

**A systematic study of the effect of chemical promoters on the precipitated Fe-based Fischer-Tropsch Synthesis catalyst**

Wonga Mpho Hexana

A thesis submitted to the Faculty of Science, University of the Witwatersrand, Johannesburg, in fulfillment of the requirements for the Degree of Doctor of Philosophy.

Johannesburg, 2009

## **Declaration**

I declare that this thesis is my own, unaided work. It is being submitted for the Degree of Doctor of Philosophy in the University of the Witwatersrand, Johannesburg. It has not been submitted before for any degree or examination in any other University.

Signature of candidate

.....day of .....2009

## Abstract

In recent years, research interest on improving the catalytic properties of precipitated Fe-based Fischer-Tropsch synthesis (FTS) catalysts has grown immensely. In particular the effect of promoters on these type of catalysts has attracted much attention. Classical promoters such as copper, potassium and silica are nowadays employed for preparing commercially used FTS catalysts. The promoted catalysts are the catalysts of choice and have been shown to possess chemical properties that improve the catalytic properties of Fe-based Fischer-Tropsch synthesis catalysts.

In this thesis we attempted to systematically study effects caused by these promoters as well as the effect of indium as a promoter for Fe. Silica which is often used as a structural promoter and often forms a large portion of the catalyst was added in significantly small amounts and its chemical promotional ability was investigated. It was found that increasing the loading of silica affected the carburization and the reduction properties of the precipitated Fe-based Fischer Tropsch synthesis catalyst. This had an effect on the Fe/Cu and Fe/K<sub>2</sub>O contacts when the loading was increased. With regard to this study, it was found that silica decreased the activity of the catalyst and shifted the hydrocarbon selectivity to low weight hydrocarbons. All catalysts used in these studies were characterized using N<sub>2</sub> physisorption, TPR, DRIFTS, XPS and XRD.

Indium was also evaluated as a chemical promoter to a precipitated Fe-based Fischer-Tropsch synthesis catalyst since it is believed that it may induce similar chemical effects as that found for copper. Indeed, it was observed that indium does possess some similar chemical properties to that of copper and also that it affected the precipitated Fe-based Fischer-Tropsch synthesis catalyst in similar ways to copper. It was also instead realized that indium acted as a poorer promoter than Cu for the Fe-based Fischer-Tropsch synthesis catalyst and this was attributed to indium having a low melting point than copper. It was also found that indium acted as a poorer promoter when it was added as a co-promoter to an iron catalyst that contained potassium and silica. It was found that indium lowered the activity of the Fischer-Tropsch synthesis reaction as well as the

Water Gas Shift reaction. This was related to a decrease in surface area of the catalyst after the addition of indium. The selectivity was shifted to the production of heavy weight hydrocarbons due to the Fe/K<sub>2</sub>O contact being promoted. Characterisation techniques such as N<sub>2</sub> physisorption, TPR and DRIFTS were employed to elucidate the findings.

## **Acknowledgements**

I am thankful to the following people and institutions:

1. My supervisor, Professor Neil Coville, for intellectual input and mental stimulation
2. School of chemistry, for providing research facilities
3. The Catomat research group, for a great research environment and invaluable assistance during the tenure of the project
4. Aberdeen University, for being a home away from home
5. Dr Dave Morgan, for XPS measurements and his immaculate XPS knowledge
6. RS (London) for funding the UK visit
7. My family for moral support
8. University of the Witwatersrand
9. Sasol
10. Canon Collins Education Trust

## **Presentations and publications arising from this study**

### **Poster Presentations**

1. CATSA Conference 2005, Midrand, Johannesburg, South Africa  
*Characterisation of iron-based Fischer Tropsch catalysts using Raman spectroscopy, XRD and TPR*
2. CATSA Conference 2006, Mossel Bay, South Africa  
*Characterisation of an Fe based Fischer Tropsch synthesis catalyst using DRIFTS*
3. SpectroCat: Vibrational Spectroscopy for Catalysis 2007, Caen, France  
*“In Situ” high pressure DRIFTS vs transmission IR*
4. International Catalysis Congress 2008, Seoul, South Korea  
*In-situ characterization of an iron based Fischer Tropsch catalyst using DRIFTS at high pressure*

### **Oral presentations**

1. University of the Witwatersrand Postgraduate Symposium 2008, Johannesburg, South Africa  
*Developing a catalyst for the production of petrol!*
2. CATSA Conference 2008, Parys, South Africa  
*Can indium be used as a promoter for an iron-based Fischer-Tropsch synthesis catalyst?*

## **Publications**

1. W. M. Hexana, N.J. Coville, "*Effect of SiO<sub>2</sub> on a promoted and unpromoted Fe-based Fischer-Tropsch synthesis catalyst*" **To be submitted**
2. W. M. Hexana, J. A. Anderson, N.J. Coville, "*Effect of Cu on a promoted and unpromoted Fe-based Fischer-Tropsch synthesis catalyst*" **To be submitted**
3. W. M. Hexana, N.J. Coville, "*Evaluating indium as a chemical promoter in Fe-based Fischer-Tropsch synthesis*" **To be submitted**
4. W. M. Hexana, N.J. Coville, "*Effect of In on a promoted and unpromoted Fe-based Fischer-Tropsch synthesis catalyst*" **To be submitted.**

# Contents

Declaration.....	i
Abstract.....	ii
Acknowledgements.....	iiiv
Presentations and publications arising from this study.....	v
Table of Contents.....	vii
List of Tables.....	xiii
List of Figures.....	xv
Abbreviations and acronyms.....	xxi

## Table of Contents

CHAPTER 1 INTRODUCTION.....	1
CHAPTER 2 FISCHER-TROPSCH SYNTHESIS (FTS): LITERATURE REVIEW ...	3
<b>2.1 Introduction.....</b>	<b>3</b>
2.2 History of the Fischer-Tropsch process.....	3
<b>2.3 Utilization of the FT process.....</b>	<b>4</b>
2.4 Three main steps in the FT process.....	7
2.4.1 Synthesis gas production.....	7
2.4.2 FT synthesis: Process conditions.....	8
2.4.3 Product Upgrading and Separation.....	8
<b>2.5 FT reactors.....</b>	<b>9</b>



2.6 The chemistry behind the FT process .....	15
2.6.1 Reactions.....	15
2.6.2 Mechanism and product selectivity .....	16
<b>2.7 Fischer-Tropsch catalysts</b> .....	23
2.7.1 Use of Fe catalysts in FTS .....	23
<b>2.8 Promoters</b> .....	26
2.8.1 Structural promoters.....	26
2.8.2 Chemical Promoters.....	29
<b>References</b> .....	34
<b>CHAPTER 3 EXPERIMENTAL</b> .....	42
<b>3.1 Catalyst preparation</b> .....	42
<b>3.2 Catalyst characterization</b> .....	43
3.2.1 X-Ray Fluorescence (XRF) spectroscopy .....	43
3.2.2 N <sub>2</sub> Physisorption .....	43
3.2.3 Temperature programmed reduction (TPR).....	44
3.2.4 Diffuse Reflectance Infrared Fourier Transform (DRIFT) Spectroscopy .....	46
3.2.5 X-Ray Diffraction (XRD) measurements .....	47
3.2.5 X-Ray Photoelectron Spectroscopy (XPS) .....	51
<b>3.3 Catalytic evaluation</b> .....	53
3.2.1. FTS reactor studies .....	53
<b>References</b> .....	68

CHAPTER 4 OPTIMISATION OF LOADING OF COPPER AND POTASSIUM PROMOTERS IN A PRECIPITATED FE-BASED FISCHER-TROPSCH SYNTHESIS CATALYST.....	69
<b>4.1 Introduction</b> .....	69
<b>4.2 Experimental</b> .....	69
<b>4.3 Results and discussion</b> .....	70
4.3.1 Optimising the weight loading of copper.....	70
4.3.2 Optimising the weight loading of potassium.....	82
<b>4.4 Conclusion</b> .....	90
<b>References</b> .....	91
CHAPTER 5 EFFECT OF SiO <sub>2</sub> ON AN UNPROMOTED Fe-BASED FISCHER- TROPSCH SYNTHESIS CATALYST.....	93
<b>5.1 Introduction</b> .....	93
<b>5.2 Experimental</b> .....	95
<b>5.3 Results and discussion</b> .....	95
5.3.1 Textural and structural properties of the catalysts.....	95
5.3.2 Reduction and carburization behaviour of the catalysts.....	96
5.3.3 Surface analysis of the catalysts.....	101
5.3.4 Adsorption properties of the catalysts.....	107
5.3.5 FTS performances.....	110
<b>5.4 Conclusion</b> .....	114
<b>References</b> .....	115

CHAPTER 6 EFFECT OF SiO <sub>2</sub> ON A PROMOTED Fe-BASED FISCHER-TROPSCH SYNTHESIS CATALYST .....	118
<b>6.1 Introduction</b> .....	118
<b>6.2 Experimental</b> .....	119
<b>6.3 Results and discussion</b> .....	119
6.3.1 Catalyst characterization .....	119
6.3.2 FTS reactor studies .....	129
<b>6.4 Conclusion</b> .....	134
<b>References</b> .....	135
CHAPTER 7 EVALUATING INDIUM AS A CHEMICAL PROMOTER IN Fe-BASED FISCHER TROPSCH SYNTHESIS .....	137
<b>7.1 Introduction</b> .....	137
7.2 Motivation to compare indium to copper as a chemical promoter .....	139
<b>7.3 Experimental</b> .....	141
<b>7.4 Results and discussion</b> .....	141
7.4.1 N <sub>2</sub> physisorption results .....	141
7.4.2 Hydrogen Temperature Programmed Reduction (H <sub>2</sub> TPR) .....	142
7.4.3 X-ray Diffraction (XRD) .....	144
7.4.4 CO adsorption measurements using DRIFTS .....	145
7.4.5 In situ FTS performances using DRIFTS .....	152
<b>7.5 Conclusion</b> .....	157
<b>References</b> .....	158

CHAPTER 8 CHEMICAL PROMOTION OF A MULTI-PROMOTED Fe-BASED FISCHER TROPSCH SYNTHESIS CATALYST BY INDIUM .....	160
<b>8.1 Introduction</b> .....	160
<b>8.2 Experimental</b> .....	160
<b>8.3 Results and discussion</b> .....	161
8.3.1 N <sub>2</sub> physisorption results .....	161
8.3.2 Temperature Programmed Reduction (TPR).....	162
8.3.3 DRIFTS.....	165
8.3.4 FTS performances.....	168
<b>8.4 Conclusion</b> .....	175
<b>References</b> .....	176
CHAPTER 9 GENERAL CONCLUSIONS.....	177

## List of Tables

### Chapter 3

Table 3.1 Characteristics of the GCs employed	57
---	----

### Chapter 4

Table 4.1 The theoretical and XRF determined Cu loadings	70
Table 4.2 XPS data for spectra given in Fig 4.1	72
Table 4.3 Reduction temperatures for the H <sub>2</sub> TPR profiles show in Fig.4.2	74
Table 4.4 %Fe reducibility as a function of Cu loading for all Cu loaded catalysts	76
Table 4.5 The calculated crystallite size of Fe <sub>2</sub> O <sub>3</sub> as a function of Cu loading	77
Table 4.6 Position of IR absorption band as a function of Cu loading	79
Table 4.7 Calculated ratios of CH <sub>2</sub> /CH <sub>3</sub> bands for all catalysts	81
Table 4.8 Reduction temperatures for the H <sub>2</sub> TPR profiles show in Fig. 4.5	83
Table 4.9 %Fe reducibility as a function of K <sub>2</sub> O loading for all K <sub>2</sub> O loaded catalysts	84
Table 4.10 The calculated crystallite size of Fe <sub>2</sub> O <sub>3</sub> as a function of K <sub>2</sub> O loading	85
Table 4.11 Peak shifts of peak at wavenumber region 2012-2015 cm <sup>-1</sup> as a function of K <sub>2</sub> O loading	87
Table 4.12 Estimation of the CH <sub>2</sub> /CH <sub>3</sub> ratio as a function of K <sub>2</sub> O loading	88

## Chapter 5

Table 5.1 The composition and textural properties of the calcined catalysts	95
Table 5.2 The calculated crystallite size of Fe <sub>2</sub> O <sub>3</sub> as a function of SiO <sub>2</sub> loading	96
Table 5.3 Peak maxima of H <sub>2</sub> TPR profiles	98
Table 5.4 Reduction temperatures for peaks of CO TPR profiles	100
Table 5.5 Areas for peaks in Figure 5.2	100
Table 5.6 Fe (2p) and Si (2p) peak areas for all catalysts	105
Table 5.7 Band maxima in the wavenumber region 2012-2015 cm <sup>-1</sup> as a function of SiO <sub>2</sub> loading	108
Table 5.8 Estimation of the CH <sub>2</sub> /CH <sub>3</sub> ratio as a function of SiO <sub>2</sub> loading	112

## Chapter 6

Table 6.1 The composition and textural properties of the catalysts	119
Reduction temperatures for peak 1 and peak 2 as well as their areas	123
Table 6.3 Reaction performances of all catalysts at steady state conditions	132

## **Chapter 7**

Table 7.1 The composition and textural properties of the catalysts as prepared	141
Table 7.2 Comparing the reducibility of Fe-based catalysts using H <sub>2</sub> TPR	144
Table 7.3 Fe <sub>2</sub> O <sub>3</sub> crystallite size determined using Rietveld refinement	145
Table 7.4 Calculated ratios of CH <sub>2</sub> /CH <sub>3</sub> for all catalysts	155

## **Chapter 8**

Table 8.1 The composition and N <sub>2</sub> physisorption results of the catalysts	161
Table 8.2 H <sub>2</sub> Reduction temperatures for all the catalysts in Figure 8.1	163
Table 8.3 CO reduction temperatures for all the catalysts in Figure 8.2	164
Table 8.4 FTS reaction performances for all the catalysts	172

## List of Figures

### Chapter 2

<b>Figure 2.1</b> Franz Fischer at work in 1918	4
<b>Figure 2.2</b> Multitubular fixed bed reactor with internal cooling	10
<b>Figure 2.3</b> Slurry bubble column reactor (or slurry bed reactor) with internal cooling tubes or three-phase fluidised (ebulating) bed reactors	11
<b>Figure 2.4</b> Fluidised fixed bed (FFB) reactor with internal cooling	13
<b>Figure 2.5</b> Circulating fluidised bed (CFB) reactor with circulating solids, gas recycle and cooling in the gas/solid recirculating loop	14
<b>Figure 2.6</b> A representation of the stepwise mechanism for hydrocarbon chain growth and chain termination	18
<b>Figure 2.7</b> Typical plot of calculated selectivities (% carbon atom basis) of carbon number product cuts as a function of the probability chain growth	21

### Chapter 3

<b>Figure 3.1</b> The TRISTAR 3000 analyzer	44
<b>Figure 3.2</b> Experimental set-up for TPR measurements	45
<b>Figure 3.3</b> DRIFTS cell with ZnSe windows	46
<b>Figure 3.4</b> Gas manifold for the introduction of gases into the DRIFTS cell	47
<b>Figure 3.5</b> The Bruker D8 X-Ray diffractometer	48



<b>Figure 3.6</b> Diffraction pattern obtained after the XRD measurement of Fe <sub>2</sub> O <sub>3</sub>	49
<b>Figure 3.7</b> Fitting of the experimental diffraction pattern (a) blue line represents the experimental pattern and red line is the fitted curve (b) difference curve produced after fitting the experimental diffraction pattern	50
<b>Figure 3.8</b> The AXIS UltraDLD XPS instrument	51
<b>Figure 3.9</b> The stainless steel bar showing the mounted catalysts ready for XPS analysis	52
<b>Figure 3.10</b> The fixed bed reactor made from a ½" Swagelok stainless steel pipe. A = Sketch portrait; B = Digital portrait	54
<b>Figure 3.11</b> The hot trap placed in a heating jacket, both situated below the reactor	55
<b>Figure 3.12</b> Traps, pressure regulator, needle valve and gas line after reactor	56
<b>Figure 3.13</b> GC on the left fitted with an FID detector and the one on the right fitted with a TCD detector	58
<b>Figure 3.14</b> Schematic representation of the reactor setup	59
<b>Figure 3.15</b> A trace for the calibration gas using the TCD GC	61
<b>Figure 3.16</b> A trace for the calibration gas product using the FID GC	61
<b>Figure 3.17</b> A trace showing the calibration of the TCD GC using syngas	62
<b>Figure 3.18</b> FTS products detected by the TCD GC	62
<b>Figure 3.19</b> FTS products detected by the FID GC	63
 <b>Chapter 4</b>	
<b>Figure 4.1.</b> (a) Cu(LLM) and (b) Cu(2p) spectra for all catalysts	71
<b>Figure 4.2</b> H <sub>2</sub> TPR profiles of all the catalysts	73
<b>Figure. 4.3</b> TPR profile of Fe <sub>2</sub> O <sub>3</sub> reduced using the reduction method employed for carrying	75

out an FTS reaction

**Figure 4.4** Comparing CO absorption spectra of Cu promoted catalysts to the unpromoted Fe catalyst 78

**Figure 4.5** H<sub>2</sub> TPR profiles of all the catalysts 82

**Figure 4.6** Comparing CO absorption spectra of K<sub>2</sub>O promoted catalysts to the unpromoted Fe catalyst 86

## Chapter 5

**Figure 5.1** H<sub>2</sub> TPR profiles of the catalysts 97

**Figure 5.2** CO TPR profiles of catalysts 99

**Figure 5.3** Survey spectrum showing elements on the surface of the 5SiO<sub>2</sub>/100Fe calcined catalyst 101

**Figure 5.4** Narrow region spectrum of Fe (2p) peak for all catalysts 103

**Figure 5.5** Narrow region spectrum of Si (2p) peak for all catalysts 104

**Figure 5.6** Oxygen core level spectra for a) 5SiO<sub>2</sub>/100Fe b) 10SiO<sub>2</sub>/100Fe c) 20 SiO<sub>2</sub>/100Fe and d) 25SiO<sub>2</sub>/100Fe 106

**Figure 5.7** CO adsorption spectra of all the catalysts (P = 2 bar, T = 25 °C, CO flow rate = 12 ml/min) 107

**Figure 5.8** DRIFTS spectra of all catalysts showing the C-H region after 5 hours of the FTS reaction (Reduction conditions: H<sub>2</sub>/CO = 2, P = 2 Bar, T = 350 °C, H<sub>2</sub>/CO flow rate = 12 ml/min, t = 1 h; FTS reaction conditions: H<sub>2</sub>/CO = 2, P = 10 Bar, T = 275 °C, H<sub>2</sub>/CO flow rate = 12 ml/min, t = 5h) 110

<b>Figure 5.9</b> CO <sub>2</sub> produced as a function of the SiO <sub>2</sub> content	113
--	-----

## Chapter 6

<b>Figure 6.1</b> H <sub>2</sub> TPR profiles for all catalysts	122
<b>Figure 6.2</b> CO adsorption on all the catalysts; Conditions: CO reduction for 1 hour (Flow rate = 12 ml/min, T = 350°C, P = 2 bar), CO adsorption for 30 min (CO Flow rate = 12 ml/min, T = 25°C, P = 2 bar)	124
<b>Figure 6.3</b> Comparing the intensity of peak at 2014 cm <sup>-1</sup> for all the catalysts	126
<b>Figure 6.4</b> DRIFTS spectra showcasing FTS reactions for all catalysts; Conditions: Reduction for 1 hour (H <sub>2</sub> /CO = 2/1, Flow rate = 12 ml/min, T = 350 °C, P = 2 bar), FTS reaction for 5 hours (H <sub>2</sub> /CO = 2/1, Flow rate = 12 ml/min, T = 275°C, P = 10 bar)	127
<b>Figure 6.5</b> DRIFTS spectra comparing FTS reactions for SiO <sub>2</sub> loaded catalysts to a non-loaded SiO <sub>2</sub> catalyst; Conditions: Reduction for 1 hour (H <sub>2</sub> /CO = 2/1, Flow rate = 12 ml/min, T = 350 °C, P = 2 bar), FTS reaction for 5 hours (H <sub>2</sub> /CO = 2/1, Flow rate = 12 ml/min, T = 275°C, P = 10 bar)	128
<b>Figures 6.6</b> The carbon monoxide conversion with time on stream for all catalysts	129
<b>Figure 6.7</b> Comparing CO conversion for all catalysts at steady state conditions	130
<b>Figures 6.8</b> The hydrogen conversion with time on stream for all catalysts	131
<b>Figure 6.9</b> Comparing H <sub>2</sub> conversion for all catalysts at steady state conditions	131

## Chapter 7

<b>Figure 7.1</b> Elements that show knight's move relationships	138
<b>Figure 7.2</b> Carbon nanotubes synthesized using the Fe-Ni/CaCO <sub>3</sub> catalyst	139
<b>Figure 7.3</b> Carbon nanotubes and coils synthesized using the Fe-Ni-Cu/CaCO <sub>3</sub> catalyst	139
<b>Figure 7.4</b> Carbon nanotubes and coils synthesized using the Fe-Ni-In/CaCO <sub>3</sub> catalyst	140
<b>Figure 7.5</b> Percentage composition of coils and tubes produced for the copper and indium promoted catalysts	140
<b>Figure 7.6</b> H <sub>2</sub> TPR profiles of Cu promoted catalysts	143
<b>Figure 7.7</b> H <sub>2</sub> TPR profiles of indium promoted catalysts	143
<b>Figure 7.8</b> Comparison of CO adsorption on the unpromoted iron catalyst and copper promoted iron catalysts; Conditions: CO reduction for 1 hour (Flow rate = 12 ml/min, T = 350°C, P = 2 bar), CO adsorption for 30 min (CO Flow rate = 12 ml/min, T = 25°C, P = 2 bar)	147
<b>Figure 7.9</b> Thermal desorption of CO on the unpromoted iron catalyst	148
<b>Figure 7.10</b> CO adsorption on the indium promoted iron catalysts	149
<b>Figure 7.11</b> Intensity of peak at 2013 cm <sup>-1</sup> for CO adsorption on the copper promoted and the indium promoted iron catalysts	149
<b>Figure 7.12</b> Intensity of peak at 2033 cm <sup>-1</sup> for CO adsorption on the copper promoted iron catalysts and the indium promoted iron catalysts	150
<b>Figure 7.13</b> CO adsorption on the indium promoted iron catalysts showing the adsorbed CO species at 2024 and 2042 cm <sup>-1</sup>	151
<b>Figure 7.14</b> Comparison of the FTS reaction over the unpromoted iron catalyst (100Fe) and copper promoted catalysts; P = 10 bar, T = 275 °C, H <sub>2</sub> /CO = 2, H <sub>2</sub> /CO flow rate = 12 ml/min,	153

Time = 5 h)

**Figure 7.15** Comparison of the FTS reaction over unpromoted iron catalyst (100Fe) and indium promoted catalysts; P = 10 bar, T = 275 °C, H<sub>2</sub>/CO = 2, H<sub>2</sub>/CO flow rate = 12 ml/min, Time = 5 h) 154

## Chapter 8

**Figure 8.1** H<sub>2</sub> TPR profiles for all the catalysts 162

**Figure 8.2** CO TPR profiles for all the catalysts 163

**Figure 8.3** CO adsorption on all the catalysts; Conditions: CO reduction for 1 hour (Flow rate = 12 ml/min, T = 350°C, P = 2 bar, CO adsorption for 30 min (CO Flow rate = 12 ml/min, T = 25°C, P = 2 Bar) 165

**Figure 8.4** Comparison of the intensities of 2014 cm<sup>-1</sup> peak 166

**Figure 8.5** DRIFTS spectra for the FTS reaction of all catalysts 167

Reaction conditions: H<sub>2</sub>/CO = 2/1, Flow rate = 12 ml/min, T = 275°C, P = 10 bar, t = 5 h

**Figure 8.6** CO conversion with time on stream 168

**Figure 8.7** H<sub>2</sub> conversion with time on stream 169

**Figure 8.8** Comparison of the CO conversion for all catalysts at steady state 170

**Figure 8.9** Comparing of the H<sub>2</sub> conversion for all catalysts at steady state 170

**Figure 8.10** H<sub>2</sub> TPR profile of In<sub>2</sub>O<sub>3</sub> 175

## Abbreviations and acronyms

African Oxygen	AFROX
Anderson, Schultz and Flory	ASF
Approximately	<i>ca.</i>
Badische Anilin und Soda Fabrik	BASF
Brunauer, Emmett and Teller	BET
Calcium carbonate	CaCO <sub>3</sub>
Carbon dioxide	CO <sub>2</sub>
Carbon monoxide	CO
Carbon number	n
Chain Growth Probability	$\alpha$
Chain propagation	$r_p$
Chain termination	$r_t$
Cobalt	Co
Copper	Cu
Copper oxide	CuO
Cubic centimeter	cm <sup>3</sup>
Degrees Celsius	°C
Fischer Tropsch	FT
Fischer-Tropsch Synthesis	FTS
Flame ionization detector	FID
Gas chromatograph	GC
Gram	g

GC integrated area of component c	$A_c$
High-temperature Fischer Tropsch	HTFT
Hydrogen	$H_2$
Indium	In
Iron	Fe
Liquid Petroleum Gas	LPG
Low-temperature Fischer Tropsch	LTFT
Methane	$CH_4$
Mole fraction	$X_i$
Moles of carbon in the feed	$N_{C, in}$
Nanometer	nm
Nickel	Ni
Nitrogen	$N_2$
Percentage	%
Product selectivity for hydrocarbons	$S_i$
United States	U.S.
Rates of reaction for FTS	$r_{FTS}$
Rates of reaction for water gas shift WGS	$r_{WGS}$
Ruthenium	Ru
Sigma	$\sigma$
Square meter	$m^2$
Temperature Programmed Reduction	TPR
Thermal conductivity detector	TCD

Total feed flow rate	$F_{in}$
Total reactor exit stream	$F_{out}$
Tin	Sn
Ultra High Purity	UHP
Water gas shift	WGS
Weight Percentage	wt. %
X-ray Diffraction	XRD
X-ray Fluorescence	XRF
X-ray Photoelectron Spectroscopy	XPS
Zinc	Zn



# Chapter 1

## *Introduction*

This chapter is written to introduce the work that was performed in this thesis and to give a comprehensive breakdown of the thesis content. The thesis is composed of nine chapters including Chapter 1. The aim of this work as illustrated by the title was to systematically study the effect that promoters have on a precipitated Fe-based Fischer-Tropsch synthesis (FTS) catalyst. A catalyst promoter is classified as a chemical substance that enhances the chemical or physical properties of a catalyst.

Over many decades various promoters have been evaluated in catalysis and extensive publications on their effects have been published. In this thesis we undertook an approach to studying the effects caused by copper, potassium, silica and indium on a precipitated Fe-based Fischer-Tropsch synthesis catalyst. A literature review on the well established Fischer-Tropsch synthesis process is first presented in Chapter 2. This describes pertinent issues such as the reaction pathways, the catalysts often used in this process, etc. Effects caused by copper, potassium and silica are well known and they are also discussed in Chapter 2. In this chapter an evaluation of prior work on FTS catalyst promoters is given. It is clear from this evaluation that little has been reported on the role of individual promoters and their relationship to the use of multiple catalyst promoters.

Chapter 3 presents all the experimental techniques and procedures that were used to carry out the studies. The actual work performed to evaluate the effects caused by these promoters on the Fe-based Fischer-Tropsch synthesis catalyst is subsequently presented (Chapter 4 to Chapter 8). Chapter 4 describes the effect of Cu and K<sub>2</sub>O on the Fe-based Fischer-Tropsch synthesis catalyst. Since the effects of these two promoters are well known and established this study was performed to optimize the weight loadings of these two promoters and provide reference data for the mixed promoter studies.

Chapter 5 deals with the effect of silica and in particular the silica content on the unpromoted Fe-based Fischer-Tropsch synthesis catalyst. The results presented in this Chapter are correlated with the silica content on the Fe-based Fischer-Tropsch synthesis catalyst.

Chapter 6 illustrates the effect of silica content on a  $K_2O$  and Cu promoted Fe-based Fischer-Tropsch synthesis catalyst. The results presented in this chapter are attributed solely to the effect of silica in the presence of Cu and  $K_2O$ . The aim of this chapter was to assess the inter-promotional effects of the promoters and what effect they have on the catalyst. It is to be noted that the optimum weight loadings obtained in Chapter 4 were used to prepare the catalysts evaluated in Chapter 6.

Chapter 7 presents the effect that indium has on the precipitated Fe-based Fischer Tropsch synthesis catalyst. The effects caused by indium on the catalyst are compared to those of Cu.

Chapter 8 describes the effect caused by indium on the precipitated Fe-based Fischer-Tropsch synthesis catalyst in the presence of potassium and silica. The aim of this study was to assess the effect of indium on the potassium and silica promoters as well as the overall effect that they have on the Fe-based Fischer Tropsch synthesis catalyst.

The general conclusions on the effect of copper, potassium, silica and indium are presented in Chapter 9. This chapter sums up all the effects caused by the above mentioned promoters and conclusions reached from each chapter are thus placed perspective.

## Chapter 2

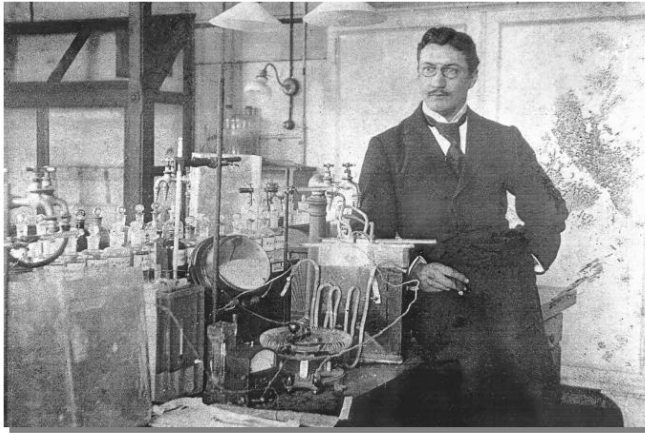
### Fischer-Tropsch Synthesis (FTS): Literature review

#### ***2.1 Introduction***

The Fischer-Tropsch Synthesis (or Fischer-Tropsch process) is a catalyzed chemical reaction in which synthesis gas (syngas), a mixture of carbon monoxide (CO) and hydrogen (H<sub>2</sub>), is converted into gaseous, liquid and solid hydrocarbons [1-12] and an appreciable amount of oxygenates [13-18]. The principal purpose of this process is to produce a synthetic petroleum substitute, typically from coal, natural gas or biomass, for use as synthetic lubrication oil or as synthetic fuel. This synthetic fuel runs trucks, cars, and some aircraft engines. The process has also been employed to produce higher value specialty chemicals, via 1-alkenes made from syngas derived from natural gas (methane) or coal [19].

#### ***2.2 History of the Fischer-Tropsch process***

In 1897, Losanitsch and Jovitschitsch reported the conversion of syngas to liquid products on electric discharge [29]. Not long after that in 1902, Sabatier and Senderens showed that methane could be produced from CO and H<sub>2</sub> mixtures using a nickel catalyst [20]. This captured the interest of many catalysis researchers and provided a platform for rigorous and intense research into this type of work. In 1913 Badische Anilin and Soda Fabrik (BASF) were awarded a patent for showcasing the catalytic production of higher hydrocarbons and oxygenated compounds from syngas under high pressures [21]. A decade later in 1923, two German researchers Franz Fischer (Fig. 2.1) and Hans Tropsch, working at the Kaiser Wilhelm Institute reported on related studies. Their work involved the reaction of syngas over alkalised iron and many other catalysts to produce a mixture of hydrocarbons and oxygenated compounds [22]. This was the start of what was to be later known as the Fischer-Tropsch Synthesis.



Fischer, H. A., 2000

**Figure 2.1** Franz Fischer at work in 1918 [23]

Since the invention of the original process many refinements and adjustments have been made, and the term "Fischer-Tropsch" now applies to a wide variety of similar processes (Fischer-Tropsch reaction or Fischer-Tropsch chemistry). The bulk of the refinements have been reported and a useful website for the location of publications relating to the research and development of the Fischer-Tropsch Synthesis can be accessed at <http://www.fischer-tropsch.org> [24]

### ***2.3 Utilization of the FT process***

The application of FTS at an industrial level started in Germany (rightfully so) since the process emanated from this country. By 1938, nine plants with a combined production capacity of about  $660 \times 10^3$  t per year were in operation [25]. Even though the nine FT plants in Germany ceased to operate after World War II, the fear of an impending shortage of petroleum kept the interest in the FT process alive. An FT plant with a capacity of  $360 \times 10^3$  t per year was built and operated in Brownsville, TX, during the 1950s. This plant was based on syngas produced from methane but a sharp increase in the price of methane caused the plant to be shut down [26, 27].

Then in 1955, Sasol, now a world-leader in the commercial production of liquid fuels and chemicals from coal and natural gas, started Sasol I in Sasolburg, South Africa. Due to the oil crises of the mid 1970s and the success of Sasol I, Sasol constructed two much larger coal-based FT plants which came on line in 1980 (Sasol II) and 1982 (Sasol III) respectively. The combined capacity of these three Sasol plants was about  $6000 \times 10^3$  t per year [27].

Some commercial ventures in FTS by Shell international in Malaysia for the production of waxes and the Moss gas project in South Africa were subsequently initiated. Based on methane, the Moss gas plant in South Africa and the Shell plant at Bintuli, Malaysia, came on stream in 1992 and 1993, respectively [12]. The Moss gas plant which converts natural gas to FT products uses a high temperature process and an iron catalyst. This plant is still running and is now under the auspices of PetroSA. The Shell commissioned plant in Bintuli, Malaysia uses the Shell Middle Distillate Synthesis process (SMDS), which is essentially, an enhanced FT synthesis.

In the last few years the interest for FTS has significantly grown due to the increase in oil price as well as the high demand for energy. Recent commercial ventures include the development of a Gas-To-Liquid (GTL) plant, Oryx GTL, in a joint venture of Sasol with Qatar Petroleum at Ras Laffan in Qatar. Sasol is also developing a GTL plant at Escravos in Nigeria. Currently, Syntroleum Corporation (a United States company) is building a 10 000 barrels per day (bpd) specialty chemicals and lube oil plant located in Northwestern Australia, also using the GTL process [28, 29].

Rentech (a small US-based company) is currently focusing on converting nitrogen-fertiliser plants from using a natural gas feedstock to using coal or coke, and producing liquid hydrocarbons as a by-product. In September 2005, Pennsylvania governor Edward Rendell announced a venture with Waste Management and Processors Inc. - using technology licensed from Shell and Sasol - to build an FT plant that will convert so-

called waste coal (leftovers from the mining process) into low-sulfur diesel fuel at a site outside of Mahanoy City, northwest of Philadelphia [30].

The state of Pennsylvania has committed to buy a significant percentage of the plant's output and together with the U.S. Dept. of Energy, has offered over \$140 million in tax incentives. Other coal-producing states are exploring similar plans. Governor Brian Schweitzer of Montana has proposed developing a plant that would use the FT process to turn his state's coal reserves into fuel in order to help alleviate the United States' dependence on foreign oil [30]

With demand for energy expected to grow 5 % a year to 2020 (according to the Carbon Sequestration Leadership Forum: [www.cslforum.org/china.htm](http://www.cslforum.org/china.htm)), China has been looking at exploiting its abundant coal reserves to meet its energy requirements. Pre-feasibility studies focusing on exploring the potential of developing two Coal-To-Liquid (CTL) plants, using Sasol's low temperature Fischer-Tropsch technology, each with a capacity of about 80000 barrels per day were concluded in November 2005 [27].

In October 2006, Finnish paper and pulp manufacturer UPM announced its plans to produce biodiesel by the Fischer-Tropsch process alongside manufacturing processes at its European paper and pulp plants, using waste biomass from the paper and pulp manufacturing processes as the source material [30].

In August 2007, Louisiana State University announced they had received funding from the US Department of Energy and Conoco Phillips for development of new nanotechnologies for catalysis of coal syngas to ethanol conversion. Conoco-Phillips is currently building a gas-to-liquids pilot plant in Bartlesville, Oklahoma to produce diesel, naphtha, and waxes from natural gas via FT catalysis [30]. The above reports show that the FT process is an established technology and already well applied on a large scale in some industrial sectors.

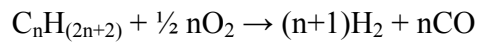
The commercial FT process itself involves three main steps, namely: syngas production, FT synthesis and product upgrading. These three main steps will be described next.

## ***2.4 Three main steps in the FT process***

### **2.4.1 Synthesis gas production**

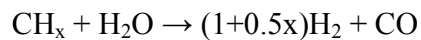
The initial reactants (syngas) used in the Fischer-Tropsch process are hydrogen gas (H<sub>2</sub>) and carbon monoxide (CO). These chemicals are usually produced by one of two methods:

1. The partial combustion of a hydrocarbon:



When n=1 (methane), the equation becomes  $2CH_4 + O_2 \rightarrow 4H_2 + 2CO$

2. The gasification of coal, biomass, or natural gas:



The value of "x" depends on the type of fuel. For example, natural gas has a greater hydrogen content (x=2 to x=4) than coal (x<2). The energy needed for this endothermic reaction is usually provided by the (exothermic) combustion of oxygen and the hydrocarbon source.

Given its availability methane is preferred to coal for syngas production.

When using natural gas as the feedstock, many authors [31-36] have recommended autothermal reforming or autothermal reforming in combination with steam reforming as the best option for syngas generation. This is primarily attributed to the resulting H<sub>2</sub>/CO ratio and the fact that there is a more favourable economy of scale for air separation units than for tubular reactors (steam methane reforming - SMR).

#### **2.4.2 FT synthesis: Process conditions**

Generally, the Fischer-Tropsch process is operated in the temperature range of 180-350°C. Higher temperatures lead to faster reactions and higher conversion rates, but also tend to favor methane production. As a result the temperature is usually maintained at the low to middle part of the range. Increasing the pressure leads to higher conversion rates and also favours formation of long-chain alkanes both of which are desirable. Typical pressures are in the range of one to several tens of bars. Even higher pressures would be more favourable, but the benefits may not justify the additional costs of high-pressure equipment [30].

#### **2.4.3 Product Upgrading and Separation**

Conventional refinery processes can be used for the upgrading of Fischer-Tropsch liquid and wax products. A number of possible processes for FT products are: wax hydrocracking, distillate hydrotreating, catalytic reforming, naphta hydrotreating, alkylation and isomerisation [37]. Fuels produced by the FT synthesis are of a high quality due to their very low aromaticity and zero sulfur content. The product stream consists of various fuel types: LPG, gasoline, diesel fuel, jet fuel, etc. The diesel fraction has a high cetane number resulting in superior combustion properties and reduced emissions [37]. New and stringent regulations may promote replacement or blending of conventional fuels by sulfur and aromatic free FT products [38, 39]. Also, other products besides fuels can be manufactured with Fischer-Tropsch catalysts in combination with upgrading processes, for example, ethene, propene,  $\alpha$ -olefins, alcohols, ketones, solvents, specialty waxes, and so forth. These valuable by-products of the FT process have higher added values, resulting in an economically more attractive process economy.



## ***2.5 FT reactors***

The FTS is operated in two modes. The high-temperature (300 - 350 °C) mode with iron-based catalysts is used for the production of gasoline and linear low molecular mass olefins [41]. The low-temperature (200 - 240 °C) mode with either iron or cobalt catalysts is used for the production of high molecular mass linear waxes [42]. Efficient and rapid removal of heat from the highly exothermic FT reaction from the catalyst particles is essential [43-45]. If this is not adequately performed, overheating results and this adversely affects the performance of the catalyst. Therefore “state of the art” reactors are needed to circumvent such problems, inevitably making reactor design a pivotal part of the FT technology. The main types of FT reactors which have been developed since 1950 are illustrated below [37, 40, 46, 166].

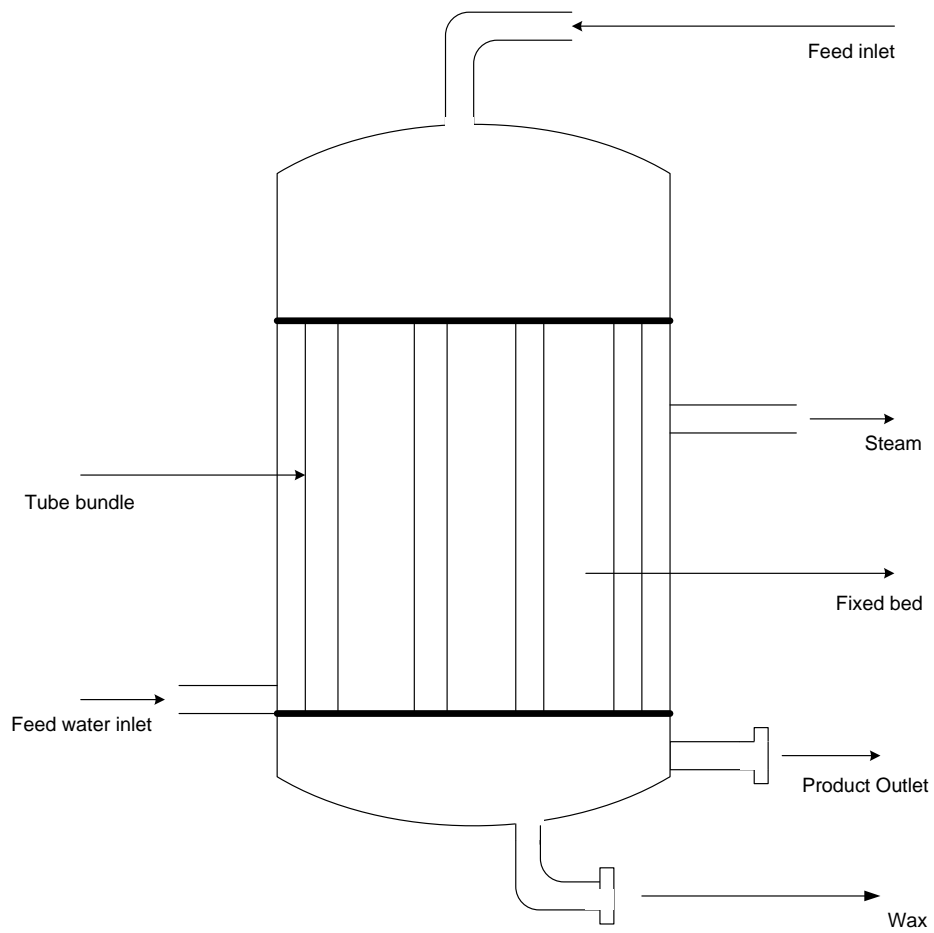


**Figure 2.2** Multitubular fixed bed reactor with internal cooling [166]

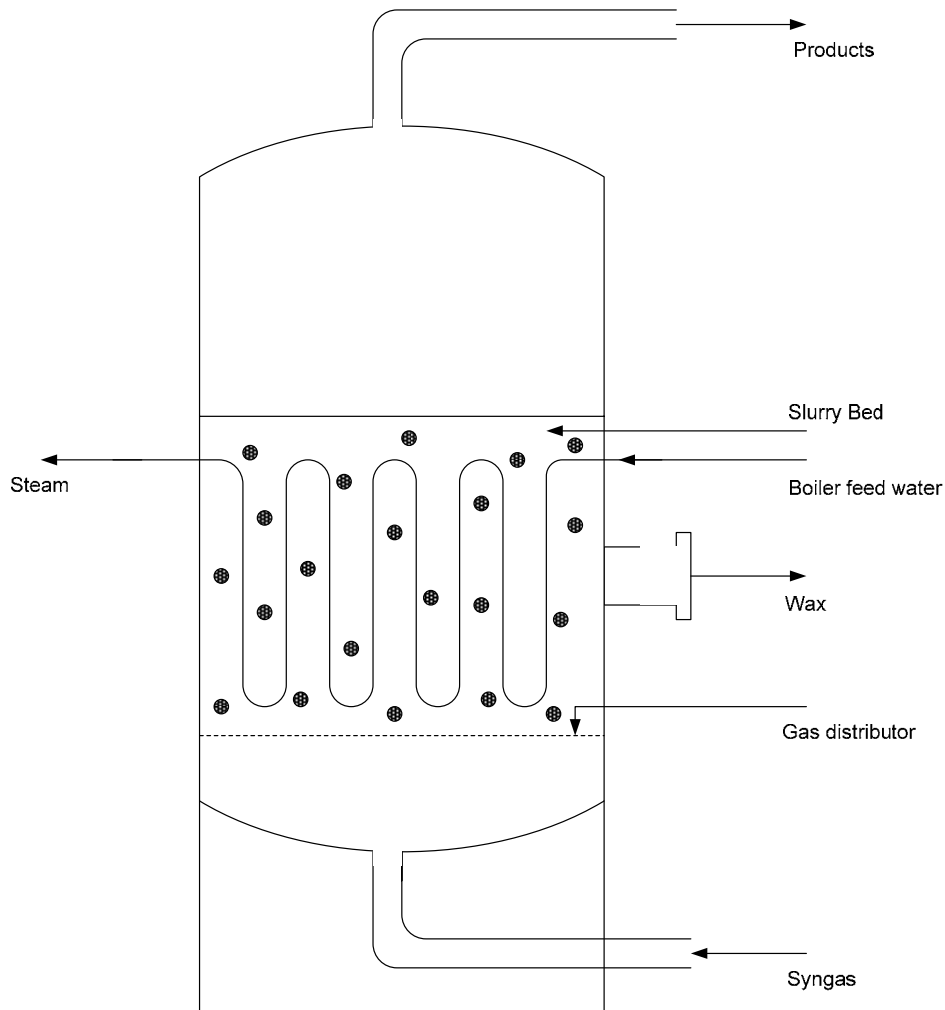


**Figure 2.3** Slurry bubble column reactor (or slurry bed reactor) with internal cooling tubes [166]

Multitubular fixed bed reactors (Fig. 2.2) are usually employed for the low temperature FT operation in producing wax. The gas flows through the bed in the downward direction and the wax produced trickles down and out of the catalyst bed. In the slurry bed reactor (Fig. 2.3), the gas flow itself provides the agitation power required to keep the catalyst bed in suspension.

The slurry bed reactor presents many advantages over the multitubular fixed bed reactor. It is cheaper to construct (only 25% of the cost of the Multitubular fixed bed reactor) and also requires less amount of catalyst. This catalyst can easily be removed or added on-line. It is also more isothermal thereby enabling it to be operated at higher temperatures which results in higher conversions. On the other hand the fixed bed is simple to operate and allows for easy separation of the catalyst from wax.

Among the disadvantages of the fixed bed reactors are: a high pressure drop over the reactor, a high temperature gradient (compared to other reactors) and tedious replacement of the used catalyst [45, 46].

The third type of reactor is the fluidized bed reactor. There are two types of fluidised bed reactors; the fluidised fixed bed (FFB) reactor (Fig. 2.4) and the circulating fluidised bed (CFB) reactor (Fig. 2.5). In the FFB reactors, there are two phases of fluidised catalyst. In the CFB reactor, the catalyst flows down the standpipe in a dense phase while it is transported up the reaction zone in a lean phase. The heat of reaction is removed from the reactor by cooling coils that generate steam. To avoid the inlet gas going up the standpipe the pressure over the standpipe, must be higher than in the reaction zone [41].

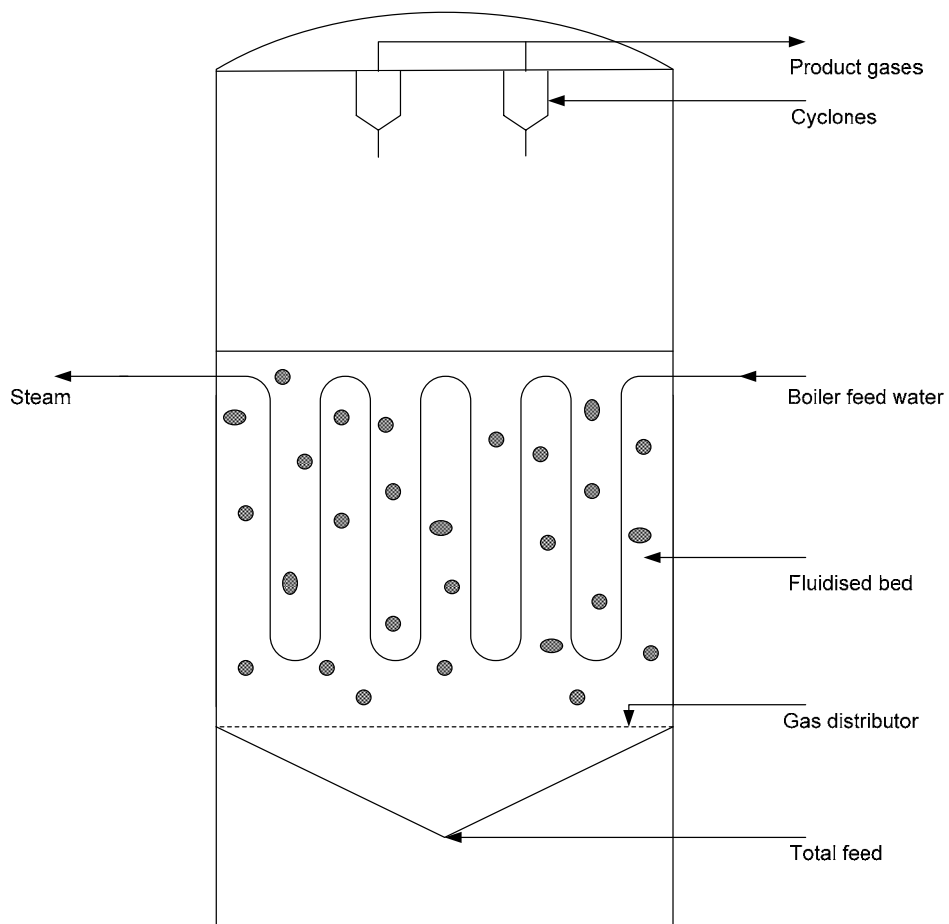


**Figure 2.4** Fluidised fixed bed (FFB) reactor with internal cooling [166]

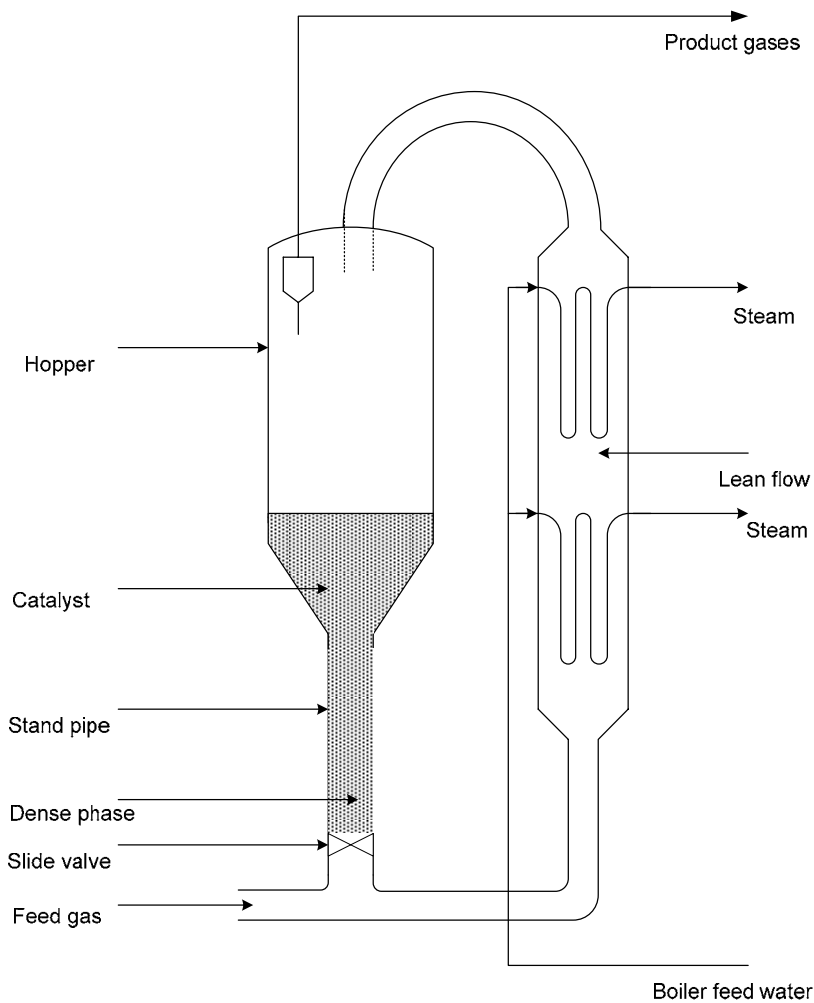


**Figure 2.5** Circulating fluidised bed (CFB) reactor with circulating solids, gas recycle and cooling in the gas/solid recirculating loop [166]

Dry [41] compared the FFB reactor to the CFB reactor. He noted that for the same production capacity, the FFB is smaller than the CFB, it is less costly to construct (cost is 40% lower), simpler to operate (more gas can be fed by either increasing the volumetric flow rate or by increasing operating pressure) and easier to build.

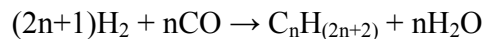
In the FFB the whole catalyst charge participates in the reaction at any moment, whereas in the CFB only a portion of it does since a portion of the catalyst is in the recirculation

loop and so not in contact with the reactant gas. The main disadvantage of the two fluidized bed reactors is that should any poison enter the reactor the entire catalyst bed is poisoned whereas in the fixed bed, the poison is adsorbed on the top layer of the catalyst leaving the rest of the bed intact.

## ***2.6 The chemistry behind the FT process***

### **2.6.1 Reactions**

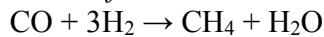
The FTS has long been recognised as a polymerisation reaction [1]. It involves a variety of competing chemical reactions, which lead to a series of desirable products and undesirable byproducts. The most important reactions are those resulting in the formation of alkanes (paraffins). These can be described by chemical equations of the form:



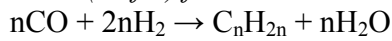
where 'n' is a *positive integer*. The simplest of these (n=1), results in formation of methane, which is generally considered to be an unwanted byproduct (particularly when methane is the primary feedstock used to produce the synthesis gas). Process conditions and catalyst composition are usually chosen, so as to favor higher order reactions (n>1) and thus minimize methane formation. Most of the alkanes produced tend to be straight-chain, although some branched alkanes are also formed.

In addition to alkane formation, competing reactions result in the formation of alkenes (olefins), as well as alcohols and other oxygenated hydrocarbons [47]. Usually, only relatively small quantities of these non-alkane products are formed, although catalysts favouring some of these products have been developed. An overview of the reactions involved is illustrated in the equations below:

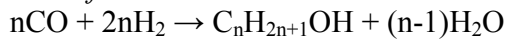
*Methane formation:*



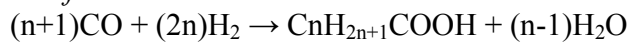
*Alkene (olefin) formation:*



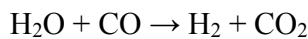
*Alcohol formation:*



*Acid formation:*

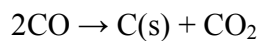


Another important reaction is the water gas shift reaction (WGS):



Although this reaction results in formation of unwanted  $\text{CO}_2$ , it can be used to shift the  $\text{H}_2/\text{CO}$  ratio of the incoming syngas. This is especially important for syngas derived from coal, which tends to have a ratio of  $\sim 0.7$  compared to the ideal ratio of  $\sim 2$ .

Another way in which  $\text{CO}_2$  can be produced in the FTS is via the Boudouard reaction:



Carbon is also produced from this reaction and can be deposited on the catalyst surface leading to catalyst deactivation. Thus, depending on a number of factors e.g.  $\text{H}_2/\text{CO}$  ratio, catalyst type, reactor type and reaction conditions used, one or the other of reactions can predominate in the synthesis [48].

### **2.6.2 Mechanism and product selectivity**

The FTS process produces a wide range of products - due to this - a detailed mechanism accounting for formation of all FTS products is yet to be achieved or reported. The detail of the mechanism has been a bone of contention for many years and an extraordinarily “hard nut” to crack. Of all the different mechanisms proposed, most of them still remain



within the original four classes put forward over the decades, namely; the surface carbide, enolic intermediate, CO-insertion and alkoxy intermediate mechanisms [49, 50]

Nonetheless there is general consensus that a stepwise growth mechanism is involved. Thus the very wide range of products formed is as a result of sequential steps taking place on the catalyst surface. These sequential steps largely resemble those of a polymerization reaction and can be summarized as follows:

- a) reactant adsorption
- b) chain initiation
- c) chain growth
- d) chain termination
- e) product desorption
- f) re-adsorption and further reaction

Consequently a mechanism of chain growth and termination has been proposed [47] and it is illustrated in Fig. 2.6.

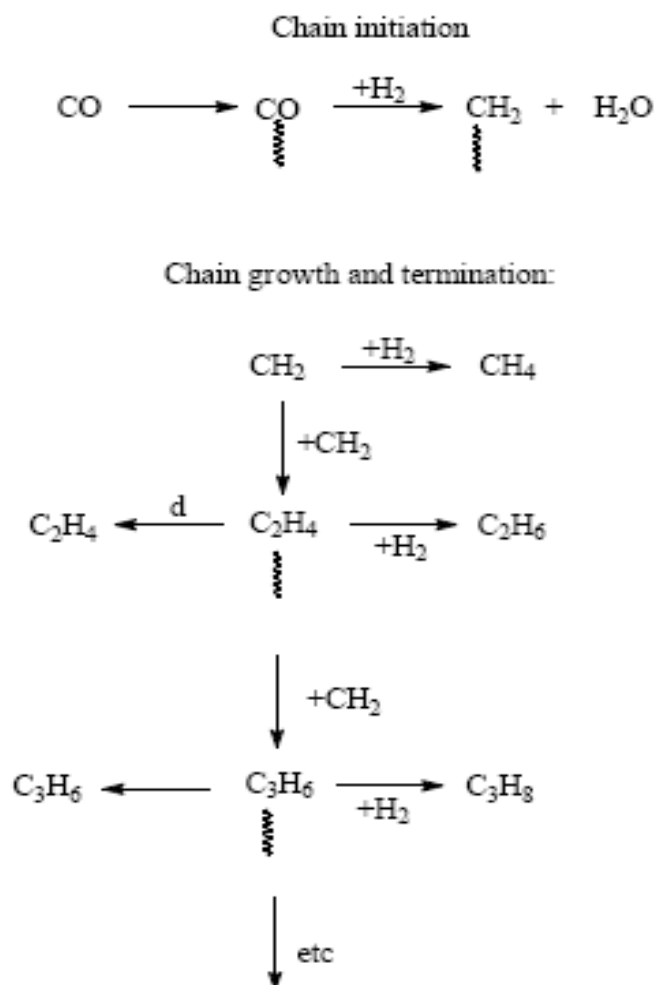


**Figure 2.6** A representation of the stepwise mechanism for hydrocarbon chain growth and chain termination [47]

The  $\text{CH}_2$  units (Fig. 2.6) formed by the hydrogenation of CO are taken as the “monomers” in this stepwise polymerization process. At each stage of growth the adsorbed hydrocarbon species has the option of desorbing or being hydrogenated to form the primary FT products or of adding another monomer to continue the chain growth.

Maitlis and co-workers have used the ideas of organometallic chemistry and homogeneous catalysis derived from model systems, combined with the results of experiments using  $^{13}\text{CH}_2=^{13}\text{CH}_2\text{-X}$  ( $\text{X} = \text{H}, \text{Br}, \text{etc}$ ) compounds as probes to propose the

“alkenyl mechanism” for the F-T reaction. In this mechanism chain growth is initiated by a vinyl + methylene coupling and it proceeds via coupling of these two groups and terminates via hydrogenation of the alkenyl to yield the 1-alkene [50]. This mechanism can explain the formation of branched products (for example, by allyl isomerisation). Labelling probe studies also suggest that oxygenates such as ethanol arise from CO but not via methylenes in F-T reactions [50].

Other mechanisms reported describe molecules such as CO and CHOH as possible “monomers” that add onto the growing chain. For instance CO insertion onto the growing chain is believed to be the way that the alcohols, acids and aldehydes are formed [51-53].

The probability of chain growth ( $\alpha$ ) is assumed to be independent of the chain length. A product distribution model known as the Anderson-Schulz-Flory (ASF) model [54, 55] is usually used to obtain the relationship between the weight fraction of formed hydrocarbons and the chain growth probability.

This model is described by the following equation:

$$W_n/n = (1-\alpha)^2 \alpha^{n-1}$$

where  $W_n$  is the weight fraction of hydrocarbon molecules containing  $n$  carbon atoms and  $\alpha$  (alpha) is the chain growth probability or the probability that a molecule will continue reacting to form a longer chain. In general,  $\alpha$  is largely determined by the catalyst and the specific process conditions. Examination of the above equation reveals that methane will always be the largest single product, however by increasing  $\alpha$  so that it is close to one, the total amount of methane formed can be minimized compared to the sum of all of the various long-chain products.

To easily illustrate the above point, the Anderson-Schulz-Flory (ASF) is usually linearised into the following equation:

$$\log (W_n/n) = n \log (\alpha) + \log ((1-\alpha)/\alpha)^2$$

This equation is used to determine the  $\alpha$  value from experimental data. A plot of  $\log (W_n/n)$  versus carbon number ( $n$ ) is linear and the chain growth probability is obtained from its slope as  $\log (\alpha)$  or from the intercept as  $\log ((1-\alpha)/\alpha)^2$  at  $n = 1$ .

Alpha ( $\alpha$ ) can also be defined in terms of the rate of chain propagation ( $r_p$ ) and chain termination ( $r_t$ ) as:

$$\alpha = \frac{r_p}{r_t + r_p}$$

Calculated product selectivities versus probability of chain growth are illustrated in Fig. 2.7 [56]. This plot shows that only the light ( $\alpha \rightarrow 0$ ) or heavy ( $\alpha \rightarrow \infty$ ) products can have a high selectivity. All other products go through a maximum yield. The product distribution is influenced by operating conditions (temperature, pressure, feed gas composition, space velocity) and catalyst type and promoters. In other words the alpha value ( $\alpha$ ) for product distribution ranges between 0 and 1 with the higher value indicating a greater selectivity towards waxy products and a lower value corresponding to gaseous products.

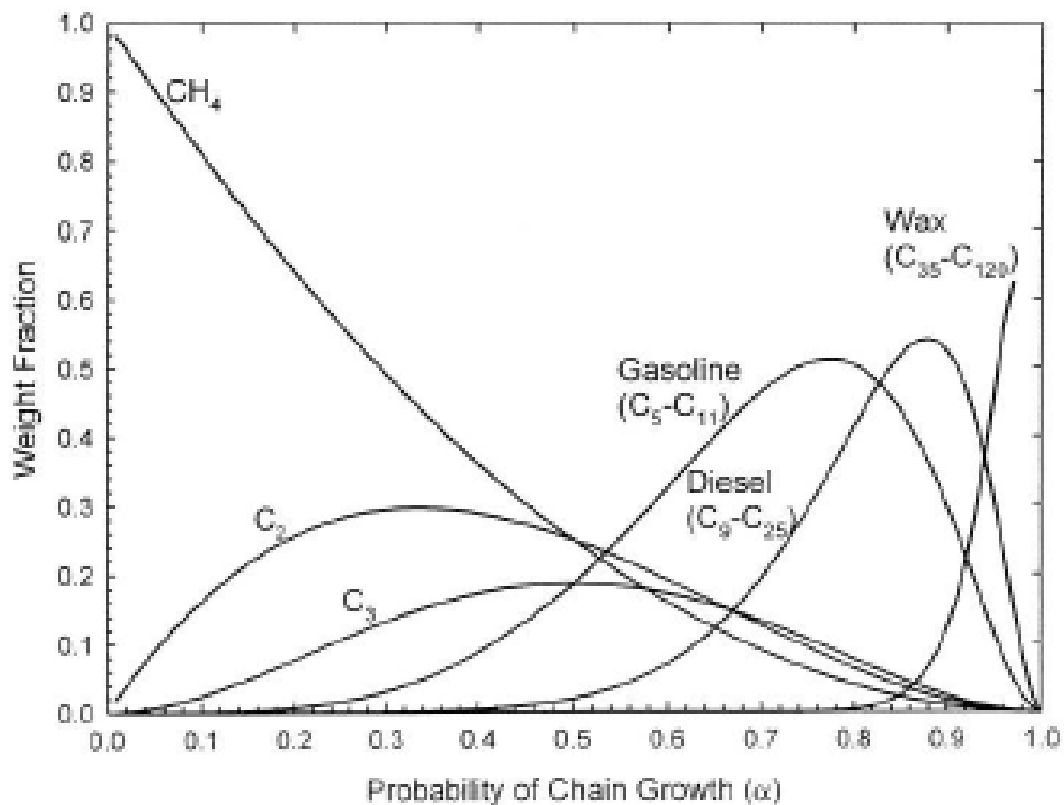


**Figure 2.7** Typical plot of calculated selectivities (% carbon atom basis) of carbon number product cuts as a function of the probability chain growth [56]

However, the FT product distributions reported in the literature [57, 58] do not always obey the simple ASF kinetic model. Some of the deviations usually observed include:

- a) A high methane selectivity. It is proposed that this is as result of methane being able to form by more than one pathway [59].
- b) A low yield of ethane, ethene and in some cases propane relative to the predicted ASF distribution. It is suggested that this could be due to the re-insertion of the very reactive olefins back into the growing chain.

c) Some negative [60] and positive [25, 55, 61-63] deviations especially when the carbon number is greater than 8 have also been reported. Various mechanisms accounting for chain-length related phenomena have been proposed. These include a vapor-liquid equilibrium phenomena, diffusion enhanced olefin readsorption model [62], different physisorption strength of the olefins [63] and the two-active-site model [55, 61]. Shi and Davis [64] have accounted for chain-length related phenomena by proposing that the apparent products of the FTS reaction is a mixture of freshly produced FTS products and the products left in the reactor. They concluded that in order to obtain correct product distribution in a FTS reaction, it is necessary to find a way to evaluate or eliminate the contribution from the products left in the reactor.

d) Further the  $\alpha$ -olefin to paraffin ratio decreases exponentially and the chain growth parameter,  $\alpha$ , is not constant with increasing chain length.

## ***2.7 Fischer-Tropsch catalysts***

A variety of catalysts can be used for the Fischer-Tropsch process, but the most common are the transition metals (group 8-10 metals) since they can dissociatively adsorb H<sub>2</sub> and CO. Fe, Ni, Co and Ru are the only metals that have the required FT activity for commercial application [12]. Ni has been reported to produce too much methane under FT conditions [11, 65-67]. On the other hand Ru has been found to be less selective to methane and more selective to the C<sub>5+</sub> hydrocarbon fraction than other metals [66]. Ru is the most expensive of these four metals and its availability in the world is insufficient for large scale application. For these reasons Fe and Co are viable catalysts for industrial applications.

Historically, Fe has been the catalyst of choice in industrial applications due to its low cost. It is also more suitable for low-hydrogen-content synthesis gases such as those derived from coal due to its promotion of the water-gas-shift reaction.

More recently emphasis in industry has been placed on using Co in industrial reactors. In this thesis, research focusing on the use of Fe has been pursued and thus only studies done using this catalyst will be described.

### **2.7.1 Use of Fe catalysts in FTS**

Fe catalysts have been extensively used for the F-T synthesis and scores of literature studies can be found that describe work in this area. Extensive reviews and government reports have also been written [6, 9, 68-70], highlighting the versatility of the Fe catalyst in the FTS.

As explained earlier, the FTS has two temperature regimes, namely the High Temperature Fischer Tropsch (HTFT) and Low Temperature Fischer Tropsch (LTFT) regimes. The Fe catalyst has found use in both these regimes. The HTFT process with iron-based catalysts, which is operated at temperatures between 300 and 350°C is used

for the production of low molecular mass olefins, gasoline (primarily) and diesel fuel range liquids. The (LTFT) process is operated in the 200-250°C temperature range is used for the production of high molecular weight waxes [71].

Thus Fe catalysts are very flexible and this is as result of much effort put into better understanding their chemical properties [72-80]. The three key properties that have always been studied for improving them is their lifetime, activity and product selectivity.

Optimizing these properties for desired commercial application has been the focus of Fe-based FTS catalyst research and development. Each one of these properties can be affected by a variety of parameters which include:

a) Catalyst preparation

Fe catalysts can be prepared by various methods varying from precipitation [81-84] to impregnation methods. Precipitation is normally the preferred preparation method for Fe catalysts employed commercially [9, 37].

b) Catalyst activation

The activation procedure used for Fe FTS catalysts has a great influence on their activity and selectivity [85-87]. Precipitated catalysts are usually activated using carbon monoxide, hydrogen or synthesis gas [85]. Activation alters the catalyst composition to what is thought to be a mixture of iron oxides ( $\text{Fe}_2\text{O}_3$ ,  $\text{Fe}_3\text{O}_4$ ), various iron carbides ( $\text{Fe}_x\text{C}$ ,  $2 \leq x \leq 3$ ) and iron metal ( $\alpha\text{-Fe}$ ) [88-95].

Over many years, reseachers have sought to find the active phase of the Fe catalyst during the FTS. Historically various studies suggested that magnetite ( $\text{Fe}_3\text{O}_4$ ) was the active phase [96–101], while other workers have linked the formation of magnetite to catalyst deactivation [102]. The starting iron oxide or the reduced iron ( $\alpha\text{-Fe}$ ) is known to transform into iron carbides during reaction. Hence, there are numerous studies that propose Fe carbides to be the active phase for F–T synthesis [103–109]. Presently there is



a resounding backing for Fe carbides to be the active species in FTS and overwhelming evidence has been presented to back this assertion [110-112].

### c) Use of promoters

One way of controlling the product selectivity in an FT reaction is to introduce promoters into the catalyst. A promoter is considered to be the component of the catalyst that does not take part in a catalytic reaction but changes the properties of the catalyst. Promoter chemistry usually contributes in two major ways to catalysis. Firstly a promoter can improve a catalyst's structural features by enhancing its surface area while maintaining its stability in a catalytic reaction. This type of a promoter is often referred to as a structural promoter. A structural promoter can also act as a barrier or spacer between active metal crystallites thereby inhibiting sintering or crystallite growth [113].

The second way in which promoters affect catalysts is electronic in nature. This occurs as a result of a change in the electronic environment of the catalyst surface. This can lead to enhanced reactant gas-active site interactions which can lead to bonding destabilization of the reactant gas. This type of promotion is chemical in nature, and the promoter is referred to as a "chemical promoter" [50].

Promoters may also serve one or more of the following purposes; they may

- (i) supply a catalytic effect not possessed by the catalytic metal alone,
- (ii) facilitate catalyst preparation, conditioning, or regeneration,
- (iii) inhibit catalyst poisoning, and/or
- (iv) improve the physical nature of the support.

The two types of promoters usually employed for improving the Fe catalysts in FTS are chemical promoters and structural promoters, and these will shortly be discussed.

## **2.8 Promoters**

### **2.8.1 Structural promoters**

Typical structural promoters used in F-T catalysis include SiO<sub>2</sub> [47, 113, 114], TiO<sub>2</sub> [47, 115-118, 119], Al<sub>2</sub>O<sub>3</sub> [47, 120-122], MnO [123], Nb<sub>2</sub>O<sub>5</sub> [124], ZrO<sub>2</sub> [115,125-128], CeO<sub>2</sub> [115,15], Cr<sub>2</sub>O<sub>3</sub> [9], ZnO [9], MgO [129] or a mixture of supports such as MgO/SiO<sub>2</sub> [130] and TiO<sub>2</sub>/SiO<sub>2</sub> [131], zeolites [132-134] and molecular sieves [135], activated carbon [136], carbon nanotubes [84, 137] and nanofibers [138]. SiO<sub>2</sub> has been shown to be a superior structural promoter for precipitated Fe based FTS catalysts [9, 139, 140]. Hence only work relating to SiO<sub>2</sub> will be discussed here.

#### **2.8.1.2 Role of SiO<sub>2</sub> as a promoter for Fe FT catalysts**

SiO<sub>2</sub> has been extensively investigated as a catalyst support in the FT reaction. In this role the support material is used in a large amount relative to the amount of catalyst used. When smaller amounts are used (typically from 1% - 20%) the materials are called binders or promoters. In many instances the interaction between the support/binder/promoter and the catalyst involve the same type of interactions. However, the concentration effect can have serious implications for the physical properties of the mixture.

SiO<sub>2</sub> can hence either be used as a support or be used in small quantities as a structural promoter for the Fe-based Fischer Tropsch catalysts. In both cases it is often added to Fe-based Fischer Tropsch catalysts to maintain surface area [26, 70].

### 2.8.1.3 Low promoter concentrations of SiO<sub>2</sub>

A major problem in using an iron catalyst without addition of a structural promoter is the formation of catalyst fines accompanying the physical breakage of the catalysts. The addition of a binder to a precipitated iron catalyst is beneficial to the formation and stabilization of small crystallites of the active phase and provides a robust skeletal structure in the catalyst. This structure is needed to keep the catalyst from breaking down (a process referred to as attrition) during the processes of activation and FTS reaction [141-144].

A study by Jothimurugesan et al. [145] on the effect of two binders - a silica-based system and a silica-kaolin-clay-phosphate-based system - on a doubly promoted Fischer-Tropsch (FT) synthesis iron catalyst (100Fe/5Cu/4.2K) has revealed that 12 wt.% binder silica gives the highest attrition resistance when the binder silica content is varied from 0 to 20 wt.%.

SiO<sub>2</sub> also has an effect on both catalytic activity and selectivity [1, 9, 144]. Work highlighting the ability of SiO<sub>2</sub> to induce chemical effects on catalytic properties has also been observed [26, 146, 147]. Mössbauer spectroscopy studies of precipitated Fe-based Fischer-Tropsch catalysts (100Fe/5Cu/4.2K/xSiO<sub>2</sub>), where x = 0, 8, 16, 24, 25, 40 or 100) have shown that reduction of the oxide precursor in CO gives rise to chi-carbide Fe<sub>3</sub>C<sub>2</sub> whose amount decreases with an increase of SiO<sub>2</sub> content [148].

From the work discussed above, it is clear that loading levels of SiO<sub>2</sub> onto Fe-based FT catalysts play a huge role in affecting their chemical properties.

#### 2.8.1.4 SiO<sub>2</sub> as a support

Apart from SiO<sub>2</sub> being used as a structural promoter, it can also be used as a support for Fe-based Fischer Tropsch catalysts. Especially in recent years, silica has been chosen as the principal support for the preparation of iron-based catalysts with high attrition resistance using popular spray-drying technologies. The ability of the silica support to prevent sintering of the Fe phases has also been observed [149].

Many other advantages of the supported catalysts, such as improved catalyst stability, decreased deactivation rate, and improved selectivity, have also been identified. The lower activity of supported Fe catalysts has been attributed to the effect of metal-support interactions that affect the reducibility of the iron phase [147, 150].

Such metal support interactions and structural properties in highly dispersed catalysts are frequently mentioned in the literature. Wielers et al. [151] studied the reduction behaviour of silica-supported iron catalysts and revealed that reduction of the Fe/SiO<sub>2</sub> catalyst proceeds via an iron (II) silicate phase. Cagnoli et al. [152] and Bukur et al. [144], respectively, investigated the influence of the support on the activity and selectivity of alumina or silica supported catalysts in FTS reaction and their results were attributed to the interactions between the metal and supports.

Lund and Dumesic [153] studied interactions in silica-supported magnetite catalysts by spectroscopy and suggested a model in which Si<sup>4+</sup> substitutes for Fe<sup>3+</sup> in the tetrahedral sites near the surface of magnetite. In the work of Yeun et al. [154], they suggested that on a 1 wt% Fe/SiO<sub>2</sub> catalyst, Fe<sup>2+</sup> strongly interacted with silica during reduction. Jun et al. [155] studied FTS over SiO<sub>2</sub> supported iron-based catalysts from biomass-derived syngas. They found that the addition of SiO<sub>2</sub> leads to the poor dispersion of iron oxide.

Therefore, SiO<sub>2</sub> is usually used as a support for FTS catalysts to obtain the desired physical strength and make it attrition resistant. However the addition of SiO<sub>2</sub> as a

support also leads to the corresponding poor reducibility due to the strong metal-support interaction.

In general, the effects of SiO<sub>2</sub> on Fe-based FTS catalysts can be summarized as follows:

- (i) Changes the catalyst stability and selectivity.
- (ii) Decreases the deactivation rate of the catalyst.
- (iii) Maintains the surface area and thereby has a chemical effect on catalyst properties.
- (iv) Prevents sintering of Fe phases.
- (v) Affects the reducibility of the iron phase, especially the transformation of magnetite to metallic iron. This is attributed to the strong interaction between the metal and the silica support. This may lead to SiO<sub>2</sub> indirectly weakening the surface basicity and severely suppressing the carburization and CO adsorption of the catalyst.
- (vi) Due to the lower surface basicity of the catalyst incorporated with SiO<sub>2</sub>, a higher selectivity to light hydrocarbons and methane is observed and a decreased selectivity to olefins and heavy products is obtained.

### **2.8.2 Chemical Promoters**

These types of promoters affect the electronic nature of the catalyst and their presence may result in a change in the activity and selectivity of the metal catalyst. Fe catalysts are significantly affected by the presence of chemical promoters. For all Fe catalysts used in the FT reaction the promotion with the optimum amount of alkali metal is vital for satisfactory FT activity as well as the required selectivity.

Potassium [156, 157] is the preferred alkali metal commercially used in FT reaction and has been known to increase wax and alkene yields while decreasing the production of undesirable methane [9]. Potassium also has been implicated in increasing FTS and water-gas shift activity [158].

However, the use of potassium as a chemical promoter may be hampered by its readiness to form an alkali compound with common catalyst supports, or structural promoters such

as alumina or silica. Also, high potassium loadings may cover too large of a fraction of the surface of the iron catalyst, resulting in a limited promotion effect or even a decrease in FTS conversions.

Work done by O'Brein et al. [157], showed that a high potassium loading is required when the FTS reaction temperature is decreased because it becomes harder to dissociate the C-O bond. They found that the optimum potassium promotion was 4-5 atomic% relative to iron.

On the contrary, Dry [41] reported that catalytic activity decreases for the low temperature FTS as the potassium loading is increased but the opposite effect is observed when performing a high temperature FTS reaction. He reported that at 200 °C, the relative catalyst activity decreased when the relative K<sub>2</sub>O content is increased from 0 to 2.6 %. At 330 °C, the catalytic activities first increased and stabilised at a certain level as the relative K<sub>2</sub>O content increased above 3 %. Furthermore, Davis and co-workers [68] have found that potassium loading to give a K/Fe atomic ratio of greater than 5 failed to further enhance the CO conversion.

It is apparent that when potassium is added in moderation to Fe-based FTS catalysts, it enhances its characteristics. This is because when potassium containing catalysts are heated the potassium migrates to the top (the surface) of the catalyst [57] and has a direct influence on the active catalyst sites. Therefore if a high loading of potassium is used, this may be detrimental to the catalyst as more of it will move to the surface and block some of the catalyst active sites leading to lower FTS activity.

Therefore the FTS activity either increases [158] or passes through a maximum as a function of potassium loading [9, 159], and potassium either has no effect on the activity for FTS [157] or suppresses it [57, 159].

From the findings above, it appears as if the optimum positive effects of potassium on Fe-based FTS catalysts are obtained at low loadings not greater than 1 - 5 atomic % relative to Fe. This is obviously dependent on the reaction conditions that are employed.

Most researchers that have studied the influence of potassium on the Fe-based FTS catalysts have come to a general consensus that potassium has the following effects on Fe-based FTS catalysts:

- (i) Influences FTS activity. The FTS activity either increases or passes through a maximum as a function of potassium loading
- (ii) Increases the activity of the WGS reaction
- (iii) Potassium and other alkali metals decrease the sticking probability of the CO and H<sub>2</sub> molecules over the iron surface and increase their probability of dissociation
- (iv) Potassium leads to higher olefin-to-paraffin ratio and decreases the methane selectivity
- (v) Produces longer hydrocarbon chains. This is favorable for gasoline production because the yield of liquid hydrocarbons increases.
- (vi) Increases its heat of adsorption of CO, rate of carbon deposition and rates of hydrocarbon chain growth

Another promoter that is commercially employed for the Fe-based FTS catalyst is copper. Copper has traditionally been added in precipitated iron catalysts to facilitate reduction of iron oxide to metallic iron during hydrogen activation [157]. Copper has been shown to minimize sintering of iron catalysts when activating with hydrogen by lowering the reduction temperature [9].

It has also been found that copper promotion appears to favour the formation of iron carbides [160]. It may be possible that copper increases the activity of iron catalysts by increasing the number of active sites that are formed. Assuming that the active site(s) is a zero valence surface species, copper may serve as a means of preventing oxidation of the active metallic iron or iron carbide.

Wachs et al. [161], Anderson [25] and O'Brein et al. [157] observed that copper had no effect on product selectivity. However, Bukur et al. [158] have reported that incorporating Cu into iron-based catalysts results in an increase in the average molecular weight of hydrocarbon products.

Copper also appears to influence the WGS reaction and carburization. As demonstrated earlier, the water-gas-shift reaction produces H<sub>2</sub> from the reaction of H<sub>2</sub>O and CO ( $\text{CO} + \text{H}_2\text{O} \rightarrow \text{CO}_2 + \text{H}_2$ ) and this enables the Cu-promoted Fe-based catalyst to be used for syngas with low levels of H<sub>2</sub> for the FTS reaction. This is also consistent with copper being used in commercial low-temperature water-gas shift catalysts. Bukur et al. [158] have also found a high water-gas shift activity for their Cu-promoted Fe-based catalyst when performing FT synthesis reactions at 260°C. A higher carbon dioxide amount was obtained for the catalyst with copper which indicated that copper is a promoter for the water-gas shift reaction.

Dry [9] has stated that the precipitated iron catalyst developed by Ruhrchemie and used in the fixed-bed reactors at SASOL contains about 5% wt. Cu. Work carried out by Linder and Papp [162] using XPS and ISS (Ion Scattering Spectroscopy) have shown that the degree of reduction of the Fe catalyst is strongly influenced by the amount of Cu that is added to the catalyst. They observed that the highest amount of Fe<sup>0</sup> (which gets converted to the active iron carbide phase during the FT reaction) in the surface of their Cu containing samples was obtained when 1 atomic% of Cu was added

When adding Cu above 1 %, they noticed a slight decrease in the metallic Fe (Fe<sup>0</sup>) content of the surface. They speculated that the decrease may be due to a decrease in dispersion of Fe and that this was as a result of sintering at higher Cu contents to bigger Fe agglomerates leading to a lower relative amount of Fe<sup>0</sup> measured on the surface. They went on to conclude that all their Cu containing samples should have a higher activity in the FT synthesis than the unpromoted Fe oxide catalyst and that those with  $\leq 1$  atomic% of Cu should have the highest activity.



Meanwhile work performed by O'Brein et al. [157] has shown that reduction of iron oxide using hydrogen is accelerated with increasing levels of copper promotion (2.6-5.0 atomic % relative to iron). They argued that the acceleration of the iron oxide reduction (with increasing levels of copper promotion) is in agreement with more nucleation sites being available with an increasing amount of copper.

From the findings given above, it is clear that the effect of copper loading is very much dependent on the experimental conditions used. Also, not much work has been reported on obtaining the optimum loading of Cu on Fe-based FTS catalysts.

The effects of Cu on Fe-based FTS catalysts can be summarized as follows:

- (i) Aids in the reduction of iron oxide
- (ii) Has an influence on the FTS and WGS activities
- (iii) Plays a small role in FTS product selectivity

#### **2.8.2.1 Use of indium as a chemical promoter for Fe-based catalysts**

Indium as a chemical promoter for Fe-based catalysts has been reported in the literature [163]. To the best of our knowledge it has not been used in the Fischer-Tropsch Synthesis. It has mainly been employed in reactions such as the selective catalytic reduction (SCR) of NO<sub>x</sub> using hydrocarbons [163-165].

## References

- [1] R.B. Anderson, *The Fischer-Tropsch Synthesis*, Academic Press, Orlando, 1984
- [2] T. Bromfield, *The effect of low-level sulfide addition on the performance of precipitated-iron Fischer-Tropsch catalysts*, PhD Thesis, University of the Witwatersrand, Johannesburg, 1997
- [3] G.C. Bond, *Catalysis by Metals*, Academic Press, London, 1962
- [4] L. Guzzi, *Stud. Surf. Sci. Catal. 64 Series: New Trends in CO Activation*, Elsevier, Amsterdam, (1991)
- [5] H.H. Storch, N. Golombic, R.B. Anderson, *The Fischer-Tropsch and related syntheses: including a summary of theoretical and applied contact catalysis*, John Wiley, New York (1951)
- [6] B.H. Davis, Final Report, *Technology development for iron Fischer-Tropsch catalysis*, Contract No. DE-AC22-94PC94055—13 (1999)
- [7] M.E. Dry, *Appl. Catal. A: Gen.* 138 (1996) 319
- [8] J.G. Price, *An investigation into novel bimetallic catalysts for use in the Fischer-Tropsch reaction*, PhD Thesis, University of the Witwatersrand, Johannesburg, 1994
- [9] M.E. Dry, *The Fischer-Tropsch Synthesis*, in *Catalysis Science and Technology*, J. R. Anderson, M. Boudart (Eds.) 1, Springer-Verlag, New York (1981) 159
- [10] E. Iglesia, *Stud. Surf. Sci. Catal.* 107 (1997) 153
- [11] M.E. Dry, *Appl. Catal. A: Gen.* 276 (2004) 1
- [12] M.E. Dry, *Catal. Today* 71 (2002) 227
- [13] G. Blyholder, D. Shihabi, W.V. Wyatt, R. Bartlett, *J. Catal.* 43 (1976) 43
- [14] G. Henrici-Olivé, S. Olivé, *J. Mol. Catal.* 3 (1977/78) 443
- [15] J.T. Kummer, P.H. Emmett, *J. Am. Chem. Soc.* 75 (1953) 5177
- [16] J.T. Kummer, H. H. Podgurski, W.B. Spencer, P.H. Emmett *J. Am. Chem. Soc.*, 73 (1951) 564
- [17] M. J. Overett, R. O. Hill, J. R. Moss, *Coord. Chem. Rev.* 206–207 (2000) 581
- [18] R. George, J.M. Andersen, J.R. Moss, *J. Organomet. Chem.* 505 (1995) 131
- [19] P.M. Maitlis, *J. Organomet. Chem.* 689 (2004) 436

- [20] P. Sabatier, J.B. Senderens, *C.R. Acad. Sci.* 134 (1902) 514
- [21] BASF, *German Patent* 293 (1913) 787
- [22] H. Pichler, *Adv. Catal.* 4 (1952) 271
- [23] <http://www.fischer-tropsch.org>
- [24] K. Khoabane, *Synthesis of nanostructured silica for use as a support for iron Fischer-Tropsch catalysts*, PhD Thesis, University of the Witwatersrand, Johannesburg, 2007
- [25] R.B. Anderson, in *Catalysis*, P.H. Emmet (Ed.), 4, Von Norstand–Reinhold, New Jersey, 1956
- [26] M.E. Dry, in *Applied Industrial Catalysis*, B.E. Leach (Ed.) 2, Academic Press, New York, 1983
- [27] K. Jalama, *Fischer Tropsch Synthesis over supported cobalt catalysts: Effect of ethanol addition, precursors and gold doping*, PhD Thesis, University of the Witwatersrand, Johannesburg, 2007
- [28] P.L. Spath, D.C. Dayton, *Preliminary Screening — Technical and Economic Assessment of Synthesis Gas to Fuels and Chemicals with Emphasis on the Potential for Biomass-Derived Syngas*, NREL/TP-510-34929 (2003) [available at [www.fischer-tropsch.org](http://www.fischer-tropsch.org)]
- [29] [http://www1.eere.energy.gov/biomass/printable\\_versions/catalytic\\_conversion](http://www1.eere.energy.gov/biomass/printable_versions/catalytic_conversion)
- [30] [http://en.wikipedia.org/wiki/Fischer-Tropsch\\_process](http://en.wikipedia.org/wiki/Fischer-Tropsch_process)
- [31] D.K. Rider, *Energy: Hydrocarbon Fuels and Chemical Resources*, John Wiley, New York, 1981
- [32] B. Jager, M.E. Dry, T. Shingles, A.P. Steynberg, *Catal. Lett.* 7 (1990) 293
- [33] P.D.F. Vernon, M.L.H. Green, A.K. Cheetham, A.T. Ashcroft, *Catal. Lett.* 6 (1990) 181
- [34] J. Abbott, B. Crewdson, *Oil & Gas J.* 100 (2002) 70
- [35] V.R. Choudhary, K.C. Mondal, A.S. Mamman, *J. Catal.* 233 (2005) 36
- [36] P.M. Biesheuvel, G.J. *AIChE J.* 49 (2003) 1827
- [37] G.P. Van der Laan, *Kinetics, Selectivity and Scale Up of the Fischer-Tropsch Synthesis*, PhD thesis, University of Groningen, The Netherlands, 1999
- [38] J.M. Fox, III, *Catal. Rev. Sci. Eng.* 35 (1993) 169

- [39] J.H. Gregor, *Catal. Lett.* 7 (1990) 317
- [40] S.C. Saxena, M. Rosen, D.N. Smith, J.A. Ruether, *Chem. Eng. Comm.*, 40 (1986) 97
- [41] M.E. Dry, *Catal. Today* 6 (1990) 183
- [42] A.A. Adesina, *Appl. Catal. A: Gen.* 138 (1996) 345
- [43] B.H. Davis, *Catal. Today* 71 (2002) 249
- [44] B. Jager, *Stud. Surf. Sci. Catal.* 107 (1997) 219
- [45] R.L. Espinoza, A. P. Steynberg, B. Jager, A. C. Vosloo, *Appl. Catal. A: Gen.* 186 (1999) 13
- [46] B. Jager, R. L. Espinoza, *Catal. Today* 23 (1995) 17
- [47] M.E. Dry, in *Studies in Surface Science and Catalysis: Fischer-Tropsch Technology*, A. Steynberg, M. Dry, (eds.), 152, Elsevier, New York, 2004
- [48] B.H. Weil, J.C. Lane, *The Technology of the Fischer-Tropsch Process*, Constable & Co. LTD, London, 1949
- [49] D.B. Bukur, X. Lang, *Ind. Eng. Chem. Res.* 38 (1999) 3270
- [50] E.M. Mokoena, *Synthesis and Use of Silica Materials as Supports for the Fischer-Tropsch Reaction*, PhD Thesis, University of the Witwatersrand, Johannesburg, 2005
- [51] K.G. Anderson, J. G. Ekerdt, *J. Catal.* 95 (1985) 602
- [52] H. Pichler, H. Schultz, *Chem. Ing. Techn.* 42 (1970) 1102
- [53] J.W. Thomas, W.J. Thomas, *Principles and Practice of Heterogeneous Catalysis*, VCH, New York, 1996
- [54] C.N. Satterfield, G.A. Huff, J.P. Longwell, *Ind. Eng. Chem. Process. Dev.*, 21,3 (1982) 466
- [55] R.J. Madon, W.F. Taylor, *J. Catal.* 69 (1981) 32
- [56] C.N. Mbileni, *Applications of mesostructured carbonaceous materials as supports for Fischer-Tropsch metal catalyst*, PhD Thesis, University of the Witwatersrand, Johannesburg, 2006
- [57] R.A. Dictor, A.T.J. Bell, *J. Catal.* 97 (1986) 121
- [58] R.J. Madon, S.C. Reyes, E. Iglesia, *J. Phys. Chem.* 95 (1991) 7795
- [59] V. Ponec, *Coal Science* 3 (1984) 1

- [60] C.N. Satterfield, G.A. Huff, *J. Catal.* 73 (1982) 187
- [61] G.A. Huff, C.N. Satterfield, *J. Catal.* 85 (1984) 370
- [62] E. Iglesia, S.C. Reyes, R.J. Madon, *J. Catal.* 129 (1991) 238
- [63] E.W. Kuipers, C. Scheper, J.H. Wilson, I.H. Vinkenburg, H. Oosterbeek, *J. Catal.* 158 (1996) 288
- [64] B. Shi, B.H. Davis, *Appl. Catal. A: Gen.* 277 (2004) 61
- [65] G.Y. Chai and J.L. Falconer, *J. Catal.* 93 (1985) 152
- [66] M.A. Vannice, *J. Catal.* 37 (1975) 449
- [67] M.A. Vannice, *J. Catal.* 50 (1977) 228
- [68] B.H. Davis, Final Report, *Technology Development for Iron Fischer-Tropsch Catalysts*, Contract No. DE-AC22-91PC90056, 1999
- [69] M. Jonardanarao, *Ind. Eng. Chem. Res.* 29 (1990) 1735
- [70] V.U.S. Rao, G.J. Stiegel, G.J. Cinquegrane, R.D. Strvastava, *Fuel Proc. Tech.* 30 (1992) 83
- [71] M.E. Dry, *Appl. Catal. A: Gen.* 189 (1999) 185
- [72] C. Bartholomew, *Appl. Catal. A: Gen.* 212 (2001) 17
- [73] N. Sirimanothan, H. H. Hamdeh, Y. Zhang, B. H. Davis, *Catal. Lett.* 82 (2002) 181
- [74] D.B. Bukur, W.-P. Ma, V. Carreto-Vazquez, *Topics Catal.* 32 (2005) 135
- [75] H. Schulz, T. Riedel, G. Schaub, *Topics. Catal.* 32 ( 2005) 117
- [76] S.A. Eliason, C.H. Bartholomew, *Appl. Catal. A: Gen.* 186 (1999) 229
- [77] L.D. Mansker, Y. Jin, D. B. Bukur , A. K. Datye, *Appl. Catal. A: Gen.* 186 (1999) 277
- [78] R.J. O'Brien, L. Xu, R.L. Spicer, S. Bao, D.R. Milburn, B.H. Davis *Catal. Today* 36 (1997) 325
- [79] D.B. Bukur, K. Okabe, M.P. Rosynek, C. Li, D. Wang, K.R.P.M. Rao, G.P. Huffman, *J. Catal.* 155 (1995) 353
- [80] D.B. Bukur, M. Koranne, X. Lang, K.R.P.M. Rao, G.P. Huffman, *Appl. Catal. A: Gen.* 126 (1995) 85
- [81] D.J. Duvenhage, N.J. Coville, *Appl. Catal. A: Gen.* 298 (2006) 211
- [82] T.C. Bromfield, N.J. Coville, *Appl. Catal. A: Gen.* 186 (1999) 245

- [83] T.C. Bromfield, N.J. Coville, *Appl. Surf. Sci.*, 119 (1997) 19
- [84] M.C. Bahome, L.L. Jewell, D. Hilderbrandt, D. Glasser, N.J. Coville, *Appl. Catal. A: Gen.* 287 (2005) 60
- [85] B.H. Davis, E. Iglesia, *Technology Development for Iron and Cobalt Fischer-Tropsch Catalysis*, Final Report, Contract No. DE-FC26-98FT40308, University of Kentucky Research Foundation, Lexington, 2002
- [86] D.B. Bukur, L. Nowicki, X. Lang, *Energy and Fuels* 9 (1995) 620
- [87] R.J. O'Brien, L. Xu, R.L. Spicer, B.H. Davis, *Energy and Fuels* 10 (1996) 921
- [88] D.J. Dwyer, G.A. Somorjai, *J. Catal.* 52 (1978) 291
- [89] J.A. Amelse, J.B. Butt, L.J. Schwartz, *J. Phys. Chem.* 82 (1978) 558
- [90] G.B. Raupp, W.N. Delgass, *J. Catal.*, 58 (1979) 348
- [91] H. Jung, W.J. Thomson, *J. Catal.* 134 (1992) 654
- [92] D.J. Dwyer, J.H. Hardenbergh, *J. Catal.* 87 (1984) 66
- [93] K.R.P.M. Rao, F.E. Huggins, V. Mahajan, G.P. Huffman, V.U.S. Rao, B.L. Bhatt, D.B. Bukur, B.H. Davis, R.J. O'Brien, *Top. Catal.* 2 (1995) 71
- [94] E.S. Lox, G.B. Marin, E. de Grave, P. Bussière, *Appl. Catal.* 40 (1988) 197
- [95] H.-B. Zhang, G.L. Schrader, *J. Catal.* 95 (1985) 325
- [96] F.B. Blanchard, J.P. Raymond, B. Pommier, S.J. Teichner, *J. Mol. Catal.* 17 (1982) 171
- [97] J.P. Raymond, P. Meriadeau, S.J. Teichner, *J. Catal.* 75 (1982) 39
- [98] F. Blanchard, J.P. Raymond, B. Pommier, S.J. Teichner, *J. Mol. Catal.* 17 (1982) 171
- [99] S. Soled, E. Iglesia, R.A. Fiato, *Catal. Lett.* 7 (1990) 271
- [100] C.S. Kuivila, P.C. Stair, J.B. Butt, *J. Catal.* 118 (1989) 299
- [101] J.B. Butt, *Catal. Lett.* 7 (1990) 61
- [102] D.J. Duvenhage, R.L. Espinoza, N.J. Coville, *Stud. Surf. Sci. Catal.* 88 (1994) 351
- [103] G.B. Raupp, W.N. Delgass, *J. Catal.* 58 (1979) 348
- [104] J.A. Amelse, L.H. Schwartz, J.B. Butt, *J. Catal.* 72 (1981) 95
- [105] M.D. Shroff, D.S. Kalakkad, K.E. Coulter, S.D. Kohler, M.S. Harrington, N.B. Jackson, A.G. Sault, A.K. Datye, *J. Catal.* 156 (1995) 185

- [106] J.W. Niemantsverdriet, A.M. van der Kraan, W.L. van Dijk, H.S. van der Baan, *J. Phys. Chem.* 84 (1980) 3363
- [107] J.W. Niemantsverdriet, A.M. van der Kraan, *J. Catal.* 72 (1981) 375
- [108] D.S. Kalakkad, M.D. Shroff, S.D. Köhler, N.B. Jackson, A.K. Datye, *Appl. Catal. A: Gen.* 133 (1995) 335
- [109] D.B. Bukur, L. Nowicki, R.K. Manne, X. Lang, *J. Catal.* 155 (1995) 366
- [110] J.T. Kummer, T.W. Dewitt, E.H. Emmet, *J. Am. Chem. Soc.* 70 (1948) 3632
- [111] D.M. Stockwell, D. Bianchi, C.O. Bennet, *J. Catal.* 113 (1988) 13
- [112] J.A. Amelse, J.B. Butt, L.H. Schwartz, *J. Phys. Chem.* 82 (1978) 558
- [113] M.E. Dry, J.A.K. du Plessis, G.M. Leuteritz, *J. Catal.* 6 (1966) 194
- [113] A. Khodakov, A. Griboval-Constant, R. Bechara, V.L. Zholobenko, *J. Catal.* 206 (2002) 230
- [114] G.H. Haddad, B. Chenand, J.G. Goodwin, *J. Catal.* 160 (1996) 43
- [115] M. Kraun, M. Baerns, *Appl. Catal. A: Gen.* 186 (1999) 189
- [116] R.C. Reuel, C.H. Bartholomew, *J. Catal.* 85 (1984) 63
- [117] E. Iglesia, S.L. Soled, R.A. Fiato, G.H. Via, *J. Catal.* 143 (1993) 345
- [118] E. Iglesia, S.L. Soled, R.A. Fiato, *J. Catal.* 137 (1992) 212
- [119] E. Iglesia, *Appl. Catal.* 161 (1997) 59
- [120] R. Bechara, D. Balloy, D. Vanhove, *Appl. Catal. A: Gen.* 207 (2001) 343
- [121] D. Schanke, A.M. Hillmen, E. Bergene, K. Kinnari, E. Rytter, E. Ådnes, A. Holmen, *Energy and Fuels* 10 (1996) 867
- [122] A. Holmen, D. Schanke, S. Vada, E.A. Blekkan, A.M. Hillmen, A. Hoff, *J. Catal.* 156 (1995) 85
- [123] F. Morales, E. de Smit, F.M.F. de Groot, T. Visser, B.M. Weckhuysen, *J. Catal.* 246 (2007) 91
- [124] F.B. Noronha, A. Frydman, D.A.G. Aranda, C. Perez, R.R. Soares, B. Morawek, D. Castner, C.T. Campbell, R. Frety, M. Schmal, *Catal. Today* 28 (1996) 147
- [125] L.A. Bruce, M. Hoang, A.E. Hughes, T.W. Turney, *Appl. Catal. A: Gen.* 100 (1993) 51
- [126] J. van der Loosdrecht, M. van der Haar, A.M. van der Kraan, A.J. van Dillen, J.W. Geus, *Appl. Catal.* 150 (1997) 365

- [127] M.K. Niemelä, A.O.I. Krause, T. Vaara, J. Lathinen, *Top. Catal.* 2 (1995) 45
- [128] M.K. Niemelä, A.O.I. Krause, T. Vaara, J.J. Kiviaho, M.K.O. Reikainen, *Appl. Catal. A. Gen.* 147 (1996) 325
- [129] G.S. Sewell, E. van Steen, C.T. O'Connor, *Catal. Lett.* 37 (1996) 255
- [130] R.J. O'Brien, L. Xu, S. Bao, A. Rajee, B.H. Davis, *Appl. Catal. A: Gen.* 196 (2000) 173
- [131] B. Jongsomjit, T. Wongsalee, P. Praserthdam, *Mater. Chem. Phys.* 97 (2006) 343
- [132] J. Eilers, S.A. Posthuma, S.T. Sie, *Catal. Lett.* 37 (1997) 253
- [133] S. Bessel, *Appl. Catal. A: Gen.* 96 (1993) 253
- [134] V.U.S. Rao, R.J. Gormley, *Catal. Today* 6 (1990) 207
- [135] D. Yin, W. Li, W. Yang, H. Xiang, Y. Sun, B. Zhong, S. Peng, *Microporous and Mesoporous Mat.* 47 (2001) 15
- [136] H.-J. Jung, P.L. Walker Jr., M.A. Vannice, *J. Catal.* 75 (1982) 416
- [137] E. van Steen, F.F. Prinsloo, *Catal. Today* 71 (2002) 327
- [138] G.L. Bezemer, J.H. Bitter, H.P.C.E. Kuipers, H. Oosterbeek, J.E. Holewijn, X. Xu, F. Kaptein, A.J. van Dillen, K.P. de Jong, *J. Am. Chem. Soc.* 128 (2006) 3956
- [139] Y. Yang, H. Xiang, L. Tian, H. Wang, C. Zhang, Z. Tao, Y. Xu, B. Zhong, Y. Li, *Appl. Catal. A: Gen.* 284 (2005) 105
- [140] H. Dlamini, T. Motjope, G. Joost, G. ter Stege, M. Mdleleni, *Catal. Lett.* 78 (2002) 201
- [141] R. Zhao, J.G. Goodwin Jr., K. Jothimurugesan, S.K. Gangwal, J.J. Spivey, *Ind. Eng. Chem. Res.* 40 (2001) 1065
- [142] K. Sudsakorn, J.G. Goodwin Jr. K. Jothimurugesan, A.A. Adeyiga, *Ind. Eng. Chem. Res.* 40 (2001) 4778
- [143] H.N. Pham, A. Viergutz, R. Gormley, A.K. Datye, *Powder Technol.* 110 (2000) 196
- [144] D.B. Bukur, X. Lang, D. Mukesh, W.H. Zimmerman, M.P. Rosynek, C. Li, *Ind. Eng. Chem. Res.* 29 (1990) 1588
- [145] K. Jothimurugesan, J.G. Goodwin, S.K. Gangwal, J.J. Spivey, *Catal. Today* 58 (2000) 335



- [146] J.L. Rankins, C.H. Bartholomew, *J. Catal.* 100 (1986) 533
- [147] S.L. Soled, E. Iglesia, S. Miseco, B.A. DeRites, R.A. Fiato, *Top. Catal.* 2 (1995) 193
- [148] K.R.P.M Rao, F.E. Huggins, V. Mahajan, G.P. Huffman, D.B. Bukur, V.U.S. Rao, *Hyperfine Interactions* 93 (1994) 1751
- [149] Y. Jin, A.K. Datye, *J. Catal.* 196 (2000) 8
- [150] M.A. Vannice, *J. Catal.* 37 (1975) 462
- [151] A.F.H. Wielers, A.J.H.M. Kock, C.E.A. Hop, J.W. Geus, A.M. van der Kraan, *J. Catal.* 117 (1989) 1
- [152] M.V. Cagnoli, S.G. Marchetti, N.G. Gallegos, M. Alvarez, R.C. Mercader, A.A. Yeramin, *J. Catal.* 123 (1990) 21
- [153] C.R.F. Lund, J.A. Dumensic, *J. Phys. Chem.* 85 (1981) 3175
- [154] S. Yuen, Y. Chen, J.E. Dumesic, *J. Phys. Chem.* 86 (1982) 3022
- [155] K.W. Jun, H.S. Roh, K.S. Kim, J.S. Ryu, K.W. Lee, *Appl. Catal. A: Gen.* 259 (2004) 221
- [156] M. Luo, R.J. O'Brien, S. Bao, B.H. Davis, *Appl. Catal. A: Gen.* 239 (2003) 111
- [157] R. J. O'Brien, L. Xu, R. L. Spicer, S. Bao, D. R. Milburn, B. H. Davis, *Catal. Today* 36 (1997) 325
- [158] D.B. Bukur, D. Mukesh, S.A. Patel, *Ind. Eng. Chem. Res.* 29 (1990) 194
- [159] D.G. Miller, M. Moskovits, *J. Phys. Chem.* 92 (1988) 6081
- [160] K.R.P.M. Rao, F.E. Huggins, G.P. Huffman, R.J. Gormly, R.J. O'Brein, B.H. Davis, *Energy and Fuels* 10 (1996) 546
- [161] I.E. Wachs, D.J. Dwyer, E. Iglesia, *Appl. Catal.* 12 (1984) 201
- [162] U. Lindner, H. Papp, *Appl. Surf. Sci.* 32 (1988) 75
- [163] X. Wang, T. Zhang, X. Sun, W. Guan, D. Liang, L. Lin, *Appl. Catal. B: Environmental* 24 (2000) 169
- [164] R. Serra, M. J. Vecchiotti, E. Miró, A. Boix, *Catal. Today* 133–135 (2008) 480
- [165] X. Wang, X. Zhao, J. Shen, X. Sun, T. Zhang, L. Lin, *Phys. Chem. Chem. Phys.* 4 (2002) 2846
- [166] M.C. Bahome, *Synthesis and use of carbon nanotubes as a support for the Fischer-Tropsch Synthesis*, PhD Thesis, University of the Witwatersrand, Johannesburg, 2007

# Chapter 3

## Experimental

### *3.1 Catalyst preparation*

All the catalysts were prepared using the co-precipitation method [1, 2].  $\text{Fe}(\text{NO}_3)_3 \cdot 9\text{H}_2\text{O}$ ,  $\text{Cu}(\text{NO}_3)_2 \cdot 3\text{H}_2\text{O}$ ,  $\text{In}(\text{NO}_3)_3$  and  $\text{KNO}_3$  were used as precursors, while the ammonia solution (25%  $\text{NH}_3$ ) was used as a precipitating agent (All were purchased from MERCK Chemicals (PTY) LTD).  $\text{SiO}_2$  (purchased from Davisil with BET surface area =  $303 \text{ m}^2/\text{g}$  and pore volume =  $1.05 \text{ cm}^3/\text{g}$ ) in form of a white powder was also employed as part of the reagents.

The nitrate precursors were dissolved in distilled water. This was followed by stirring using an overhead stirrer. While stirring,  $\text{SiO}_2$  was added (when needed for the preparation of catalysts that contained  $\text{SiO}_2$ ). The ammonia solution was then added dropwise to produce a brown slurry. The resultant slurry (precipitate) was stirred for 15 minutes and the final pH (pH = 8-9) was recorded. The slurry was dried at  $120^\circ\text{C}$  overnight to give a brown solid. The dried slurry was then calcined for 4 hours at  $350^\circ\text{C}$ . The calcined catalyst was ready for analysis using  $\text{N}_2$  physisorption, XRF, XPS, XRD, TPR, DRIFTS and FTS reactor studies.

## ***3.2 Catalyst characterization***

### **3.2.1 X-Ray Fluorescence (XRF) spectroscopy**

The XRF experiments were carried out using a PW2404 wavelength dispersive XRF spectrometer from Panalytical. A Rh target tube was used to generate the X-Rays with  $K\alpha = 24.9$  and  $K\beta = 22$ . The samples were mixed with polyvinyl glue (Mowiol) and were pressed to pellets using 10 MPa pressure prior to analysis.

### **3.2.2 N<sub>2</sub> Physisorption**

N<sub>2</sub> physisorption was employed for surface-area determination and pore volume measurements of the calcined catalysts. It is noted that the surface areas could change significantly following various pretreatments and could be different from those determined after calcination. For consistency and comparison purposes, surface areas reported in this thesis were determined on only calcined samples. The samples were degassed using N<sub>2</sub> at 150 °C for 2 hours before measurement. N<sub>2</sub> adsorption-desorption isotherms at N<sub>2</sub> boiling point (-196 °C) were measured on a Micromeritics TRISTAR 3000 analyzer (Fig. 3.1). The surface areas were determined by the Brunauer-Emmett-Teller (BET) method.



**Figure 3.1** The TRISTAR 3000 analyzer

### **3.2.3 Temperature programmed reduction (TPR)**

Temperature programmed reduction (TPR) was used to assess the reducibility of the catalysts. The home-built apparatus used (Fig. 3.2) was the same as that used by Duvenhage [3], Mokoena [4] and Bahome [5].



**Figure 3.2** Experimental set-up for TPR measurements

The catalyst sample was first weighed before being loaded into a U-shaped quartz tube. Typical mass values weighed were *ca.* 20 mg. A glass wool plug was inserted into the U-tube before the catalyst was added. This was to circumvent any of the catalyst material being carried into the reactor outlet. The ends of the U-tube were then attached to the gas-inlet and outlet points of the apparatus.

The flow rate of the affluent gas stream was kept at 50 ml/min and a thermal conductivity detector (TCD) was used to monitor the concentration variation of the gas stream. The TCD output was calibrated based upon 100% reducibility of Ag<sub>2</sub>O powder.

For CO TPR measurements the temperature was ramped from room temperature to 800°C under a flow of 10% CO balanced in Helium. For the H<sub>2</sub> TPR measurements the temperature was ramped from room temperature to 900 °C under a flow of 5% H<sub>2</sub> balanced in Argon. The temperature of the sample was monitored by a thermocouple placed in the catalyst bed.

### 3.2.4 Diffuse Reflectance Infrared Fourier Transform (DRIFT) Spectroscopy

A Bruker Tensor 27 infrared spectrometer fitted with a Harrick Praying Mantis Diffuse Reflectance accessory was employed. Typically 50 mg of the catalyst was loaded into the DRIFTS cell fitted with ZnSe windows (Fig. 3.3).

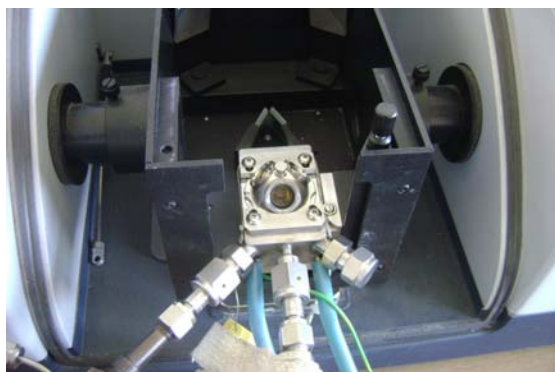


**Figure 3.3** DRIFTS cell with ZnSe windows

The cell was equipped with a heating system that allowed operation under different temperatures and pressures. Spectra were collected at a resolution of  $4\text{ cm}^{-1}$  and an average of 64 scans were employed during the measurements. Gases were led into the cell using a homemade gas manifold (Fig. 3.4).



**Figure 3.4** Gas manifold for the introduction of gases into the DRIFTS cell

### **3.2.5 X-Ray Diffraction (XRD) measurements**

Powder samples were loaded on a sample holder and their diffraction patterns were recorded from 5 to 90°  $2\theta$  on a Bruker D8 X-Ray diffractometer using monochromatized Cu  $K_{\alpha}$  radiation (40 kV, 40 mA). The Bruker D8 X-Ray diffractometer employed for carrying out the measurements is shown below (Fig. 3.5).



**Figure 3.5** The Bruker D8 X-Ray diffractometer

Typically a diffraction pattern as illustrated in Fig. 3.6 was obtained after XRD analysis. From this pattern the iron oxide phase was identified using the reported diffraction patterns in the *Diffrac<sup>plus</sup>* evaluation package with the aid of the EVA (V11.0) software package. It is to be noted that this was done for all the catalysts employed in this thesis and the only phase identified after calcination was the hematite ( $\text{Fe}_2\text{O}_3$ ) phase.



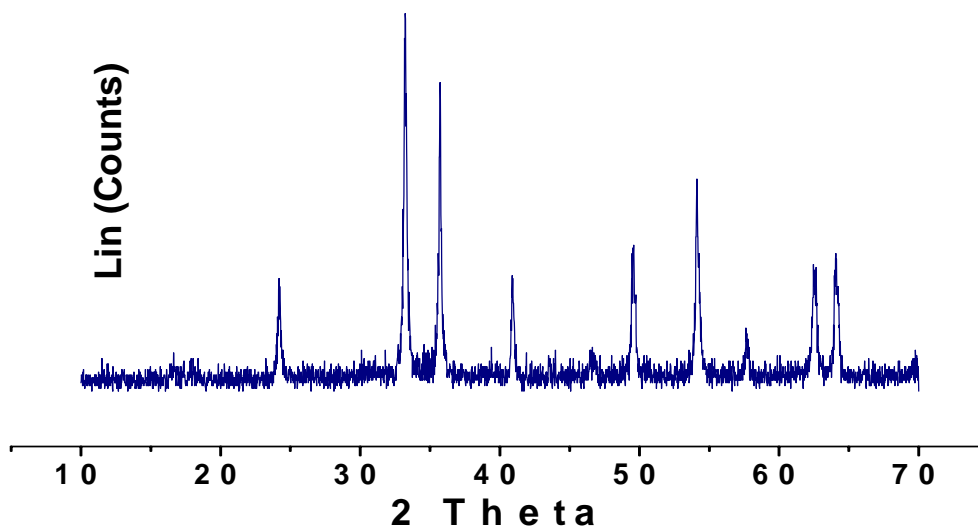


**Figure 3.6** Diffraction pattern obtained after the XRD measurement of Fe<sub>2</sub>O<sub>3</sub>

Rietveld refinement was also employed to estimate the average crystallite size of Fe<sub>2</sub>O<sub>3</sub>. During Rietveld refinement the diffraction peaks were fitted using mathematical functions (Gaussian, Lorentzian and Pearson functions). The idea was to try and minimize the differences between the fitted curve and the experimental diffraction pattern. A fit was deemed excellent, if the difference curve between the observed and calculated curves was minimized and revealed as a straight line as illustrated in Fig. 3.7b. The average crystallite size was estimated using the fit and mathematical equations within the EVA software package.

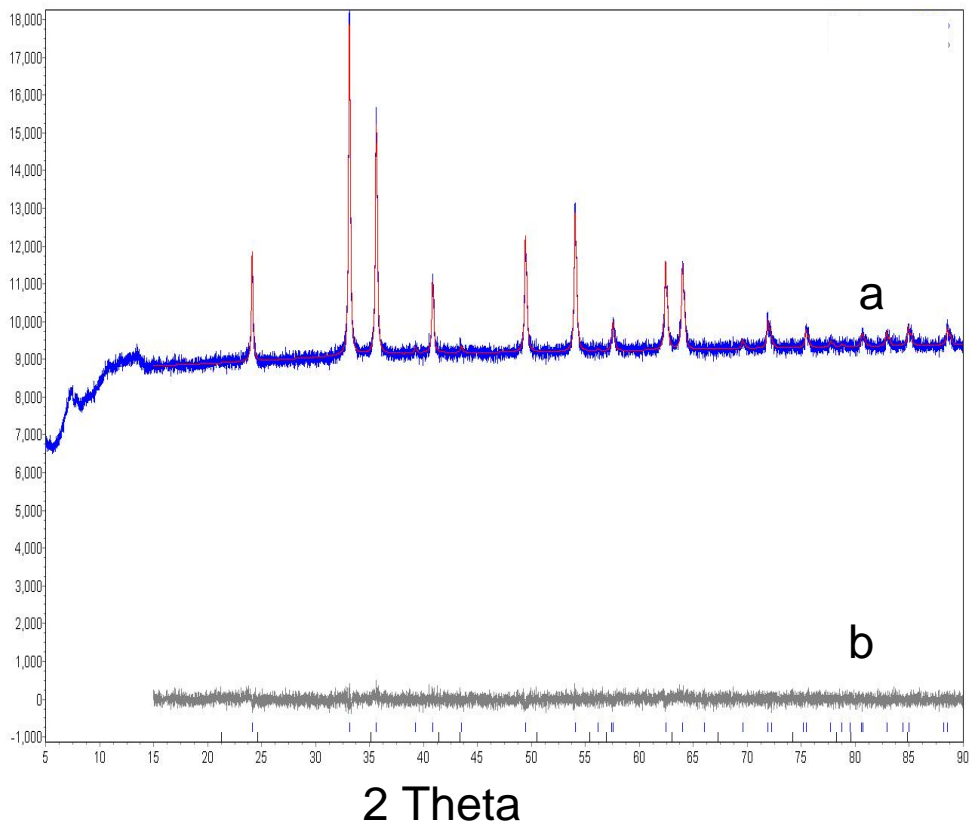


**Figure 3.7** Fitting of the experimental diffraction pattern (a) blue line represents the experimental pattern and red line is the fitted curve (b) difference curve produced after fitting the experimental diffraction pattern

### 3.2.6 X-Ray Photoelectron Spectroscopy (XPS)

The surface analysis of all the catalysts was performed using the XPS instrument based at the University of Cardiff in Wales, United Kingdom. The AXIS Ultra<sup>DLD</sup> manufactured by KRATOS Analytical (A Shimadzu Group Company) was employed and the set-up is illustrated below (Fig. 3.8).

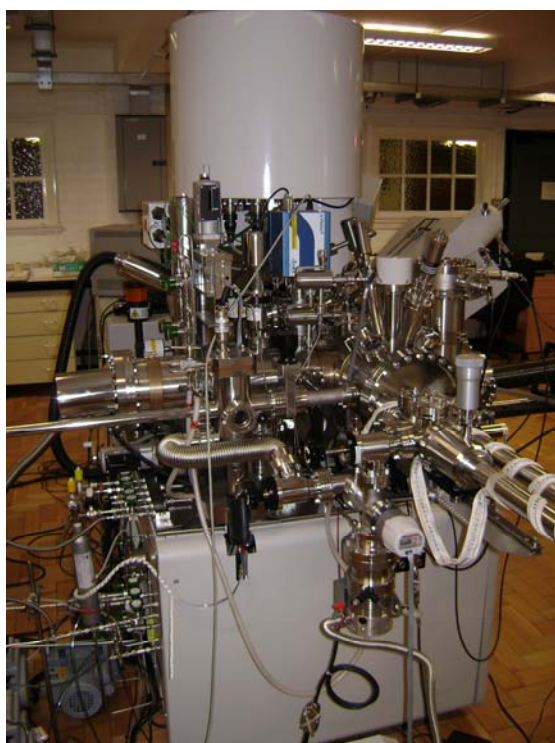


**Figure 3.8** The AXIS UltraDLD XPS instrument

The samples were placed on a stainless steel bar as depicted in Fig. 3.9 below and were transferred into the analysis chamber of the XPS instrument.

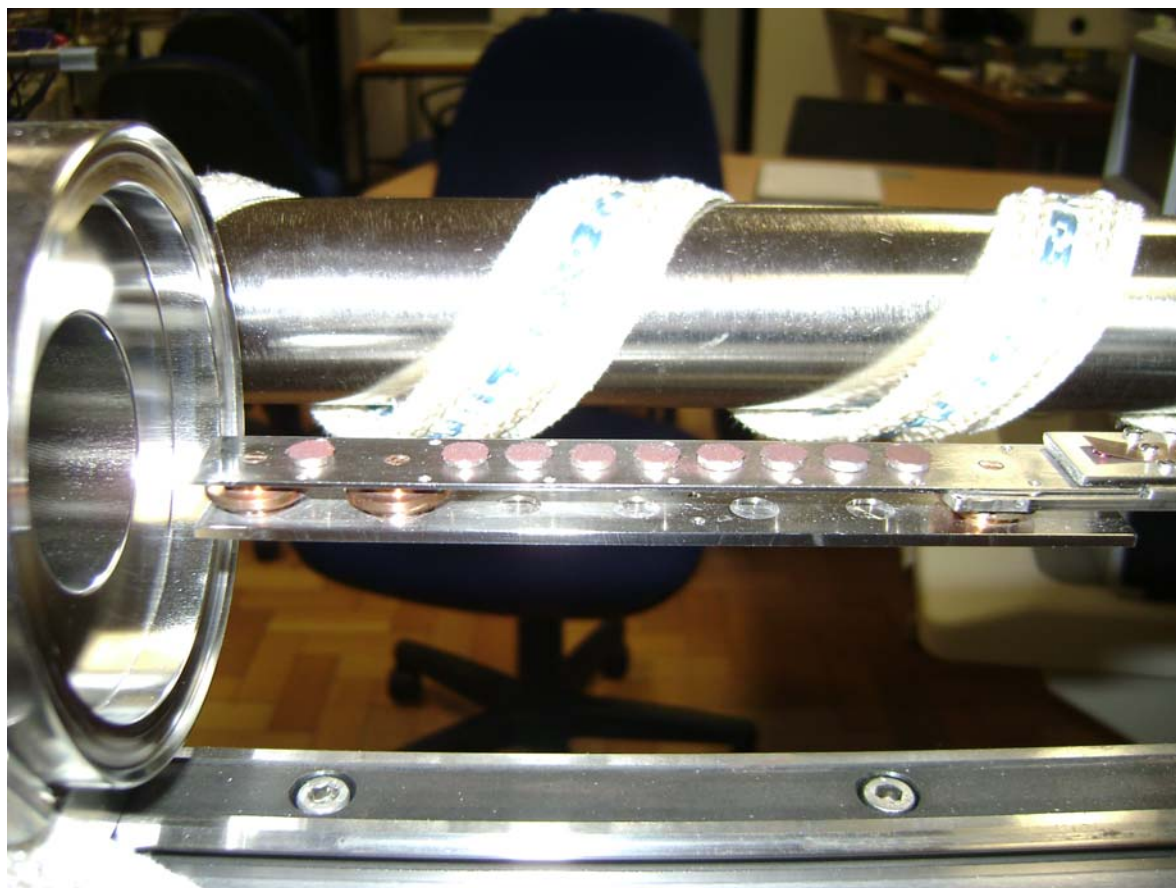


**Figure 3.9** The stainless steel bar showing the mounted catalysts ready for XPS analysis

### ***3.3 Catalytic evaluation***

#### **3.3.1 FTS reactor studies**

##### **3.3.1.1 Gases**

All gases used were supplied by AFROX (African Oxygen) Ltd. The gas used for catalyst reduction prior to the FT synthesis was an Ultra High Purity (UHP) grade Carbon monoxide gas (99.97 % purity) and only this gas was used for all the reduction reactions. Gas cylinders containing H<sub>2</sub>/CO/N<sub>2</sub> mixtures (60.2 %/29.6 %/10.2 % v/v) were used to supply the reactant gas stream to the catalyst. N<sub>2</sub> was used as an internal standard in order to ensure accurate mass balances.

##### **3.3.1.2 Catalyst reactor setup**

The fixed bed reactor system is shown in Fig. 3.10 and was used for all the FT reactions. It consisted of a 1/2" Swagelok stainless steel pipe and this served as the reactor. The reactor was placed into a heating jacket to maintain a constant temperature profile across it and inside the reactor a 1/4" Swagelok stainless steel pipe was placed. Quartz wool was placed on top of this 1/4" pipe so that the catalyst bed could rest on it. The 1/4" pipe had an opening at the bottom for the ejection of liquid and wax products into the traps.

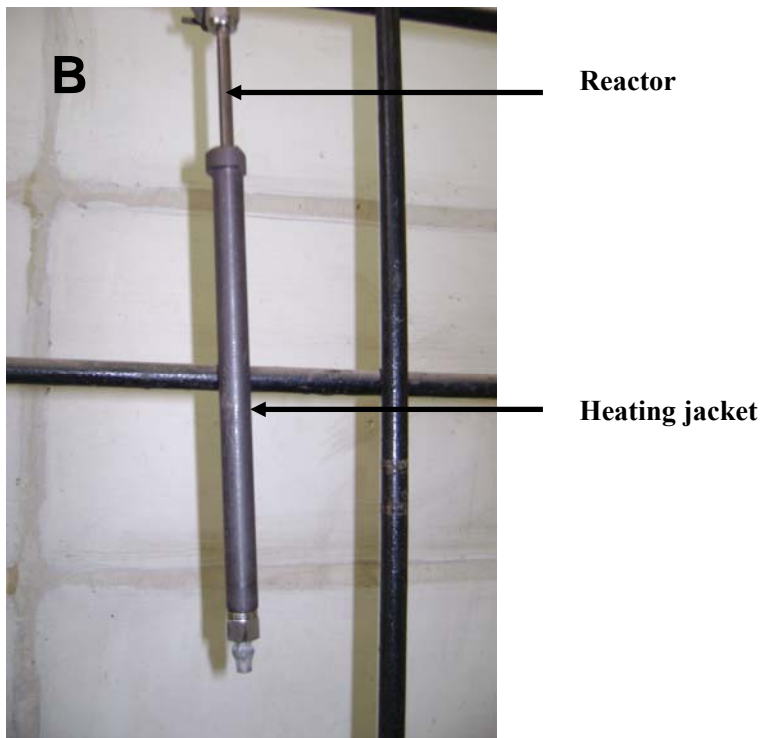
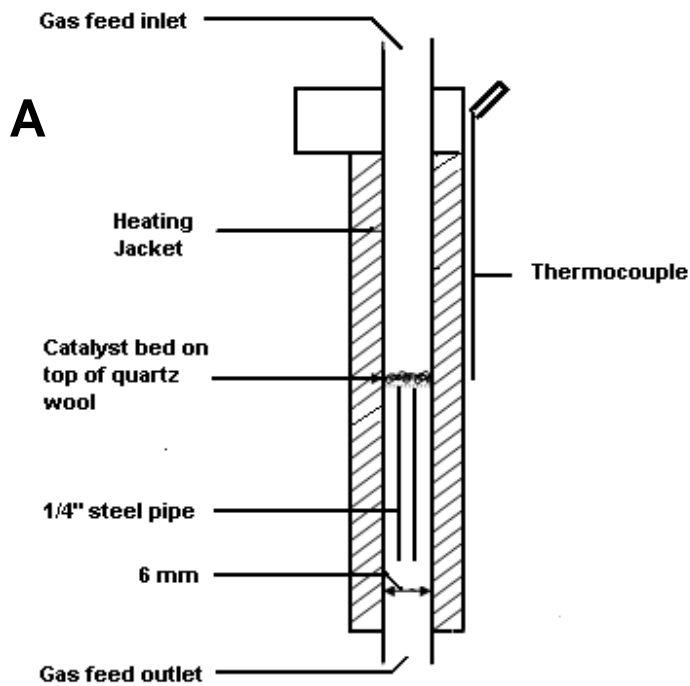


**Figure 3.10** The fixed bed reactor made from a  $\frac{1}{2}$ " Swagelok stainless steel pipe.  
 A = Sketch portrait; B = Digital portrait

All gas lines after the reactor were kept at 150 °C as shown in Fig. 3.12 and a hot trap (Fig. 3.11) placed immediately after the reactor was held at this temperature in order to collect wax. A second trap kept at ambient temperature was used to collect the oil and water mixture. The flow rate was controlled using a needle valve and measured by a means of a bubble meter.

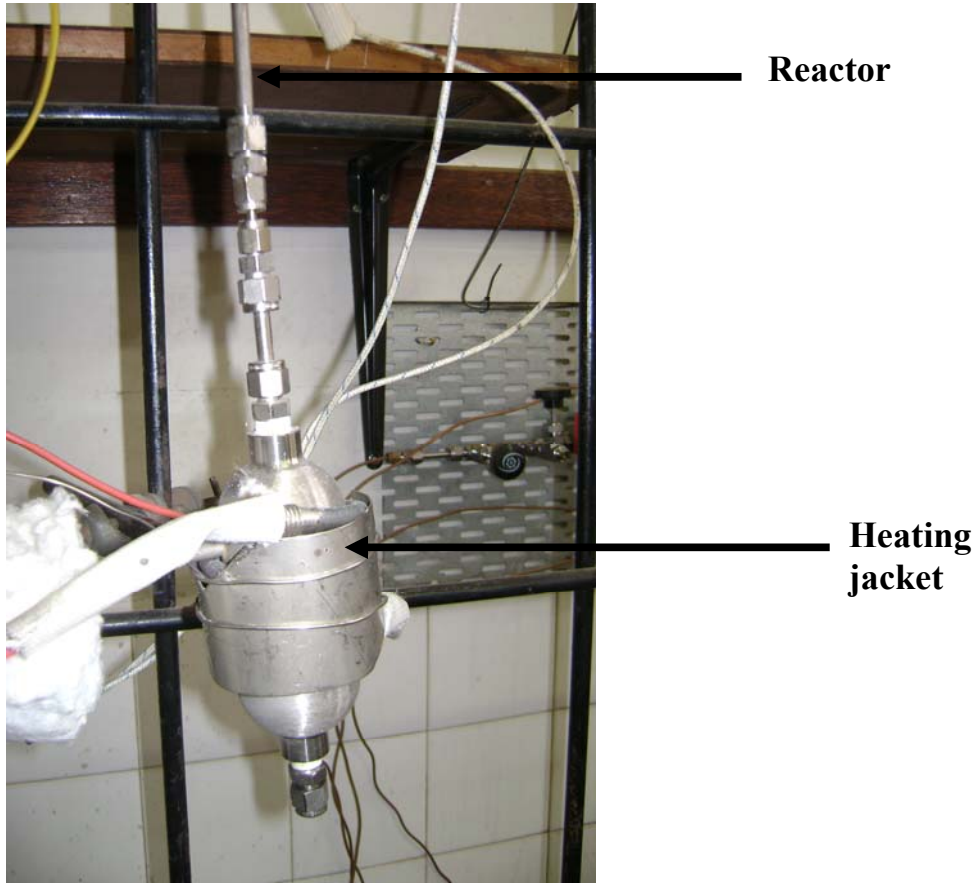


**Figure 3.11** The hot trap placed in a heating jacket, both situated below the reactor

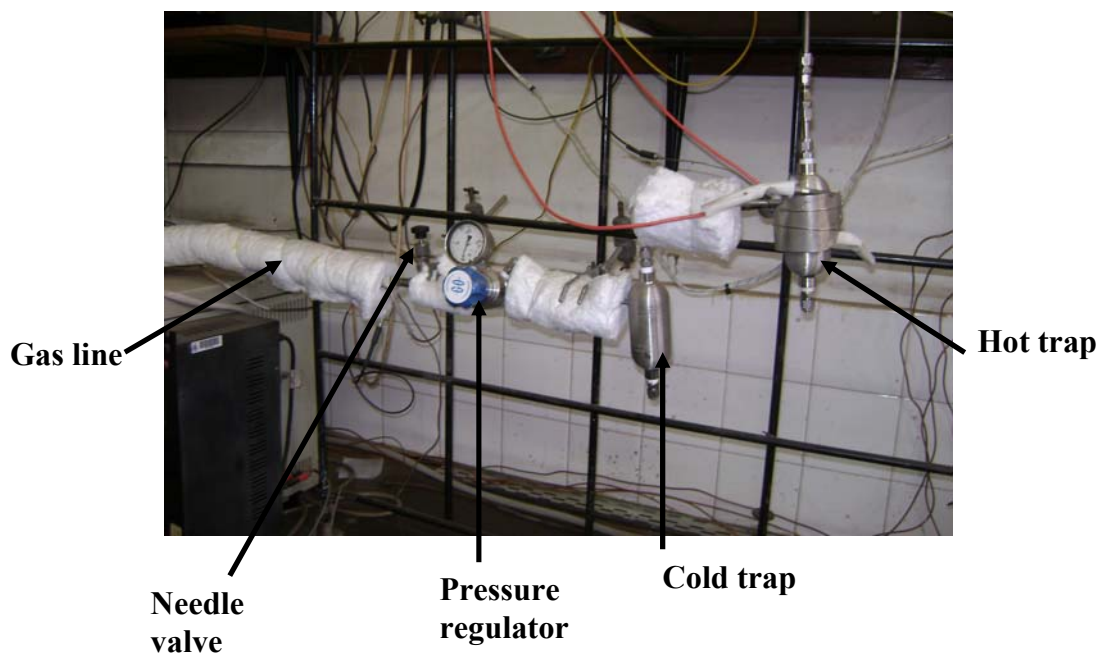


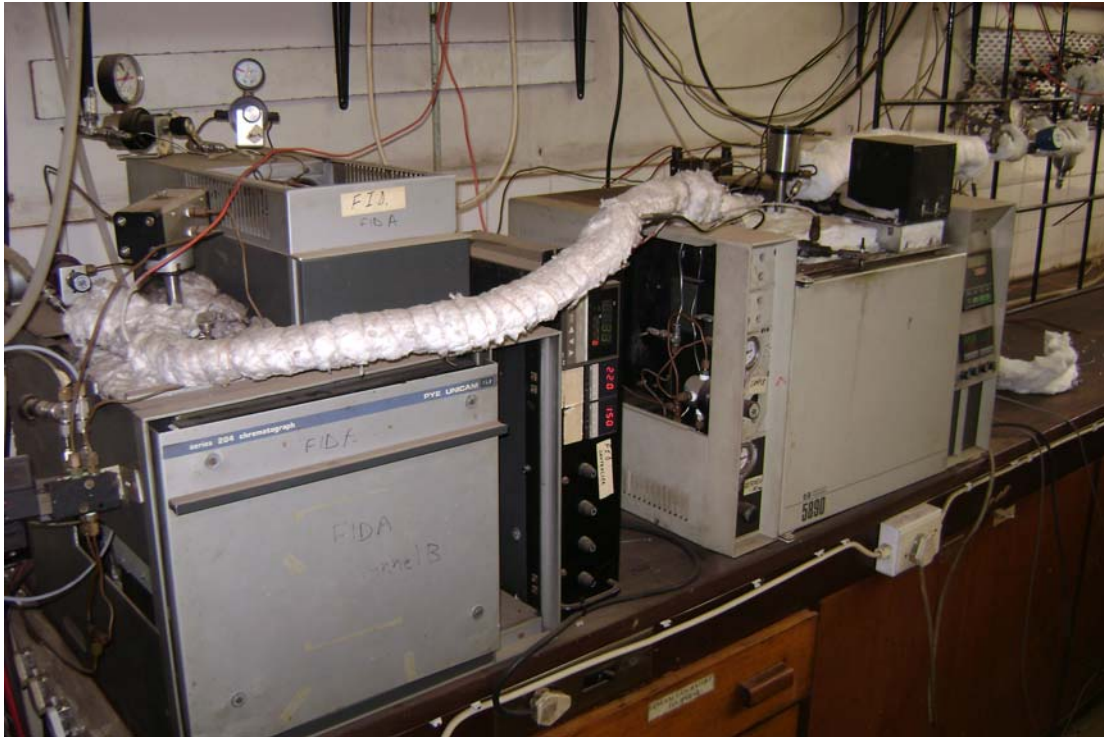
**Figure 3.12** Traps, pressure regulator, needle valve and gas line after reactor

Both the collected wax and liquid products were decanted and were analysed using an offline gas chromatograph (G.C.). The gaseous stream which was not collected in the hot and cold traps was analysed online using two GCs and both of them are depicted in Fig. 3.13. Table 3.1 below illustrates the instrumental characteristics for the GCs used [6] and an overview of the detailed schematic representation of the reactor setup is depicted in Fig 3.14.

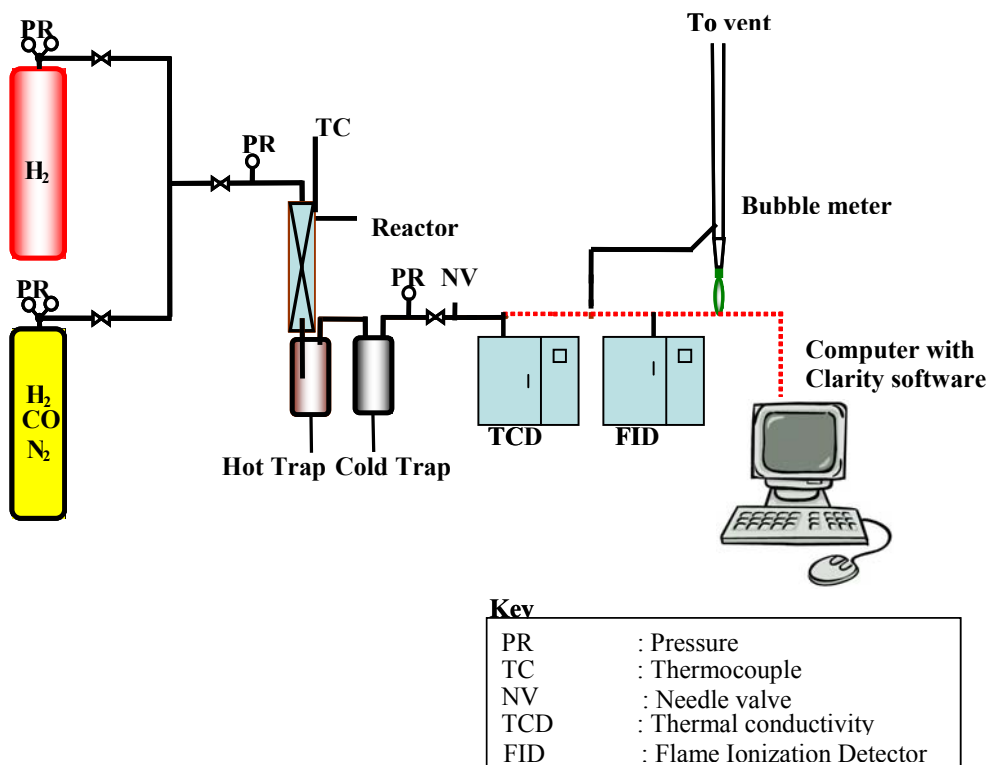


Table 3.1 Characteristics of the GCs employed

<b>Online GC</b>	
Make	<i>PYE Unicam (Series 204)</i>
Column type	<i>Packed, stainless steel, 2m x 2.2mm, O.D = 1/8"</i>
Stationary phase	<i>Carbosieve S-II, 60-80 mesh</i>
Detector	<i>Thermal conductivity detector (TCD)</i>
<b>Online GC</b>	
Make	<i>Hewlett Packard 5890</i>
Column type	<i>Packed, stainless steel, 1.5 m x 2.2 mm, O.D = 1/8"</i>
Stationary phase	<i>ZB-5, 80/100 mesh</i>
Detector	<i>Flame ionization detector (FID)</i>
<b>Offline GC</b>	
Make	<i>Varian 3700</i>
Column type	<i>30 m x 5 <math>\mu</math>FT, O.D. = 0.53 mm</i>
Stationary phase	<i>ZB-1</i>
Detector	<i>Flame ionization detector (FID)</i>



**Figure 3.13** GC on the left fitted with an FID detector and the one on the right fitted with a TCD detector



**Figure 3.14** Schematic representation of the reactor setup

### 3.3.1.3 Activity measurement of catalysts

Catalyst (0.1 g) was added to the reactor and reduced in situ at 350 °C for 20-24 hours under a stream of CO (2 bar pressure, 12 ml/min). After reduction, the temperature was decreased to room temperature. Synthesis gas was introduced and the pressure was gradually increased to 10 bar. The temperature was then ramped to 200°C for 40 minutes and thereafter, ramped from 200 °C to 275 °C for a period of 1 hour. The FTS reaction was then carried out at 275°C for a period of 140 hours

#### 3.3.1.4. Product analysis

The analysis of the product spectrum was divided into two parts. The first part being the online analysis of the gaseous product stream using two GCs. The second part being that of the analysis of the liquid (oil and water) and wax products using an offline GC.

For the online analysis, the two GCs employed were respectively equipped with a thermal conductivity detector (TCD) and a flame ionization detector (FID). The TCD was used to analyze H<sub>2</sub>, N<sub>2</sub>, CO, CH<sub>4</sub>, CO<sub>2</sub> whereas the FID was mainly employed for the analysis of hydrocarbons, primarily C<sub>1</sub>-C<sub>8</sub>.

Prior to the gas product analyses, the two online gas chromatographs (GC) were calibrated using a gas mixture of a known concentration. The gas mixtures employed were 20.6 % H<sub>2</sub>/20.3 % N<sub>2</sub>/20.3 % CO/19.1 % CH<sub>4</sub>/19.7 % CO<sub>2</sub> (v/v) and 2.5 % CH<sub>4</sub>/0.20% C<sub>2</sub>H<sub>4</sub>/0.50 % C<sub>2</sub>H<sub>6</sub>/10 % CO/5 % CO<sub>2</sub>/81 % Ar. Syngas (10 % N<sub>2</sub>/29.6 % CO/60.2 % H<sub>2</sub> ) was also used as a calibration gas for the estimation of the number of moles of reactants entering the reactor (feed stream) prior to the FT reaction. Typical traces produced from the calibration and reaction analyses were recorded and plotted using a DataApex Chromatograph software package known as Clarity (v. 2.5). These plots are illustrated in Figures 3.15, 3.16, 3.17, 3.18 and 3.19.

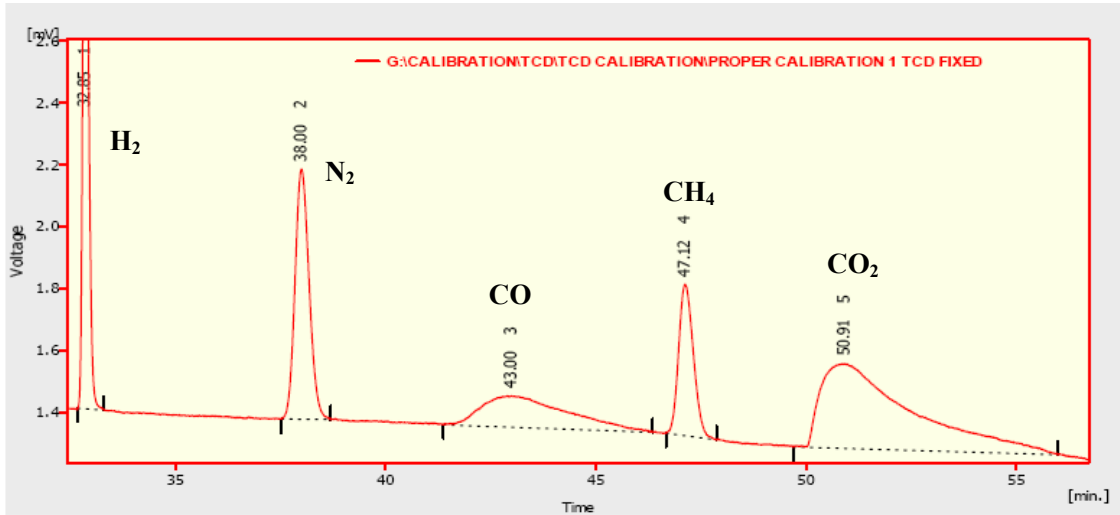


**Figure 3.15** A trace for the calibration gas using the TCD GC

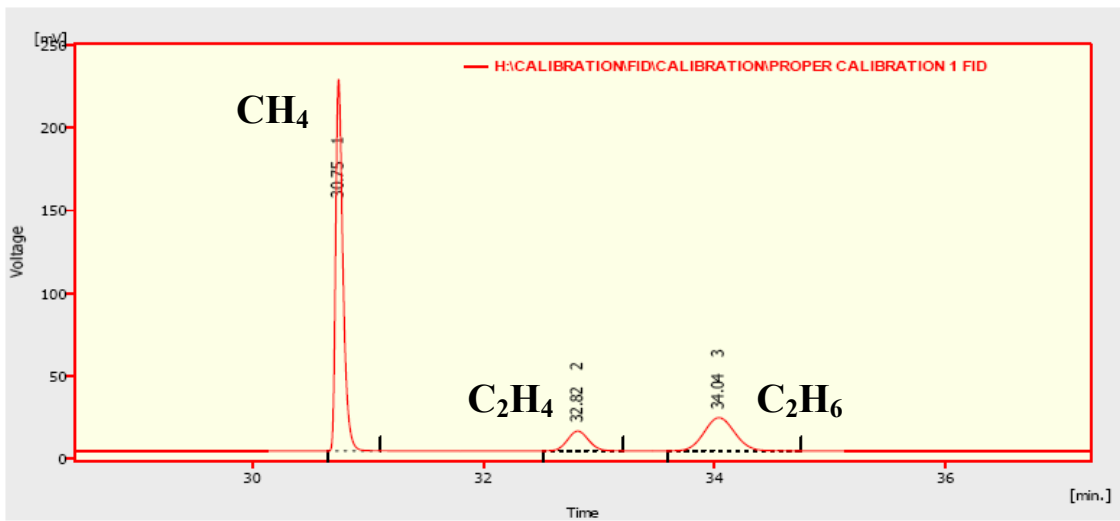


**Figure 3.16** A trace for the calibration gas product using the FID GC

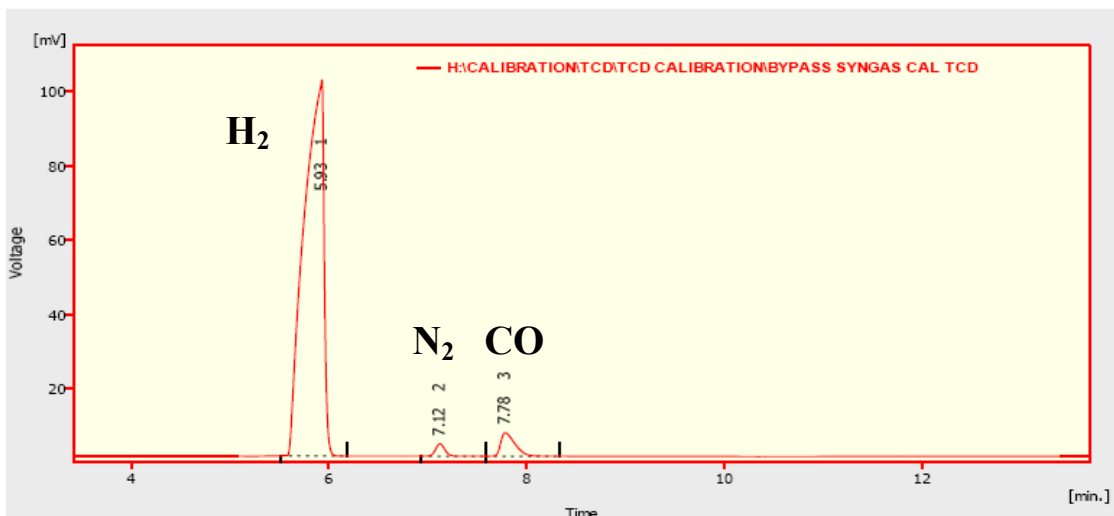


**Figure 3.17** A trace showing the calibration of the TCD GC using syngas

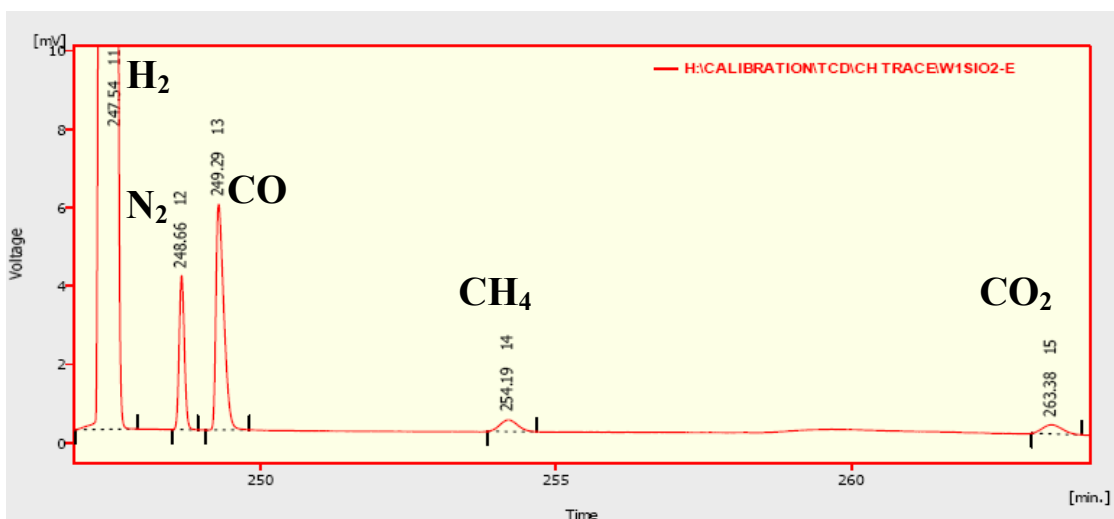


**Figure 3.18** FTS products detected by the TCD GC

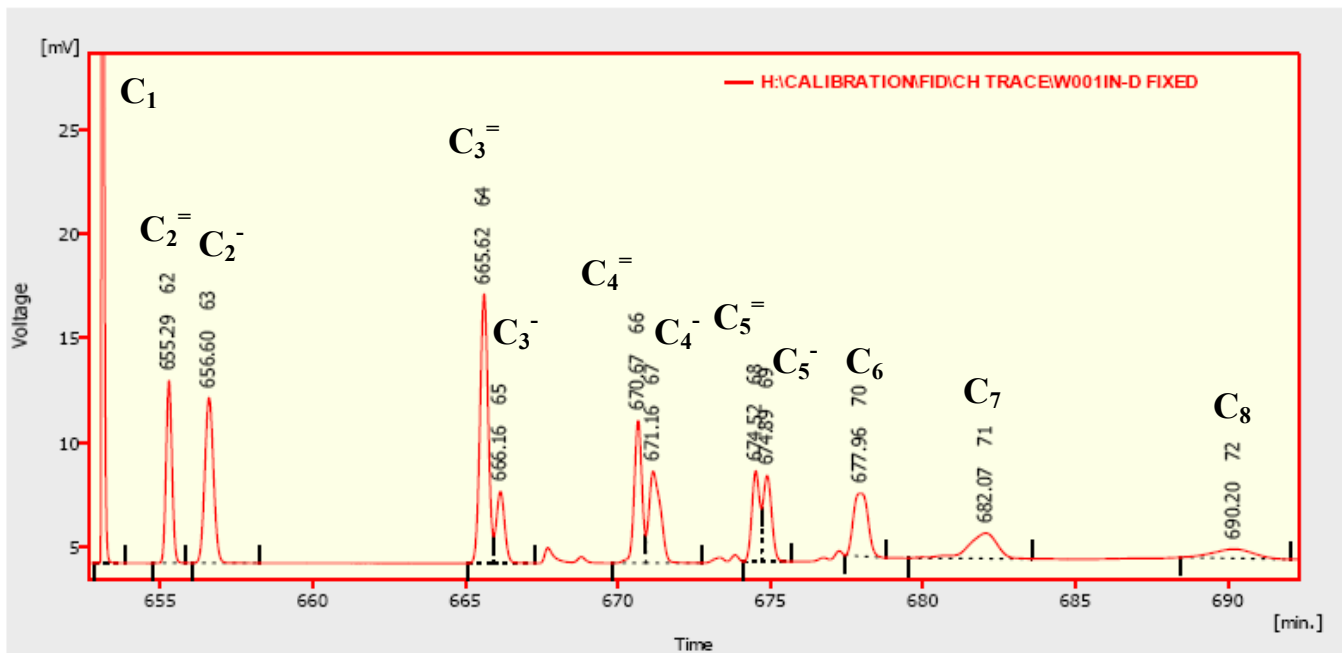


Figure 3.19 FTS products detected by the FID GC

### 3.3.1.5 Mass balance calculations

The calculations used to determine the mass balance are similar to those used by Duvenhage [3], Mokoena [4], Bahome [5], Phadi [6], and Price [7]. The mass balance was performed on carbon and oxygen. Mass balance data of 95% to 105% was accepted as adequate.

The analysis of feed and products in the two gas chromatographs was recorded and plotted using the Clarity software as explained in the previous section. The areas of the components were converted to molar composition by calculation.

The reaction steady state was typically reached 24 hours after the beginning of the reaction. Once this period was reached, the mass balance period was initiated and was recorded till the end of the experiment. The liquid and the wax products were then collected separately from the cold trap and hot trap successively and weighed. They were then analysed using the offline GC. It is to be noted that the oil was separated from water before analysis. The actual offline analysis involved syringe injection (0.02  $\mu$ l) of liquid (oil) and wax products into the GC.

The outlet flow stream was measured on a daily basis using a bubbler at ambient pressure and temperature. The feed inlet flow rate to the reactor was determined using N<sub>2</sub> gas contained in the syngas cylinder. The equation used to determine the feed flow rate is given below:

$$F_{in} = \left[ \frac{X_{N_2, in}}{X_{N_2, out}} \right] \times F_{out} \quad (3.1)$$

where  $F_{in}$  is the total feed flow rate in mol/s,  $X_{N_2, in}$  and  $X_{N_2, out}$  are mole fractions of nitrogen in the feed (Syngas) and reactor exit streams respectively and  $F_{out}$  is the total reactor exit stream in mol/s.



The number of moles of carbon in the feed stream in the total mass balance period was calculated by:

$$N_{c,in} = F_{in} \cdot t \cdot X_{CO,in} \quad (3.2)$$

where  $N_{C,in}$  is the moles of carbon in the feed,  $F_{in}$  is the total feed flow rate in mol/s,  $t$  is the total mass balance time and  $X_{CO,in}$  is the mole fraction of CO in the feed gas.

Calibration of the components was carried out with a premixed gas of known composition containing CH<sub>4</sub>, C<sub>2</sub>H<sub>6</sub>, C<sub>2</sub>H<sub>4</sub>, CO, CO<sub>2</sub>, and Ar. The moles product of each of the component present in the calibration gas was calculated using the following equation:

$$N_{c,out} = \frac{A_c}{A_{c,cal}} \cdot X_{c,cal} \cdot F_{out} \cdot t \quad (3.3)$$

where  $A_c$  is the GC integrated area of component  $c$ ,  $A_{c,cal}$  is the area of the component  $c$  in the calibration gas and  $X_{c,cal}$  is the mole fraction of the component  $c$  in the calibration gas.

The hydrocarbon product areas were corrected for C<sub>2</sub>H<sub>4</sub> (olefins) and C<sub>2</sub>H<sub>6</sub> (paraffins) by using the response factors based on those presented by Bahome [5] and Phadi [6]. The mole fractions of hydrocarbons  $X_{HC,i}$  were calculated using the equation below:

$$X_{HC,i} = \frac{RF_i \cdot A_{HC,i}}{A_{C_2,cal}} \cdot X_{C_2,cal} \quad (3.4)$$

where  $RF_i$  is the response factor for carbon number  $i$ ,  $A_{HC,i}$  is the integrated GC area for a hydrocarbon with carbon number  $i$ ,  $A_{C_2,cal}$  and  $X_{C_2,cal}$  refer to peak area and mole fraction of the C<sub>2</sub> hydrocarbon in the calibration gas [3, 4].

The mass response factors for the hydrocarbon with carbon number greater than 15 were assumed to be one. The mass fractions of these hydrocarbons ( $i > 15$ ) were thus determined directly from the GC integrated areas using the following equation:

$$m_i = \frac{A_{HC,i}}{\sum A_{HC,i}} \quad (3.5)$$

The product selectivity for hydrocarbons  $S_i$  was calculated for component  $x_i$  as follows:

$$S_i = \left[ \frac{\text{mass component } x_i}{\sum x_i} \right] \times 100\% \quad (3.6)$$

The olefin to paraffin ratio  $x_2$  was given as:

$$\text{Olefin to Paraffin ratio } x_2 = \frac{\text{Mass olefin } x_2}{\text{Mass total hydrocarbon } x_2} \quad (3.7)$$

Carbon and oxygen mass balances were determined using the information obtained from the above analysis and calculations:

$$\% \text{ Mole balance} = 100 \times \frac{N_{CO,in} - N_{CO,out} - N_{CO,in \text{ solid}} - N_{CO,in \text{ vapour}} - N_{CO_2}}{N_{CO,in}} \quad (3.8)$$

The % CO conversion was calculated as:

$$\left[ \frac{CO_{in} - CO_{out} \times \text{Gas contraction}}{CO_{in}} \right] \times 100 \quad (3.9)$$

where the gas contraction was determined from the  $\frac{N_{2,in}}{N_{2,out}}$  calibration

The individual rates of reaction for FTS ( $r_{\text{FTS}}$ ) and water gas shift WGS ( $r_{\text{WGS}}$ ) were calculated from experimentally obtained quantities as:

$$r_{\text{WGS}} = r_{\text{CO}_2} \quad (3.10)$$

$$r_{\text{FTS}} = r_{\text{CO}} - r_{\text{CO}_2} \quad (3.11)$$

where  $r_{\text{CO}_2}$  is the rate of carbon dioxide formation and  $r_{\text{CO}}$  is rate of carbon monoxide conversion.

## **References**

1. M. Bowker, *The Basis and Applications of Heterogeneous Catalysis*, Oxford University Press, New York (1998)
2. A. Y. Khodakov, W. Chu, P. Fongarland, *Chem. Rev.* 107 (2007) 1692
3. D.J. Duvenhage, *The Preparation, Characterization and Evaluation of Titania Supported Fe:Co Bimetallic Catalysts for the Hydrogenation of CO*, PhD Thesis, University of the Witwatersrand, Johannesburg (1994)
4. E.M. Mokoena, *Synthesis and use of silica materials as support for the Fischer-Tropsch reaction*, PhD Thesis, University of the Witwatersrand, Johannesburg (2005)
5. M.C. Bahome, *Synthesis and use of carbon nanotubes as a support for the Fischer-Tropsch Synthesis*, PhD Thesis, University of the Witwatersrand, Johannesburg (2007)
6. T.T. Phadi, *Titanates and titania coated titanates as supports in the Fischer-Tropsch synthesis*, MSc Dissertation, University of the Witwatersrand, Johannesburg (2008)
7. J.G. Price, *An investigation into novel bimetallic catalysts for use in the Fischer-Tropsch reaction*, PhD Thesis, University of the Witwatersrand, Johannesburg (1994)

## Chapter 4

### Optimisation of the weight loading of copper and potassium promoters in a precipitated Fe-based Fischer-Tropsch synthesis catalyst

#### *4.1 Introduction*

Copper and potassium are classic chemical promoters often used in the iron-based Fischer-Tropsch synthesis catalyst. They are typical promoters used to prepare FTS catalysts employed in industrial catalysts. The effects caused by copper and potassium are well documented and most of these have been described in Chapter 2. The aim of this study was to optimize the weight loadings of these two promoters and the studies were carried out systematically. The weight loading range investigated was 1 – 5 wt. %

#### *4.2 Experimental*

All the catalysts were prepared using the precipitation method as outlined in Chapter 3. The catalysts were characterized using XRF, XPS, TPR, XRD and DRIFTS techniques. A comprehensive discussion of how these characterisation experiments were carried out is also given in Chapter 3.

### **4.3 Results and discussion**

The optimum weight loading of copper in Fe FTS catalysts will be presented first. The results obtained on studying potassium will be presented after the copper results.

#### **4.3.1 Optimising the weight loading of copper**

##### **4.3.1.1 XRF**

The intended weight loadings of Cu and those determined using XRF are displayed in Table 4.1

Table 4.1 The theoretical and XRF determined Cu loadings

Catalyst composition	Theoretical value of Cu (wt. %)	XRF determined (wt. %)
1Cu/100Fe	1	1.2
2Cu/100Fe	2	2.2
3Cu/100Fe	3	3.5
4Cu/100Fe	4	4.8
5Cu/100Fe	5	6.0

It is noticed that the intended weight loadings are similar to those determined using XRF. The maximum error that exists between the theoretical values and the XRF determined values is 1 wt. %. The catalysts were then characterised using the techniques mentioned above. All the comparisons were done relative to a catalyst containing only Fe (100Fe). In other words 100Fe was used as the benchmark catalyst.

### 4.3.1.2 XPS

XPS spectra of the copper loaded catalysts are shown in Fig. 4.1 where the Cu(2p) spectra and copper Auger spectra are presented. The Cu(2p) spectra show several peaks, the most intense of which is centered at 934.5 eV, and is assigned to the Cu(2p<sup>3/2</sup>) photoelectron line of CuO. The other peaks are ascribed to the satellites of Cu(II) [1-2]. The copper Auger spectra were recorded to aid exact determination of the copper oxidation state within each sample. From the Cu(LLM) spectra (Fig 4.1a), it is clear that the copper exists as CuO rather than Cu<sub>2</sub>O or metallic copper, due to the presence of a peak having a binding energy at 569.3 eV. For copper metal, the LLM peak would have shifted to a lower binding energy (*ca.* 568 eV) [3].

It is noticeable that as the copper loading is increased, the peak at 934.5 eV increases in intensity. This is an indication that the copper content on the surface is increasing. Evidence of this assertion is illustrated in Table 4.2 and it is observed that as the atomic % of Fe (Fe 2p peak) decreases the atomic % of Cu (Cu 2p peak) increases.

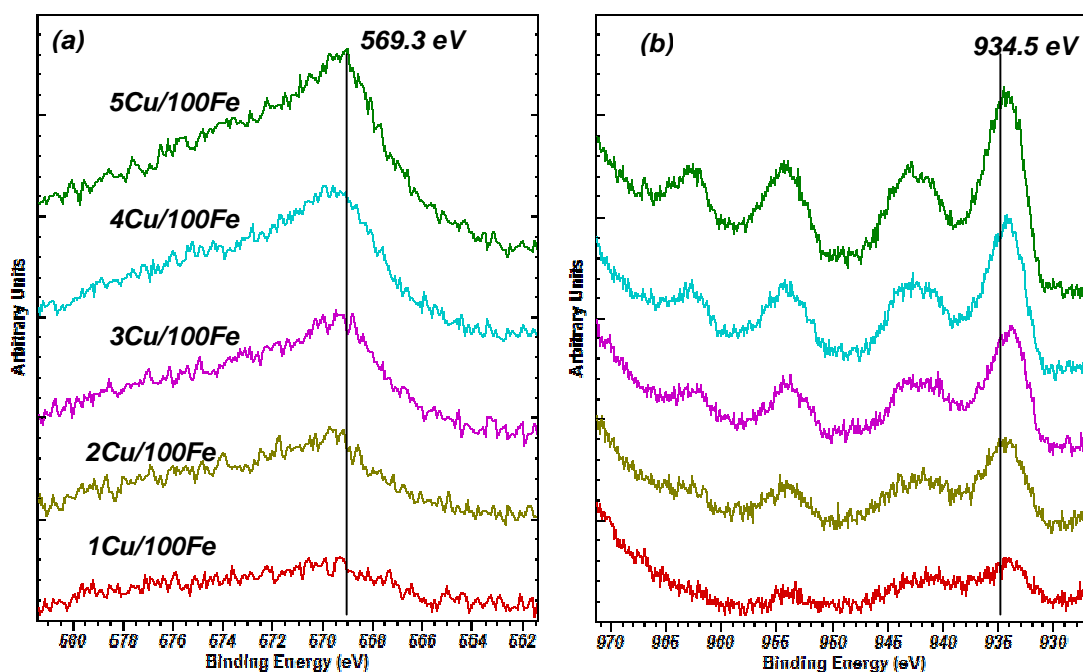


Figure 4.1 (a) Cu(LLM) and (b) Cu(2p) spectra for all catalysts

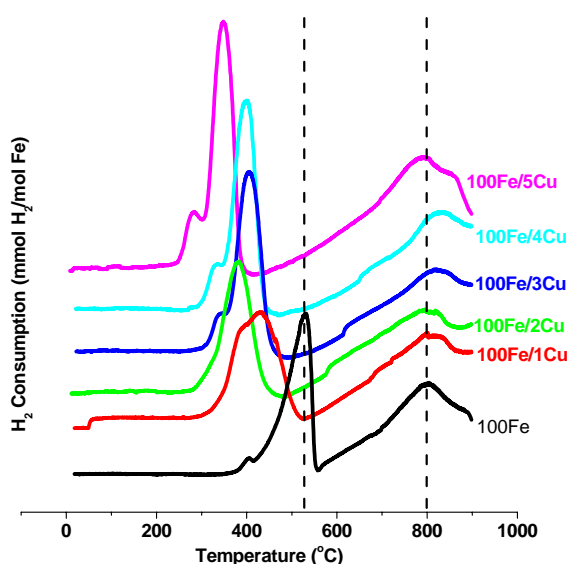
Table 4.2 XPS data for spectra given in Fig 4.1

Catalyst composition (parts by weight)	Peak identity	Binding energy (eV)	Peak area	Atomic %
1Cu/100Fe	Fe 2p	711.4	24662	43.7
	Cu 2p	935.4	587	0.58
2Cu/100Fe	Fe 2p	711.9	18595	42.0
	Cu 2p	935.4	576	0.72
3Cu/100Fe	Fe 2p	711.4	20683	40.8
	Cu 2p	935.4	849	0.93
4Cu/100Fe	Fe 2p	711.4	20445	42.7
	Cu 2p	933.9	1156	1.34
5Cu/100Fe	Fe 2p	711.4	19159	39.5
	Cu 2p	934.4	1668	1.91



### 4.3.1.3 H<sub>2</sub> TPR

The H<sub>2</sub> TPR results are shown in Fig. 4.2, Tables 4.3 and 4.4. All TPR profiles show 2 distinct reductions peaks with the last three profiles showing an extra small peak before the first peak. This peak is ascribed to the reduction of CuO to Cu. The occurrence of this peak has also been reported in the literature [4, 5]. It has also been reported that the H<sub>2</sub> reduction of Fe<sub>2</sub>O<sub>3</sub> occurs via 2 main steps: Fe<sub>2</sub>O<sub>3</sub> → Fe<sub>3</sub>O<sub>4</sub> → Fe. These two elementary reactions are assigned to the first and second peaks in the H<sub>2</sub> TPR profiles, respectively [6-8]. It is noticeable that the addition of Cu shifts the reduction peaks to lower temperatures. This is also a well known effect and has been widely published [4, 5]. As the Cu loading is increased the reduction temperature of the first peak is lowered, demonstrating a linear relationship between copper loading and the iron oxide reduction temperature. An increase in the copper content generally increases the reduction temperature of the second peak. The peak is only decreased to a lower temperature for the catalyst loaded with 5 wt. % of Cu. From these results it is seen that the 5 wt. % loading of Cu greatly improves the reduction of the iron oxide phase more than the other loadings.



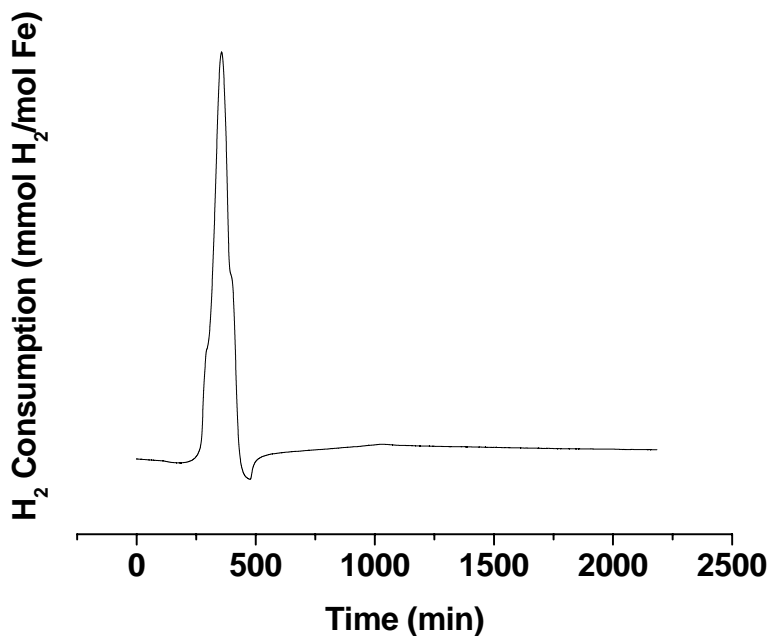
**Figure 4.2** H<sub>2</sub> TPR profiles of all the catalysts

Table 4.3 Reduction temperatures for the H<sub>2</sub> TPR profiles show in Fig.4.2

Catalyst composition (parts by weight)	Reduction temperature (°C)		
	Peak 1	Peak 2	Peak 3
100Fe	-	529	798
1Cu/100Fe	-	430	815
2Cu/100Fe	-	379	815
3Cu/100Fe	336	404	823
4Cu/100Fe	332	396	828
5Cu/100Fe	285	345	789

When carrying out an FTS reaction, reduction is normally carried out for longer than the time employed when performing an H<sub>2</sub> TPR experiment. An isothermal temperature is employed instead of the changing temperature as is the case for a TPR experiment. TPR is often employed for relative comparisons and does represent the reduction process used for the FTS reaction.

In order to be able to determine the amount of Fe reduced prior to reaction, the reduction conditions normally employed for an FTS reaction were employed in a TPR reaction. The 100Fe catalyst was used for these experiments and the experimental procedure involved heating the catalyst from room temperature to 350 °C under the flow of H<sub>2</sub> and then holding the temperature at 350 °C for 24 hours. The TPR profile obtained is shown in Fig. 4.3.



**Figure 4.3** TPR profile of  $\text{Fe}_2\text{O}_3$  reduced using the reduction method employed when carrying out an FTS reaction

It is noticeable from Fig. 4.3 that only one peak is present and this represents the transformation of  $\text{Fe}_2\text{O}_3$  to  $\text{Fe}_3\text{O}_4$ . However, it is likely that some  $\text{Fe}_2\text{O}_3$  could be reduced to  $\text{Fe}_3\text{O}_4$  and then to Fe rapidly for small crystallites when Cu is present. This could also be possible in the absence of Cu as is with the current situation. Fig. 4.3 also shows that holding the temperature at 350 °C for 24 hours does not increase the reducibility of Fe. As a result only the first reduction peak during TPR, accounts for the reduction of Fe under the standard reduction procedure used. The %Fe reducibility shown in Table 4.4, therefore, was calculated only from the first TPR peak shown in Fig. 4.2 and represents the degree of reducibility of the catalyst prior to reaction. Another way of determining %Fe reducibility could be to reduce the catalyst at 350 °C for 24 hrs, followed by cooling

to room temperature (all under H<sub>2</sub>) and then performing an H<sub>2</sub> TPR experiment thereafter. But for the purpose of our studies the former method was employed.

Table 4.4 %Fe reducibility as a function of Cu loading for all Cu loaded catalysts

<sup>a</sup> Catalyst composition (parts by weight)	%Fe reducibility <sup>b</sup>
100Fe	15
1Cu/100Fe	30
2Cu/100Fe	33
3Cu/100Fe	38
4Cu/100Fe	39
5Cu/100Fe	46

<sup>a</sup>Parts by weight

<sup>b</sup>Maximum error = ± 5%

From Table 4.4 it is observed that varying the loading amount of Cu has some effect on the %Fe reducibility. The catalyst loaded with 5 wt. % Cu gives the highest %Fe reducibility.

Dry [9] has stated that the precipitated iron catalyst developed by Ruhrchemie and used in the fixed-bed reactors at Sasol contains about 5 wt. % Cu. Meanwhile work performed by O'Brein et al. [10] has shown that reduction of iron oxide using hydrogen is accelerated with increasing levels of copper promotion (2.6-5.0 atomic % relative to iron). They argued that the acceleration of the iron oxide reduction (with increasing levels of copper promotion) is in agreement with more nucleation sites being available with an increasing amount of copper.

Based on these findings, the 5 wt. % loading of Cu can be nominated as the best loading amount for enhancing the reduction properties of the Fe based catalyst.

#### 4.3.1.4 XRD

The XRD experiments were performed to determine the crystallite size of  $\text{Fe}_2\text{O}_3$ . The actual crystallite size was determined using Rietveld refinement and the crystallite sizes determined are given in Table 4.5.

Table 4.5 The calculated crystallite size of  $\text{Fe}_2\text{O}_3$  as a function of Cu loading

<sup>a</sup> Catalyst composition	$\text{Fe}_2\text{O}_3$ crystallite size (nm)
100Fe	33
1Cu/100Fe	44
2Cu/100Fe	46
3Cu/100Fe	48
4Cu/100Fe	46
5Cu/100Fe	45

<sup>a</sup>Parts by weight

It is noticeable that the introduction of even 1 wt. % Cu increases the crystallite size of  $\text{Fe}_2\text{O}_3$ . The crystallite size increases irrespective of the loading amount of Cu added and the crystallite sizes for all the Cu loaded catalysts are comparable to one another.

### 4.3.1.5 CO adsorption measurements using DRIFTS

CO adsorption on the copper loaded catalysts was also performed and the results are illustrated in Fig 4.4 and Table 4.6. It is noticeable that adsorption of CO on Fe produces two CO bands at around 2013 and 2033  $\text{cm}^{-1}$ . These two bands show that CO is adsorbed on Fe in a linear fashion [11, 12]. The CO adsorption measurements indicate that the presence of Cu causes a red shift of the 2013.7  $\text{cm}^{-1}$  peak to 2011.7  $\text{cm}^{-1}$ . This red shift by Cu indicates that Cu enhances the backdonation ability of Fe. This means that in the presence of Cu, the ability of Fe to transfer electrons via backdonation into the antibonding orbitals ( $2\pi^*$ ) of carbon is enhanced [13, 14]. This strengthens the Fe-C bond making it possible to increase the hydrocarbon chain during the FTS reaction. This postulation is further confirmed by the number increase of the calculated  $\text{CH}_2/\text{CH}_3$  ratio (see below). In fact for all the copper loaded catalysts the 2013  $\text{cm}^{-1}$  band shifts to lower wavenumbers. The results are illustrated in Table 4.6.

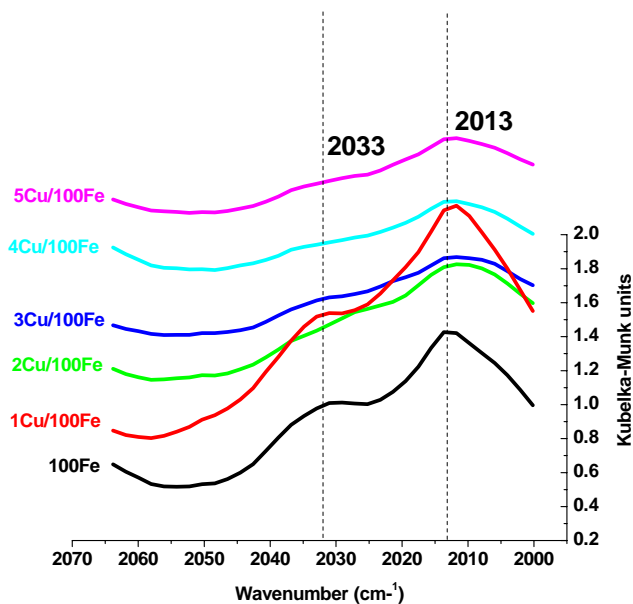


**Figure 4.4** Comparing CO absorption spectra of Cu promoted catalysts to the unpromoted Fe catalyst

Table 4.6 Position of IR absorption band as a function of Cu loading

Catalyst	Peak wavenumber (cm <sup>-1</sup> )
100Fe	2014
1Cu/100Fe	2012
2Cu/100Fe	2012
3Cu/100Fe	2012
4Cu/100Fe	2012
5Cu/100Fe	2012

#### 4.3.1.6 In situ CO hydrogenation using DRIFTS

In situ CO hydrogenation reactions were performed using the DRIFTS reactor. Only the part of the spectrum that monitors the production of C-H species ( $2750 - 3100 \text{ cm}^{-1}$ ) was assessed. This C-H species gives an indication of the hydrocarbon molecules produced during the reaction.

To estimate the average carbon chain length of the hydrocarbon molecules produced after 5 hours of reaction, the ratio of  $\text{CH}_2/\text{CH}_3$  species was calculated using the following formula:

$$\frac{\text{Area}(-\text{CH}_2 - \text{species})}{\varepsilon_1} / \frac{\text{Area}(-\text{CH}_3 - \text{species})}{\varepsilon_2}$$

where

- 1) Area of  $-\text{CH}_2-$  species is the area of the peak at  $2925-2930 \text{ cm}^{-1}$  representing the asymmetric stretch of  $\text{CH}_2$  species
- 2) Area of  $-\text{CH}_3$  species is the area of the peak at  $2955-2960 \text{ cm}^{-1}$  representing the asymmetric stretch of  $\text{CH}_3$  species
- 3)  $\varepsilon_1$  is the molar extinction coefficient of the  $\text{CH}_2$  species ( $75 \text{ mole}^{-1} \cdot \text{l} \cdot \text{cm}^{-1}$ ) [15]
- 4)  $\varepsilon_2$  is the molar extinction coefficient of the  $\text{CH}_3$  species ( $70 \text{ mole}^{-1} \cdot \text{l} \cdot \text{cm}^{-1}$ ) [15]

The calculated ratios are given in Table 4.7. It is evident that addition of copper leads to an increase in the average chain length of the hydrocarbons.



Table 4.7 Calculated ratios of CH<sub>2</sub>/CH<sub>3</sub> bands for all catalysts

Catalyst	Ratio of CH <sub>2</sub> /CH <sub>3</sub>
100Fe	1
100Fe/1Cu	7
100Fe/2Cu	6
100Fe/3Cu	7
100Fe/4Cu	6
100Fe/5Cu	6

As stipulated in the previous section the addition of Cu leads to an increase in the CH<sub>2</sub>/CH<sub>3</sub> ratio indicating an increase in the chain length of the hydrocarbon molecules. Further when the loading of Cu is varied, the CH<sub>2</sub>/CH<sub>3</sub> ratio is not drastically changed, indicating that changing the Cu loading does not significantly change the FTS product spectrum. This could mean that the FTS product selectivity is not affected by varying the loading of Cu. This again could mean Cu plays a small role in changing the FTS product selectivity. Zhang et al. [16] have also reported that copper plays only a small role in FTS product selectivity.

It was also important to make sure that deductions made on the results presented above were real and did not necessarily constitute a scenario of a one point deduction. To verify this postulation, two unpromoted 100Fe samples were prepared and DRIFTS experiments (i.e. calculation of CH<sub>2</sub>/CH<sub>3</sub>) were done on both samples. The results obtained came out to be similar (not presented here). Clearly, confirming that deductions made above were true. Unfortunately the XRD experiment was performed only on one sample (as already discussed above). But it is logical to conclude that if the DRIFTS results came out to be the same for both prepared samples surely the XRD results of the two samples would give similar results.

### 4.3.2 Optimising the weight loading of potassium

#### 4.3.2.1 H<sub>2</sub> TPR

The H<sub>2</sub> TPR results are presented in Fig. 4.5, Tables 4.8 and 4.9. All the catalysts show the two dominant peaks for the reduction of Fe<sub>2</sub>O<sub>3</sub>. These peaks represent the two step reduction of Fe<sub>2</sub>O<sub>3</sub> into metallic Fe as explained earlier. It is noticeable that catalysts loaded with a loading amount of  $\geq 2$  wt. % K<sub>2</sub>O show 3 peaks. The first peak in all these profiles could reflect the reduction of easily reducible iron oxide crystallites. This still reflects the transformation of Fe<sub>2</sub>O<sub>3</sub> into Fe<sub>3</sub>O<sub>4</sub>.

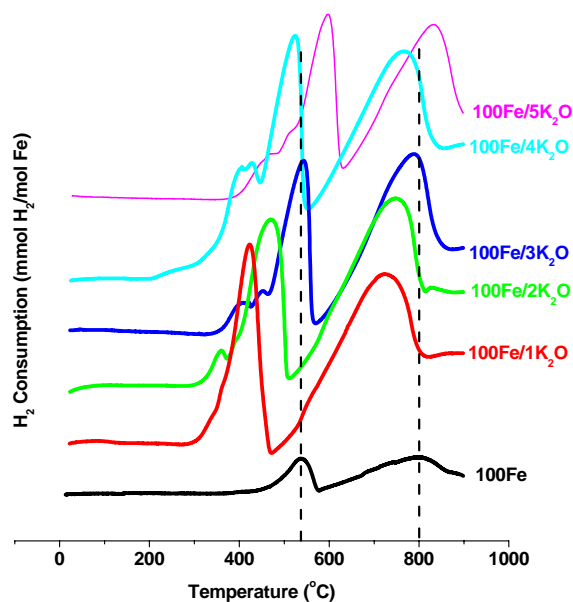


**Figure 4.5** H<sub>2</sub> TPR profiles of all the catalysts

Table 4.8 Reduction temperatures for the H<sub>2</sub> TPR profiles show in Fig. 4.5

Catalyst composition (parts by weight)	Reduction temperature (°C)		
	Peak 1	Peak 2	Peak 3
100Fe	-	537	802
1K <sub>2</sub> O/100Fe	-	422	721
2K <sub>2</sub> O /100Fe	358	469	747
3K <sub>2</sub> O /100Fe	426	537	785
4K <sub>2</sub> O/100Fe	417	520	764
5K <sub>2</sub> O/100Fe	486	597	832

From Table 4.8 it is observed that K<sub>2</sub>O loading up to 2 wt. % lowers the reduction temperature of peak 2, thereafter the reduction temperatures are shifted to higher temperatures.

The %Fe reducibility was also determined in the same manner as it was done for the Cu/Fe loaded catalysts. It is clear that as the loading of potassium is increased the %Fe reducibility is decreased. This could be attributed to potassium suppressing the ability of Fe to adsorb H<sub>2</sub> [17, 19]. The catalyst loaded with 2 wt. % K<sub>2</sub>O gives the highest %Fe reducibility.

Table 4.9 %Fe reducibility as a function of K<sub>2</sub>O loading for all K<sub>2</sub>O loaded catalysts

<sup>a</sup> Catalyst composition	%Fe reducibility <sup>b</sup>
100Fe	15
1K <sub>2</sub> O/100Fe	64
2K <sub>2</sub> O/100Fe	70
3K <sub>2</sub> O/100Fe	55
4K <sub>2</sub> O/100Fe	54
5K <sub>2</sub> O/100Fe	41

<sup>a</sup>Parts by weight

<sup>b</sup>Maximum error = ± 5%

#### 4.3.2.2 XRD

XRD was employed to determine the crystallite size of  $\text{Fe}_2\text{O}_3$ . The crystallite size was determined in the same way as it was done for the Cu loaded catalysts. Table 4.9 below illustrates the calculated crystallite size of  $\text{Fe}_2\text{O}_3$  for all the  $\text{K}_2\text{O}$  loaded catalysts.

Table 4.10 The calculated crystallite size of  $\text{Fe}_2\text{O}_3$  as a function of  $\text{K}_2\text{O}$  loading

<sup>a</sup> Catalyst composition	$\text{Fe}_2\text{O}_3$ crystallite size (nm)
100Fe	33
1 $\text{K}_2\text{O}$ /100Fe	51
2 $\text{K}_2\text{O}$ /100Fe	52
3 $\text{K}_2\text{O}$ /100Fe	52
4 $\text{K}_2\text{O}$ /100Fe	52
5 $\text{K}_2\text{O}$ /100Fe	47

<sup>a</sup>Parts by weight

It is seen that the presence of  $\text{K}_2\text{O}$  increases the crystallite size of  $\text{Fe}_2\text{O}_3$  but increasing the  $\text{K}_2\text{O}$  loading from 1-4 wt. % does not significantly change the crystallite size of  $\text{Fe}_2\text{O}_3$ .

### 4.3.2.3 CO adsorption measurements using DRIFTS

The CO adsorption results are presented in Fig. 4.6 and Table 4.10. Again it is noticeable that all the catalysts have two bands showcasing CO adsorbed linearly on Fe. The adsorbed CO bands on the benchmark catalyst are around 2013 and 2033  $\text{cm}^{-1}$  and no other peaks could be identified.

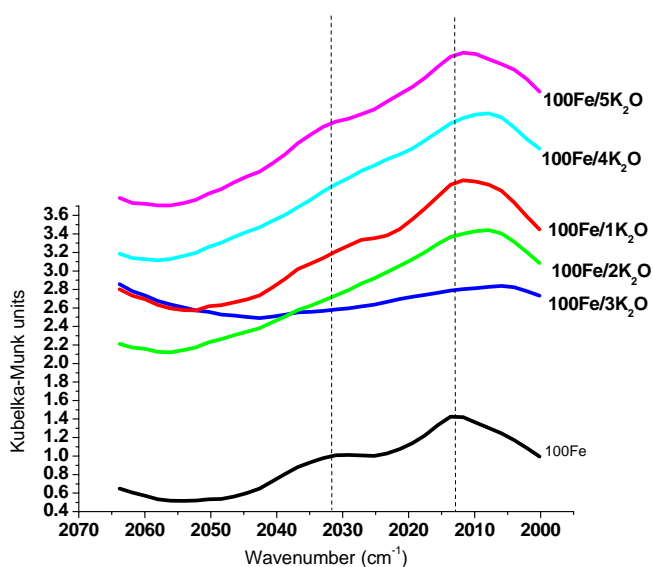


**Figure 4.6** Comparing CO absorption spectra of  $\text{K}_2\text{O}$  promoted catalysts to the unpromoted Fe catalyst

These bands are shifted to lower wavenumbers for all the  $\text{K}_2\text{O}$  loaded catalysts as illustrated in Table 4.10. This red shift illustrates that the Fe-C bond is strengthened and that potassium enhances CO adsorption on Fe. It is well known that potassium increases the CO adsorption ability of Fe [18, 19].

Table 4.11 Peak shifts of peak at wavenumber region 2012-2015  $\text{cm}^{-1}$  as a function of  $\text{K}_2\text{O}$  loading

Catalyst	Peak wavenumber ( $\text{cm}^{-1}$ )
Fe	2014
1 $\text{K}_2\text{O}$ /100Fe	2012
2 $\text{K}_2\text{O}$ /100Fe	2008
3 $\text{K}_2\text{O}$ /100Fe	2006
4 $\text{K}_2\text{O}$ /100Fe	2008
5 $\text{K}_2\text{O}$ /100Fe	2012

The catalyst loaded with 3 wt. %  $\text{K}_2\text{O}$  shifts the 2013  $\text{cm}^{-1}$  peak to the lowest wavenumber (2006.0  $\text{cm}^{-1}$ ). This peak is then shifted to ca. 2007.9  $\text{cm}^{-1}$  at a loading of 4 wt. %  $\text{K}_2\text{O}$  and to 2011.7  $\text{cm}^{-1}$  for the 5 wt. % loading. It is clear that weight loadings above 3 wt. % do not significantly enhance the adsorption of CO.

#### 4.3.2.4 In situ CO hydrogenation using DRIFTS

The CH<sub>2</sub>/CH<sub>3</sub> ratio was also determined for all the catalysts. The ratio was determined as explained in section 4.2.1.6. All the “in situ” CO hydrogenation reactions were performed as explained in Chapter 3.

Table 4.12 Estimation of the CH<sub>2</sub>/CH<sub>3</sub> ratio as a function of K<sub>2</sub>O loading

Catalyst	Ratio of CH <sub>2</sub> /CH <sub>3</sub>
100Fe	1
1K <sub>2</sub> O/100Fe	2
2K <sub>2</sub> O/100Fe	8
3K <sub>2</sub> O/100Fe	8
4K <sub>2</sub> O/100Fe	7
5K <sub>2</sub> O/100Fe	7

Increasing the loading of K<sub>2</sub>O increases the CH<sub>2</sub>/CH<sub>3</sub> ratio. It is also noticeable that 2 and 3 wt. % loadings of K<sub>2</sub>O give the highest CH<sub>2</sub>/CH<sub>3</sub> ratio. These results are consistent with the CO adsorption results. It can also be noted that an increased CH<sub>2</sub>/CH<sub>3</sub> ratio on addition of K<sub>2</sub>O promotion reflects that the hydrocarbon chain length is increased. This is consistent with literature reports since it is well known that K<sub>2</sub>O promotes chain growth and shifts selectivity to longer chained hydrocarbons [19-23].

It is apparent that when potassium is added in moderation to Fe-based FTS catalysts, it enhances its characteristics (e.g. FTS activity is enhanced and selectivity to methane lowered). This is because when potassium containing catalysts are heated potassium moves to the top (the surface) of the catalyst [24] and has a direct influence on the active sites of the catalyst. Therefore if a high loading of potassium is used, this may be detrimental to the catalyst as more of it will move to the surface and block some of the catalyst active sites leading to a lower FTS activity.



Therefore the FTS activity either increases [22, 25] or passes through a maximum as a function of potassium loading [23], and potassium either has no effect on the activity for FTS [10] or suppresses it [23, 24].

Not much systematic work has been carried out on the effect of the level of potassium loading on Fe-based FTS catalysts. Work done by O'Brein et al. [10] in 1997, showed that a high potassium loading is required when the FTS reaction temperature is decreased because it becomes harder to dissociate the C-O bond. They found that the optimum potassium promotion was 4-5 atomic % relative to iron. They further found that potassium promotion increased wax selectivity.

In these studies we have noticed that 2 – 3 wt. % loading amount of K<sub>2</sub>O significantly enhanced the chemical properties of the precipitated Fe-based FTS catalyst. It improved the reduction properties (TPR results) and the CO adsorption ability of the catalyst. It also increased the CH<sub>2</sub>/CH<sub>3</sub> ratio which can be used as a qualitative way of measuring the average hydrocarbon chain length.

#### ***4.4 Conclusion***

The aim of this study was to optimize the weight loadings of Cu and K<sub>2</sub>O. The weight loading range investigated was 1-5 wt. % for both promoters. Various characterization techniques were used to assess the effects caused by all the promoter loadings. It was found that the 5 wt. % loading of Cu was the optimum loading amount for the copper loaded catalysts, because this loading significantly enhanced the reduction properties of the precipitated Fe-based FTS catalyst.

For the K<sub>2</sub>O loading, the wt. % loading range of 2-3 wt. % K<sub>2</sub>O significantly improved the reduction properties as well as the CO adsorption ability of the precipitated Fe-based FTS catalyst and due to the 2 wt. % K<sub>2</sub>O loading giving the best %Fe reducibility, this loading was chosen as the optimal loading of K<sub>2</sub>O.

As a result the 5 wt. % loading of Cu and 2 wt. % loading of K<sub>2</sub>O were used to prepare all Cu/K<sub>2</sub>O containing catalysts used in this thesis. The work showcasing the use of these optimum loading amounts of Cu and K<sub>2</sub>O is illustrated in Chapter 6 and Chapter 8.

## References

- [1] F.M. Capece, V. Dicastro, C. Furlani, G. Mattocono, C. Fragale, M. Gargano, M. Rossi, *J. Electron Spec. Relat. Phenom.* 27 (1982) 119.
- [2] B. Peplinske, W.E.S. Unger, I. Grohmann *Appl. Surf. Sci.* 62 (1992)
- [3] Z. Wang, Q. Liu, J. Yu, T. Wu, G. Wang, *Appl. Catal. A: Gen.* 239 (2003) 87
- [4] D.B. Bukur, K. Okabe, M.P. Rosynek, C. P Li, D. J Wang, K. R. P. M. Rao, G. P. Huffman, *J. Catal.* 155 (1995) 353
- [5] Y. Jin, A. K. Datye, *J. Catal.* 196 (2000) 8
- [6] I.S.C Hughes, J.O.H. Newman, G.C. Bond, *Appl. Catal.* 30 (1987) 303
- [7] C.N. Mbileni, *Applications of mesostructured carbonaceous materials as supports for Fischer-Tropsch metal catalyst*, PhD Thesis, University of the Witwatersrand, Johannesburg, 2006
- [8] M. Luo, R.J. O'Brein, S. Bao, B.H. Davis, *Appl. Catal. A: Gen.* 239 (2003) 111
- [9] M.E. Dry, The Fischer–Tropsch synthesis, in: J.R. Anderson, M. Boudart (Eds.), *Catalysis Science and Technology* 1, Springer-Verlag, New York, 1981, 159
- [10] R. J. O'Brein, L. Xu, R. L. Spicer, S. Bao, D. R. Milburn, B. H. Davis, *Catal. Today* 36 (1997) 325
- [11] M.J. Heal, E.C. Leisegang, R.G. Torrington, *J. Catal.* 51 (1978) 314
- [12] G. Bian, A. Oonuki, Y. Kobayashi, N. Koizumi, M. Yamada, *Appl. Catal. A: Gen.* 219 (2001) 13
- [13] F. Morales, E. de Smit, F.M.F. de Groot, T. Visser, B.M. Weckhuysen, *J. Catal.* 246 (2007) 91
- [14] G. Blyholder, L.D. Neff, *J. Chem. Phys.* 66 (1962) 1464
- [15] K. Nakanishi, *Infrared Absorption spectroscopy – PRACTICAL -*, Nankodo Company Limited, Japan, 1964
- [16] C. Zhang, Y. Yang, Z. Tao, T. Li, H. Wan, H. Xiang, Y. Li, *Acta Physico-Chimica Sinica* 22 (2006) 1310
- [17] G. Zhao, C. Zhang S. Qin, H. Xiang, Y. Li, *J. Mol. Catal. A: Chemical* 286 (2008) 137

- [18] H.J. Wan, B.S. Wu, Z.C. Tao, T.Z. Li, X. An, H.W. Xiang, Y.W. Li, *J. Mol. Catal. A: Chemical* 260 (2006) 255
- [19] N. Lohitharn, J.G. Goodwin Jr., *J. Catal.* 260 (2008) 7
- [20] R.B. Anderson, *The Fischer-Tropsch Synthesis*, Academic Press, Orlando, 1984
- [21] Y. Yang, H.W. Xiang, Y.Y. Xu, L. Bai, Y.W. Li, *Appl. Catal. A Gen.* 266 (2004) 181
- [22] D.B. Bukur, D. Mukesh, S.A. Patel, *Ind. Eng. Chem. Res.* 29 (1990) 194
- [23] D.G. Miller, M. Moskovits, *J. Phys. Chem.* 92 (1988) 6081
- [24] R.A. Dector, A.T. Bell. *J. Catal.* 97 (1986) 121
- [25] R.B. Anderson, B. Sekigman, J.F. Schulz, M.A. Elliot, *Ind. Eng. Chem.* 44 (1952) 391

## Chapter 5

### Effect of SiO<sub>2</sub> content on an unpromoted Fe-based Fischer-Tropsch synthesis catalyst

#### **5.1 Introduction**

Many studies have been performed employing SiO<sub>2</sub> as part of the ingredient for preparing precipitated iron-based catalysts for the FTS. In most instances it has been employed as a support (structure promoter) or as a major component of the catalyst [1].

The major reason for using it as a support or structural promoter is that it lowers the deactivation rate of the catalyst especially in slurry phase reactors [2]. Deactivation of catalysts particularly those without a binder, support or structural promoter occurs via attrition. Attrition is the breakage of the catalyst leading to the formation of very small particles. These small particles are readily lost as “fines”.

Previous studies with supported iron catalysts have been reported [3-10], but there are very few studies that have looked at the effect of SiO<sub>2</sub> as a chemical promoter. SiO<sub>2</sub> has been shown to possess chemical promotional abilities [11].

Recent work by Zhang et al. [11] has highlighted that the introduction of 20 wt. % SiO<sub>2</sub> into a precipitated iron-based FTS catalyst results in improved light hydrocarbon selectivity. A deleterious effect was observed on introduction of 20 wt. % SiO<sub>2</sub> as this high loading lowered the FTS activity. They attributed this effect to the strong interaction that exists between iron and silica (iron-silica interaction) thus rendering some of the iron to be inactive for FTS. Work reported by other researchers [12-16] also confirms the latter postulation made by Zhang et al., but most of this work was performed on multi-component systems.

Surprisingly not much work has been carried out to evaluate the effect of SiO<sub>2</sub> as a sole chemical promoter for the precipitated Fe-based FTS catalysts. Employing SiO<sub>2</sub> in a multi-component system makes it difficult to establish its chemical effect. Our aim then was to evaluate the effect of SiO<sub>2</sub> as a chemical promoter for Fe-based FTS catalyst in the absence of other promoters. We were interested in studying the effect of the SiO<sub>2</sub> content (5 wt. % to 25 wt. %) on a precipitated iron-based Fischer-Tropsch catalyst.

## 5.2 Experimental

All the catalysts were prepared in the same manner as outlined in Chapter 3. The catalysts were characterised using N<sub>2</sub> physisorption, XRD, XPS, TPR and DRIFTS. A comprehensive discussion on how the characterisation experiments were performed is also outlined in Chapter 3.

## 5.3 Results and discussion

### 5.3.1 Textural and structural properties of the catalysts

The textural properties of the catalysts were determined using N<sub>2</sub> physisorption as illustrated in Table 5.1. The structural properties were examined using XRD.

Table 5.1 The composition and textural properties of the calcined catalysts

Catalyst composition (parts by weight)	BET Surface area <sup>b</sup> (m <sup>2</sup> /g)	Pore volume <sup>b</sup> (cm <sup>3</sup> /g)
100Fe	22.8	0.086
100Fe/5SiO <sub>2</sub>	72.7	0.13
100Fe/10SiO <sub>2</sub>	131	0.16
100Fe/20SiO <sub>2</sub>	196	0.22
100Fe/25SiO <sub>2</sub>	229	0.24

<sup>b</sup>Maximum error = ± 2%

As expected the addition of SiO<sub>2</sub> increased the surface area of the precipitated catalyst. The surface area as well as the pore volume increased with increasing SiO<sub>2</sub> content. This is consistent with work carried out by other researchers [17, 18].

Several authors [14, 19] have gone on to mention that SiO<sub>2</sub> provides a more dispersed rigid matrix, which helps to prevent the catalyst from a fast pore collapse and stabilizes the small iron oxide crystallites from sintering. In other words, SiO<sub>2</sub> favours a high dispersion of Fe<sub>2</sub>O<sub>3</sub>. This means that increasing the SiO<sub>2</sub> content favours a formation of a porous structure and the high dispersion of Fe<sub>2</sub>O<sub>3</sub>. Consequently, the average crystallite size of Fe<sub>2</sub>O<sub>3</sub> was decreased as shown by XRD results (Table 5.2). The crystallite size was calculated from Rietveld refinement of the XRD patterns of the catalysts.

Table 5.2 The calculated crystallite size of Fe<sub>2</sub>O<sub>3</sub> as a function of SiO<sub>2</sub> loading

<sup>a</sup> Catalyst composition	Fe <sub>2</sub> O <sub>3</sub> crystallite size (nm)
100Fe	32.8
5SiO <sub>2</sub> /100Fe	30.5
10SiO <sub>2</sub> /100Fe	23.4
20SiO <sub>2</sub> /100Fe	20.5
25SiO <sub>2</sub> /100Fe	12.5

<sup>a</sup>Parts by weight

### 5.3.2 Reduction and carburization behaviour of the catalysts

H<sub>2</sub> and CO TPR techniques were employed to investigate the effect of the silica content on the reduction and carburization behaviour of the catalysts. The TPR profiles of the H<sub>2</sub> absorption and the corresponding quantitative results are presented in Fig. 5.1 and Table 5.3.



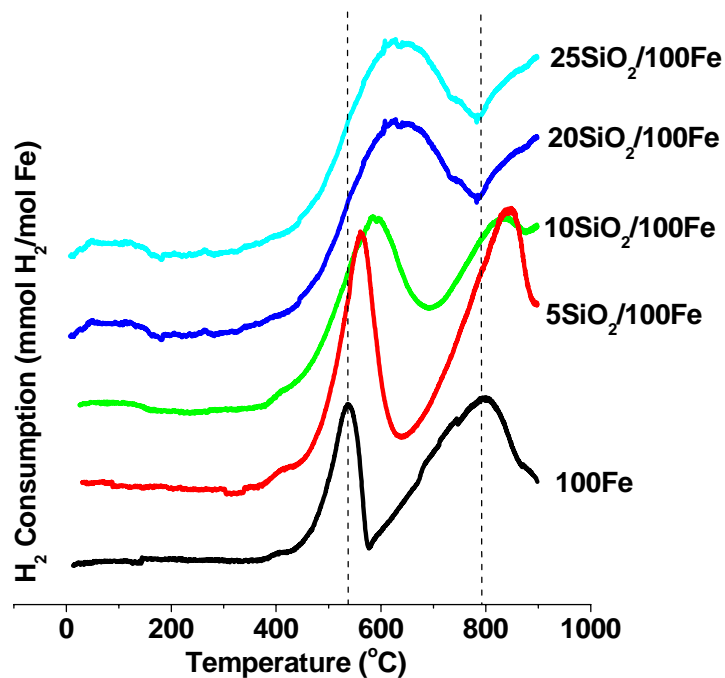


**Figure 5.1** H<sub>2</sub> TPR profiles of the catalysts

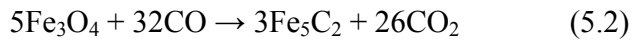
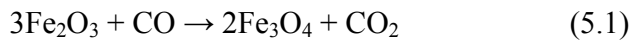
As shown in Fig. 5.1, the expected two stage reduction process of Fe<sub>2</sub>O<sub>3</sub> occurs but as the loading of SiO<sub>2</sub> is increased the reduction peaks are shifted to higher temperatures. In fact it becomes difficult to distinguish between the two reduction peaks when SiO<sub>2</sub> loading is increased above 10 wt. %. This may be attributed to increased Fe-SiO<sub>2</sub> interactions [20]. It has also been reported that adding SiO<sub>2</sub> to iron-based FTS catalyst restrains its reduction [11] and this is clearly indicated by Fig. 5.1 and Table 5.3.

Table 5.3 Peak maxima of H<sub>2</sub> TPR profiles

<sup>a</sup> Catalyst composition	Peak Maximum (°C)	
	Peak 1	Peak 2
100Fe	537	793
5SiO <sub>2</sub> /100Fe	561	845
10SiO <sub>2</sub> /100Fe	585	845
20SiO <sub>2</sub> /100Fe	630	-
25SiO <sub>2</sub> /100Fe	633	-

<sup>a</sup>Parts by weight

CO TPR results are illustrated by Fig. 5.2. It is known that CO also reduces Fe<sub>2</sub>O<sub>3</sub> via a two step process into iron carbides [21-23].



The catalyst with no SiO<sub>2</sub> shows the two peaks associated with FeO<sub>x</sub> reduction to FeC<sub>x</sub>. As soon as SiO<sub>2</sub> is added, three peaks emerge. The first peak is attributed to the reduction of easily reducible iron oxide crystallites. The second peak is ascribed to the reduction of iron oxide via Eq. 5.1 and the third peak represents the carburization of the crystallites (Eq. 5.2). It is noticeable that as the SiO<sub>2</sub> content is increased the first peak increases in intensity and broadens (Fig 5.2 and Table 5.5). This would indicate an increase in the number of easily reducible iron oxide crystallites. This is possible since increasing the SiO<sub>2</sub> content increases the surface area (N<sub>2</sub> physisorption results) which in turn improves the dispersion of the crystallites.

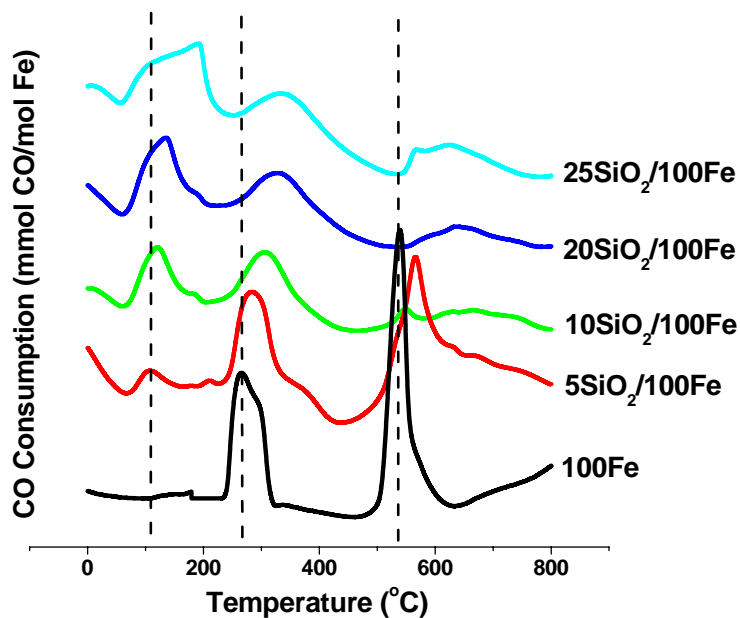


**Figure 5.2** CO TPR profiles of catalysts

It is also noticed that the first peak (for SiO<sub>2</sub> loaded catalysts) shifts to higher temperatures as the SiO<sub>2</sub> loading is increased. This is attributed to increasing Fe-SiO<sub>2</sub> interactions [17]. It is also evident that increasing the SiO<sub>2</sub> loading shifts all three peaks to higher temperatures (Table 5.4) and decreases the areas of all three peaks (Table 5.5). Again this effect is attributed to the increased Fe-SiO<sub>2</sub> interaction. It is therefore concluded that both the Fe-SiO<sub>2</sub> interaction and the iron dispersion affect the reduction and carburization behaviour of the catalyst [11, 18].

Table 5.4 Reduction temperatures for peaks of CO TPR profiles

<sup>a</sup> Catalyst composition	Peak Maximum (°C)		
	Peak 1	Peak 2	Peak 3
100Fe	-	266	536
5SiO <sub>2</sub> /100Fe	106	285	567
10SiO <sub>2</sub> /100Fe	121	304	609
20SiO <sub>2</sub> /100Fe	133	322	640
25SiO <sub>2</sub> /100Fe	186	338	640

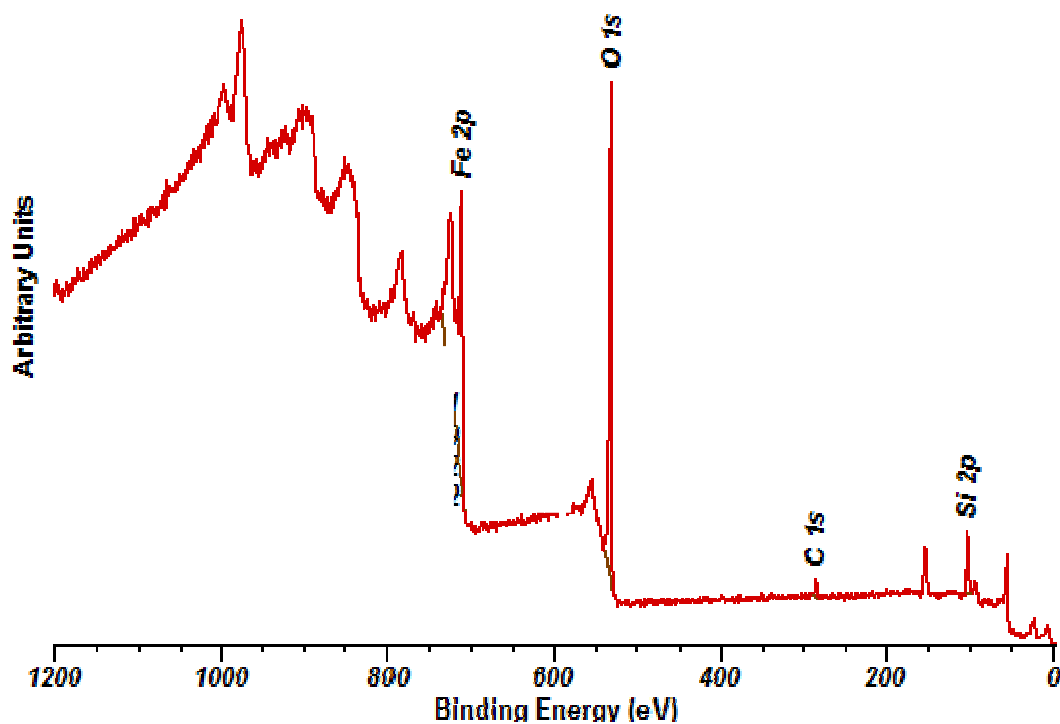
<sup>a</sup>Parts by weight

Table 5.5 Areas for peaks in Figure 5.2

<sup>a</sup> Catalyst composition	Peak Area		
	Peak 1	Peak 2	Peak 3
100Fe	-	3732	5813
5SiO <sub>2</sub> /100Fe	487	2868	2868
10SiO <sub>2</sub> /100Fe	1521	2289	2033
20SiO <sub>2</sub> /100Fe	1994	1954	1868
25SiO <sub>2</sub> /100Fe	3378	1339	1327

### 5.3.3 Surface analysis of the catalysts

The surfaces of the catalysts were studied using XPS. The regions that were looked at were the core levels of oxygen, iron and silicon, as well as C(1s) spectral regions. Survey spectra were collected for each sample and an example of this is shown in Fig. 5.3.

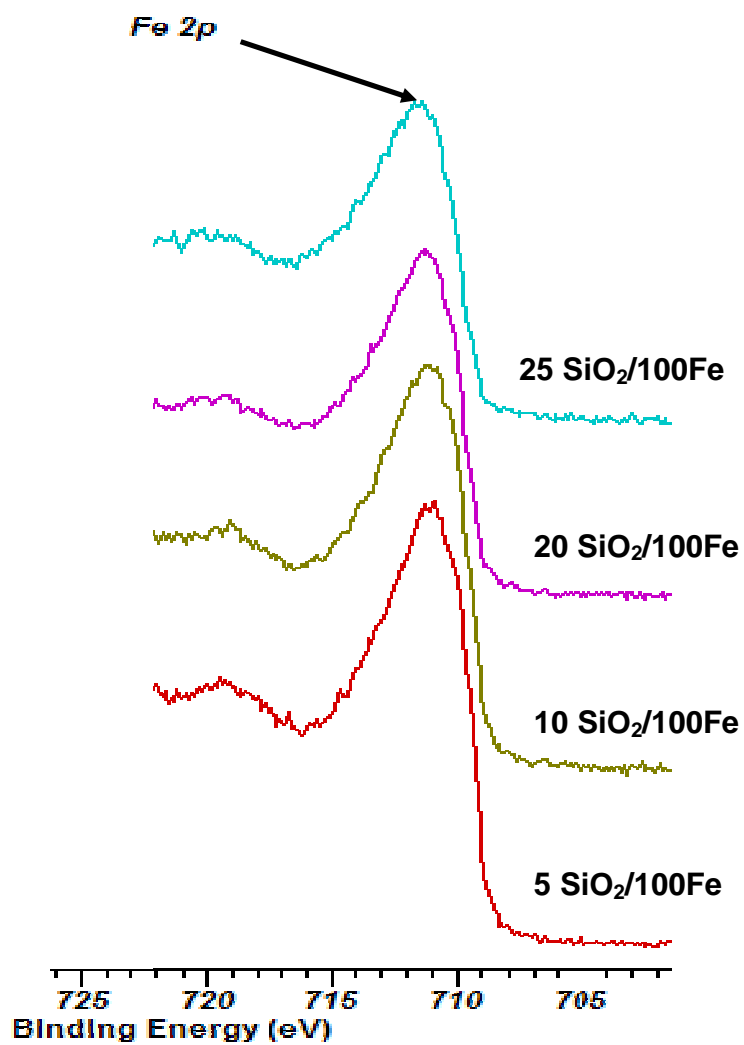


**Figure 5.3** Survey spectrum showing elements on the surface of the 5SiO<sub>2</sub>/100Fe calcined catalyst

In all the survey spectra, a peak having a binding energy of 284.7 eV (Fig. 5.3) was identified. This is assigned to adventitious carbon [37-39]. This peak was used as a reference peak for the analysis. It was also used for correction of charge compensation on the surfaces of all catalysts analysed.

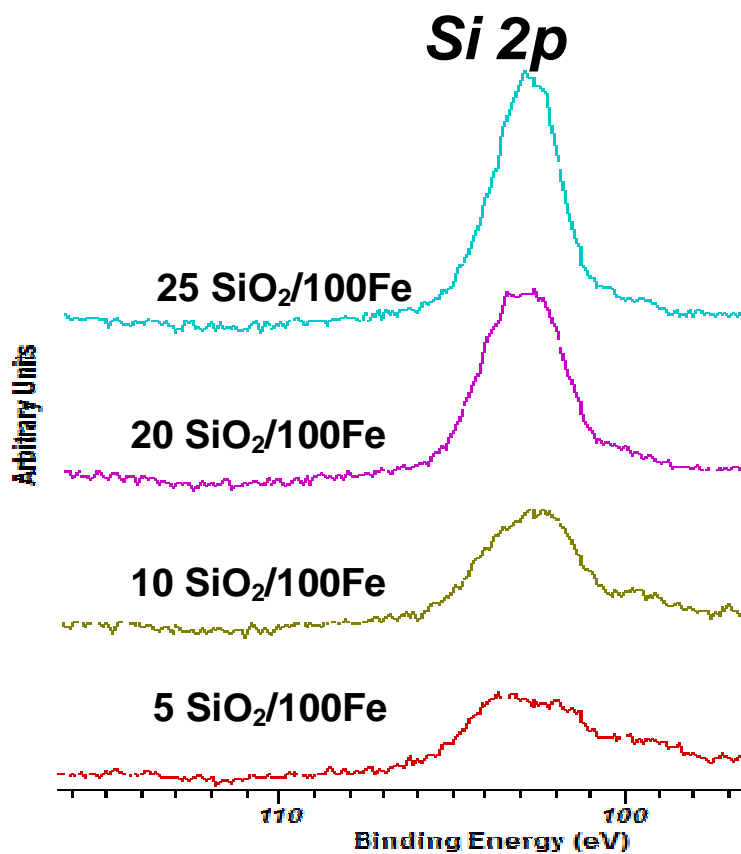
Common to all spectra, the carbon peak at 284.7 eV exhibited a shoulder at 288.2 eV. The former peak is attributed to adventitious carbon, whilst the latter is ascribed to adsorbed carbonate from reaction with CO<sub>2</sub> in the atmosphere. A peak at 529.8 eV with a shoulder at *ca.* 531 eV was identified in all the survey spectra and is clearly illustrated in Fig. 5.3. This peak is attributed to oxygen [26]. The shoulder at *ca.* 531 eV is characteristic of a more O<sup>δ-</sup> like oxygen state and is probably attributable to adsorbed surface hydroxyl groups.

The Fe (2p) spectra region (Fig. 5.4) showed a peak with binding energy in the region of 711 eV, characteristic of Fe<sub>2</sub>O<sub>3</sub> [25], in addition, the characteristic satellite for Fe(III) is clearly visible at *ca.* 719.5 eV.



**Figure 5.4** Narrow region spectrum of Fe (2p) peak for all catalysts

Fig. 5.5 shows the narrow region spectrum of the Si (2p) peak. It is observed that as the weight loading of SiO<sub>2</sub> is increased the Si (2p) peak at ~ 109.3 eV increases in size. To get a qualitative measure of the increase in size of the Si (2p) peak. The ratio of Si (2p) peak/Fe (2p) peak was calculated using the areas of the peaks. The results are shown in Table 5.6. It is noticeable from Table 5.6 that as the SiO<sub>2</sub> content is increased the ratio of the Si (2p) peak/Fe(2p) peak increases. This is indicative of the fact that more SiO<sub>2</sub> goes to the surface as its loading amount is increased. This would explain why it was extremely difficult to reduce and carburize the Fe especially at weight loadings above 10 wt. % .



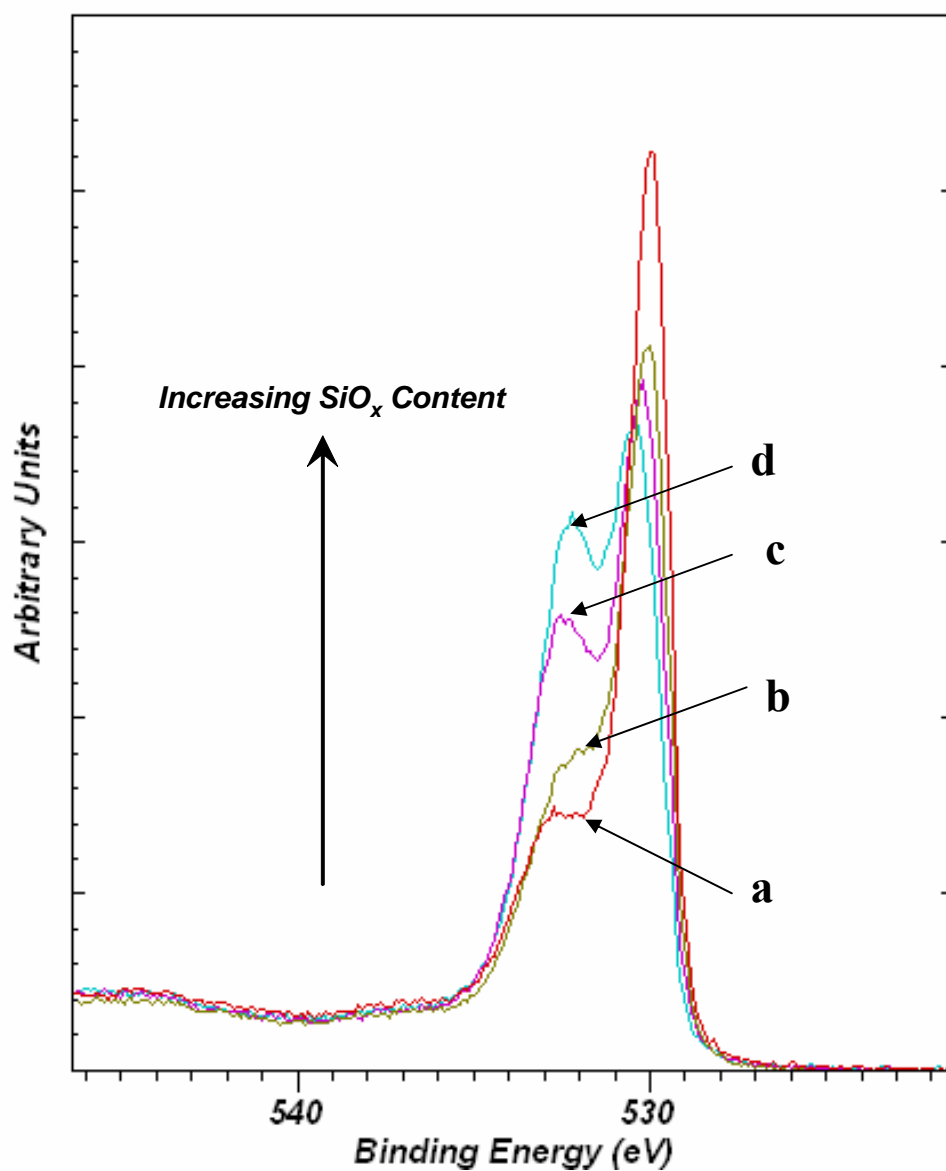
**Figure 5.5** Narrow region spectrum of Si (2p) peak for all catalysts



Table 5.6 Fe (2p) and Si (2p) peak areas for all catalysts

<sup>a</sup> Catalyst composition	Area of peak		Ratio of Si (2p) peak/ Fe (2p) peak
	Fe (2p)	Si (2p)	
5SiO <sub>2</sub> /100Fe	20723	474	0.023
10SiO <sub>2</sub> /100Fe	19177	625	0.033
20SiO <sub>2</sub> /100Fe	16818	871	0.052
25SiO <sub>2</sub> /100Fe	14191	917	0.065

The oxygen core level spectra (Fig. 5.6), shows a notable increase in the component at *ca.* 532 eV as the SiO<sub>2</sub> content of the catalyst increases. This high O (1s) binding energy is characteristic of SiO<sub>x</sub> (x=1.8 to 2) [27-30].



**Figure 5.6** Oxygen core level spectra for a) 5SiO<sub>2</sub>/100Fe b) 10SiO<sub>2</sub>/100Fe c) 20 SiO<sub>2</sub>/100Fe and d) 25SiO<sub>2</sub>/100Fe

It is clear that as the SiO<sub>2</sub> loading is increased. There is a notable increase in the amount of SiO<sub>2</sub> that goes to the surface of the catalyst. This leads to increased Fe-SiO<sub>2</sub> interactions resulting in the reduction and carburization of the catalyst to be suppressed as confirmed by the H<sub>2</sub> and CO TPR results.

### 5.3.4 Adsorption properties of the catalysts

The adsorption properties of the catalysts were studied using CO as a probe molecule. The adsorbed CO species were monitored using DRIFTS. The spectra obtained for differently SiO<sub>2</sub> loaded samples after 30 minutes of adsorption are shown in Fig. 5.7.

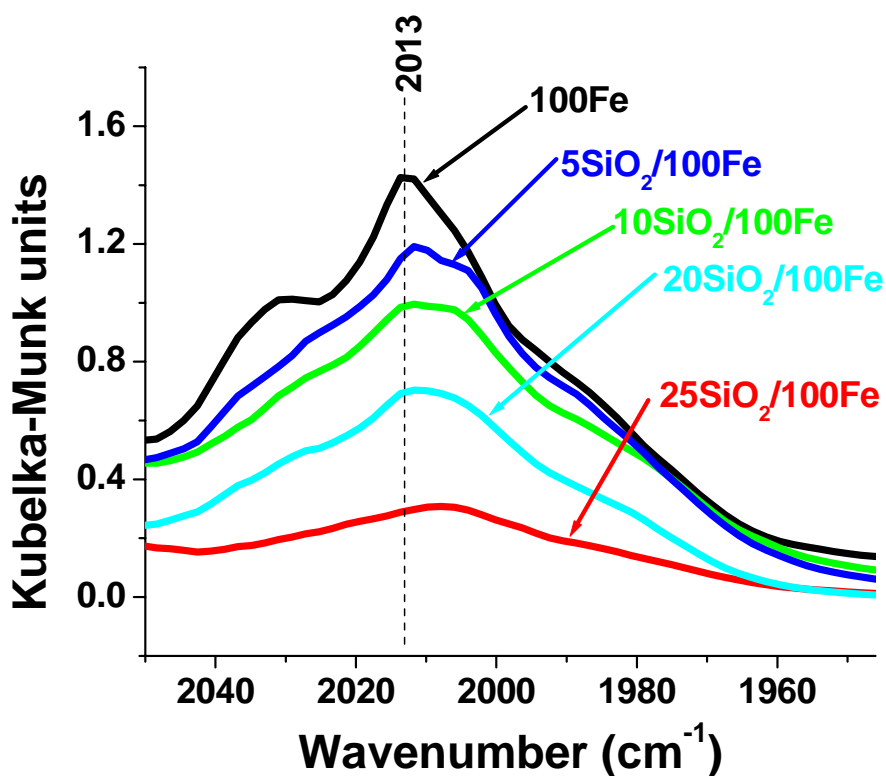


**Figure 5.7** CO adsorption spectra of all the catalysts (P = 2 bar, T = 25 °C, CO flow rate = 12 ml/min)

A band at  $2013\text{ cm}^{-1}$  could be identified for all the catalysts. It is noticeable that as the  $\text{SiO}_2$  loading is increased the intensity of this band is decreased (Fig 5.7). This indicates that fewer iron surface sites are available for binding CO, most likely due to masking by  $\text{SiO}_2$  species. This could be assumed to be the case since XPS results showed that more of the  $\text{SiO}_2$  goes to the surface as its loading amount is increased.

It is also evident from Fig. 5.7 that the addition of  $\text{SiO}_2$  shifts the band maxima to lower wavenumbers and this shift is independent of the  $\text{SiO}_2$  loading (Table 5.5).

Table 5.7 Band maxima in the wavenumber region  $2012\text{-}2015\text{ cm}^{-1}$  as a function of  $\text{SiO}_2$  loading

Catalyst	Peak maxima ( $\text{cm}^{-1}$ )
100Fe	2014
5 $\text{SiO}_2$ /100Fe	2012
10 $\text{SiO}_2$ /100Fe	2012
15 $\text{SiO}_2$ /100Fe	2012
20 $\text{SiO}_2$ /100Fe	2012
25 $\text{SiO}_2$ /100Fe	2012

It is possible that the introduction of  $\text{SiO}_2$  increases the dispersion of the  $\text{Fe}_2\text{O}_3$  crystallites (as postulated earlier). The smaller particles are more easily reduced into the iron metal phase resulting in an increased d-electron density. This in turn results in a strong Fe-C bond.

The generally accepted explanation of Fe-C bond formation of the Fe-C-O system is based on a molecular orbital model of the CO molecule. A  $\text{C} \rightarrow \text{Fe}$   $\sigma$  bond would be ineffective, being opposed by electrostatic repulsions arising from electron transfer.

An  $\text{Fe} \rightarrow \text{C}$   $\pi$  bond would be similarly ineffective. However, taken together, the two

electron transfer act in opposite directions and tend to cancel each other; Relatively strong synergetic bond processes results. The Fe  $\rightarrow$  C component arises from the availability of d-electron density from the metal which occupies an empty CO antibonding orbital. Thus as the Fe-C bond strength increases, through greater availability of d-electron density, the C-O bond strength diminishes as shown by lower C-O vibration frequencies [31].

These results may also suggest that the silica species tightly interact with the surface iron species and promote iron oxide reduction to form the fine metallic iron clusters as suggested earlier with the H<sub>2</sub>-TPR results.

### 5.3.5 FTS performance

The FTS performance of the catalysts was monitored “in-situ” using DRIFTS. Figure 5.8 below shows the C-H region of the DRIFTS spectra for all catalysts after 5 hours of reaction. Infrared absorption bands located at  $2855\text{ cm}^{-1}$  and  $2927\text{ cm}^{-1}$  can be assigned to symmetric and asymmetric stretching vibrations of  $\text{CH}_2$  groups, while the  $2960\text{ cm}^{-1}$  band is usually assumed to arise from the asymmetric stretch of  $\text{CH}_3$  groups [32]. The peak at  $3016\text{ cm}^{-1}$  is assigned to gaseous  $\text{CH}_4$  [33].

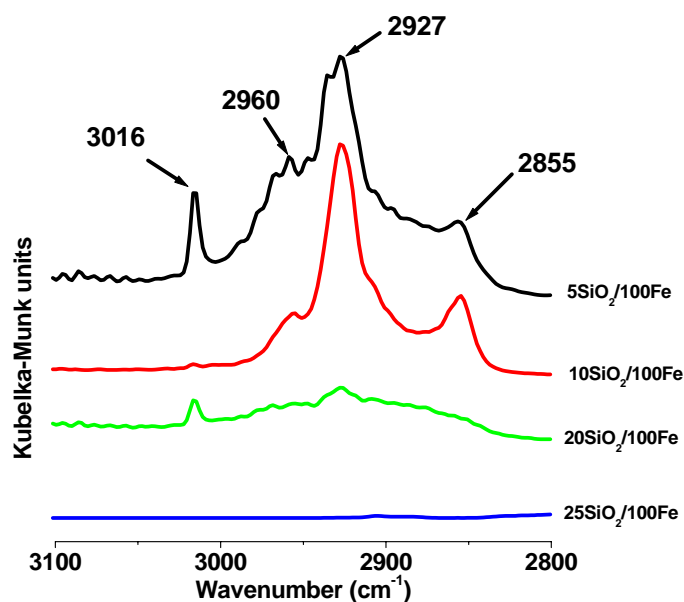


**Figure 5.8** DRIFTS spectra of all catalysts showing the C-H region after 5 hours of the FTS reaction (Reduction conditions:  $\text{H}_2/\text{CO} = 2$ ,  $P = 2\text{ Bar}$ ,  $T = 350\text{ }^\circ\text{C}$ ,  $\text{H}_2/\text{CO}$  flow rate =  $12\text{ ml/min}$ ,  $t = 1\text{ h}$ ; FTS reaction conditions:  $\text{H}_2/\text{CO} = 2$ ,  $P = 10\text{ Bar}$ ,  $T = 275\text{ }^\circ\text{C}$ ,  $\text{H}_2/\text{CO}$  flow rate =  $12\text{ ml/min}$ ,  $t = 5\text{ h}$ )

It is noticeable that as the SiO<sub>2</sub> loading is increased the intensity of C-H peaks is lowered indicating a decline in the FTS activity. These results are in agreement with H<sub>2</sub> and CO TPR results. The decrease in activity is attributed to the Fe-SiO<sub>2</sub> interaction as described earlier. This observation has been reported previously in literature [11].

It is also well known that iron carbides are the main active phases required for FTS reactions [34, 35]. CO TPR results suggest that increasing SiO<sub>2</sub> loading suppresses carburization of the precipitated Fe-based catalyst. This may mean that during syngas reduction the carburization is suppressed leading to a lower content of iron carbides. This in turn, results in lower FTS activity for catalysts with high SiO<sub>2</sub> loadings.

We also estimated the average chain length of the products produced in the FTS reaction. The estimation of the average chain distribution was done by calculating the CH<sub>2</sub>/CH<sub>3</sub> ratio using the equation illustrated below:

$$\frac{Area(-CH_2 - species)}{\epsilon_1} / \frac{Area(-CH_3 - species)}{\epsilon_2}$$

where

- 1) Area of -CH<sub>2</sub>- species is the peak at 2925-2930 cm<sup>-1</sup> which represents the asymmetric stretch of CH<sub>2</sub> species
- 2) Area of -CH<sub>3</sub> species is the peak at 2955-2960 cm<sup>-1</sup> which represents the asymmetric stretch of CH<sub>3</sub> species
- 3) ε<sub>1</sub> is the molar extinction coefficient of CH<sub>2</sub> species (75 mole<sup>-1</sup>.l.cm<sup>-1</sup>) [36]
- 4) ε<sub>2</sub> is the molar extinction coefficient of CH<sub>3</sub> species (70 mole<sup>-1</sup>.l.cm<sup>-1</sup>) [36]

It is evident that as the SiO<sub>2</sub> loading is increased the CH<sub>2</sub>/CH<sub>3</sub> ratio is decreased (Table 5.8). This equates to formation of light weight (short chain) hydrocarbons. This is in excellent agreement with work reported by other researchers who have performed full FTS reactor studies [2, 11, 18].

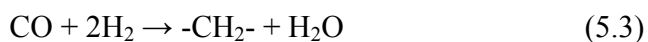
Table 5.8 Estimation of the CH<sub>2</sub>/CH<sub>3</sub> ratio as a function of SiO<sub>2</sub> loading

Catalyst	Ratio of CH <sub>2</sub> /CH <sub>3</sub>
100Fe	1
5SiO <sub>2</sub> /100Fe	4
10SiO <sub>2</sub> /100Fe	4
15SiO <sub>2</sub> /100Fe	3
20SiO <sub>2</sub> /100Fe	1
25SiO <sub>2</sub> /100Fe	-

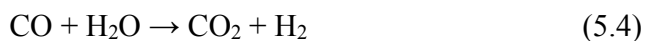
Work by Zhang et al. [11] suggests that adding SiO<sub>2</sub> to a precipitated Fe-based FTS catalyst results in enhanced high selectivity towards low weight hydrocarbons and light olefins. They attribute this to the Fe-SiO<sub>2</sub> interaction and they believe it inhibits chain growth and secondary hydrogenation reactions.

The precipitated Fe-based FTS catalyst is also known to be reactive for the Water-Gas Shift (WGS) reaction (Eq. 5.4), where H<sub>2</sub>O produced from the FTS reaction (Eq. 5.3) reacts with CO to produce H<sub>2</sub> and CO<sub>2</sub>.

FTS reaction:



WGS reaction:



The 2250-2450 cm<sup>-1</sup> region of the DRIFTS spectrum can be assigned to gaseous CO<sub>2</sub>. We notice that as the SiO<sub>2</sub> loading is increased these peaks diminish (Fig. 5.9).



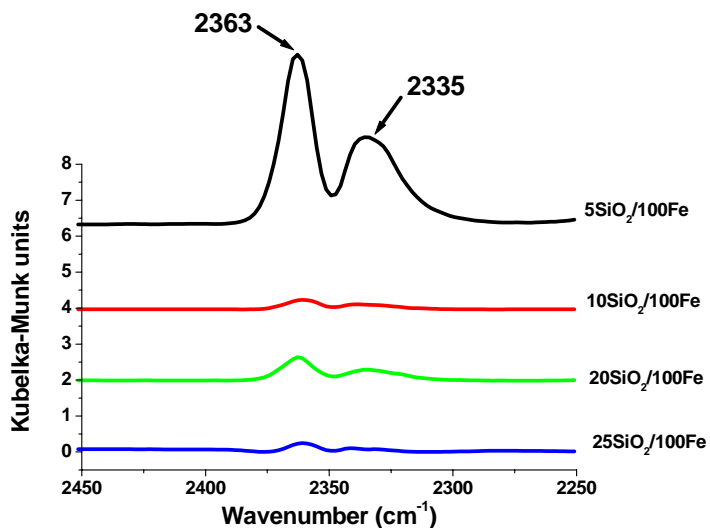


**Figure 5.9** CO<sub>2</sub> produced as a function of the SiO<sub>2</sub> content

It is also important to note that CO<sub>2</sub> can also be produced from the Boudouard reaction (Eq. 5.5), together with the carbon that deposits on the surface of the catalyst.

Boudouard reaction:



Even if the CO<sub>2</sub> was produced via this reaction clearly the addition of SiO<sub>2</sub> reduces the formation of CO<sub>2</sub>. Therefore one would assume that reaction 5.5 is also not enhanced when the SiO<sub>2</sub> content is increased.

#### ***5.4 Conclusion***

The effect of the SiO<sub>2</sub> content on a precipitated Fe-based Fischer Tropsch synthesis catalyst was investigated by comparing the textural, structural, reduction, carburization properties as well as the FTS performances. Increasing the SiO<sub>2</sub> content increased the surface area of the catalyst which improved the dispersion of the iron oxide crystallites, resulting in a decrease in the average size of the iron oxide crystallites.

But a decrease in the average size of the iron oxide crystallites strengthened the Fe-SiO<sub>2</sub> interaction, XPS surface analysis confirmed that as the SiO<sub>2</sub> loading was increased, more of the SiO<sub>2</sub> stayed on the surface allowing the Fe-SiO<sub>2</sub> interaction to be enhanced.

This resulted in the reduction and carburization ability of the catalyst to be suppressed.

This affected the FTS performance of the catalyst and lowered its activity. In general, the reduction and carburization behaviour reflects the activation capability of catalyst. Hence the effect of the Fe-SiO<sub>2</sub> interaction on the reduction/carburization behaviour, directly affects the FTS performance of the precipitated Fe-based catalyst. It therefore appears that low loadings of SiO<sub>2</sub> are required to induce chemical activation.

## References

- [1] V.U.S. Rao, G.J. Steigel, G.J. Cinquegrane, R.D. Srivastava, *Fuel Proc. Technol.* 30 (1992) 83
- [2] D.B. Bukur, C. Sivaraj, *Appl. Catal. A: Gen.* 231 (2002) 201
- [3] M.E. Dry, in *Catalysis Science and Technology* 1, J.R. Anderson, M. Boudart (Eds.), Springer, New York, 1981, p. 160
- [4] R.J. O'Brien, L. Xu, S. Bao, A. Raje, B.H. Davis, *Appl. Catal.* 196 (2000) 173
- [5] L. Guzzi, *Catal. Rev. Sci. Eng.* 23 (1981) 329
- [6] H.J. Jung, P.L. Walker, M.A. Vannice, *J. Catal.* 75 (1982) 416.
- [7] R.B. Anderson, *The Fischer–Tropsch Synthesis*, Academic Press, New York, 1984
- [8] C.H. Bartholomew, *Stud. Surf. Sci. Catal.* 64 (1990) 159
- [9] G.B. McVicker, M.A. Vannice, *J. Catal.* 63 (1980) 25
- [10] J.L. Rankins, C.H. Bartholomew, *J. Catal.* 100 (1986) 533
- [11] C.H. Zhang, H.J. Wan, Y. Yang, H.W. Xiang, Y.W. Li, *Catal. Comm.* 7 (2006) 733
- [12] Y. Yang, H.W. Xiang, L. Tian, H. Wang, C.H. Zhang, Z.C. Tao, Y.Y. Xu, B. Zhong, Y.W. Li, *Appl. Catal. A: Gen.* 284 (2005) 105
- [13] N. Egiebor, W.C. Cooper, *Can. J. Chem. Eng.* 63 (1985) 81
- [14] D.B. Bukur, X. Lang, D. Mukesh, W.H. Zimmerman, M.P. Rosynek, C. Li, *Ind. Eng. Chem. Res.* 29 (1990) 1588
- [15] P.K. Basu, S.B. Basu, S.K. Mitra, S.S. Dasandhi, S.S. Bhattacharjee, P. Samuel, *Stud. Surf. Sci. Catal.* 113 (1998)
- [16] J.J. Jothimurugesan, S.K. Spiey, S.K. Gangwal, J.G. Goodwin, *Stud. Surf. Sci. Catal.* 119 (1998) 215
- [17] W. Hou, B. Wu, X. An, T. Li, Z. Tao, H. Zheng, H. Xiang, Y. Li, *Catal. Lett.* 119 (2007) 353
- [18] W. Hou, B. Wu, Y. Yang, Q. Hao, L. Tian, H. Xiang, Y. Li, *Fuel Process. Technol.* 89 (2008) 284
- [19] K.W. Jun, H.S. Roh, K.S. Kim, J.S. Ryu, K.W. Lee, *Appl. Catal. A: Gen.* 259 (2004) 221

- [20] H. Dlamini, T. Motjope, G. Joorst, G.T. Stege, M. Mdleleni, *Catal. Lett.* 78 (2002) 201
- [21] C.H. Zhang, Y. Yang, B.T. Teng, T.Z. Li, H.Y. Zheng, H.W. Xiang, Y.W. Li *J. Catal.* 237 (2006) 405
- [22] C.N. Mbileni, *Applications of mesostructured carbonaceous materials as supports for Fischer-Tropsch metal catalyst*, PhD Thesis, University of the Witwatersrand, Johannesburg, 2006
- [23] M. Luo, R.J. O'Brein, S. Bao, B.H. Davis, *Appl. Catal. A: Gen.* 239 (2003) 111
- [24] G. Zhao, C. Zhang, S. Qin, H. Xiang, Y. Li, *J. Mol. Catal. A: Chemical* 286 (2008) 137
- [25] C.D. Wagner, W.M. Riggs, L.E. Davis, J.F. Moulder, G.E. Muilenberg, *Handbook of X-Ray Photoelectron Spectroscopy*, Perkin-Elmer Corporation, Physical Electronics Division, Eden Prairie, Minn. (1979) 55344
- [26] J.C. Dupin, D. Gonbeau, P. Vinatier, A. Levasseur, *PCCP* 2 (2000) 1319
- [27] G. Hollinger, *Appl. Surf. Sci.* 8 (1981) 318
- [28] J.R. Pitts, T.M. Thomas, A.W. Czanderna, M. Passler, *Appl. Surf. Sci.* 26 (1986) 107
- [29] J. Finster, E.-D. Klinkenberg, J. Heeg, *Vacuum* 41 (1990) 1586
- [30] A. Carnera, P. Mazzoldi, A. Boscolo-Boscoletto, F. Caccavale, R. Bertoncetto, G. Granozzi, *J. Non-cryst. Solids* 125 (1990) 293
- [31] M. J. Heal, E. C. Leisegang, R. G. Torrington, *J. Catal.* 51 (1978) 314
- [32] D. Schanke, G.R. Fredriksen, E.A. Blekkan, A. Holmen, *Catal. Today* 9 (1991) 69
- [33] G. Bian, A. Oonuki, Y. Kobayashi, N. Koizumi, M. Yamada, *Appl. Catal. A: Gen.* 219 (2001) 13
- [34] L.D. Mansker, Y. Jin, D.B. Buker, A.K. Datye, *Appl. Catal. A* 186 (1999) 277
- [35] S. Li, G.D. Meitzner, E. Iglesia, *J. Phys. Chem. B* 105 (2001) 5743
- [36] K. Nakanishi, *Infrared Absorption spectroscopy – PRACTICAL -*, Nankodo Company Limited, Japan, 1964
- [37] Y. Lei, K. Ng, L. Weng, C. Chan, L. Li, *Surf. Interface Anal.* 35 (2003) 852
- [38] D.T. Clark, A. Dilks, H.R. Thomas, *J. Polym. Sci., Polym. Chem. Ed.* 16 (1978) 1461
- [39] D.T. Clark, W.J. Feast, D. Kilcast, W.K.R. Musgrave, *J. Polym. Sci.*,

*Polym. Chem. Ed.* 11 (1973) 389

## Chapter 6

### Effect of SiO<sub>2</sub> content on a promoted precipitated iron-based Fischer-Tropsch synthesis catalyst

#### **6.1 Introduction**

There is an increasing interest in studying the structural, electronic and chemical properties of precipitated iron-based Fischer-Tropsch synthesis catalysts. In particular, the Ruhrchemie catalyst (Cu/K<sub>2</sub>O/SiO<sub>2</sub>/Fe) has received much attention due to its excellent catalytic performance.

SiO<sub>2</sub> is often incorporated into this catalyst as a structural promoter [1-4]. However, its addition suppresses the reduction as well as the activity of the catalyst due to the variations in surface structure and interaction between iron and silica [5]. To circumvent this from happening, chemical promoters such as K<sub>2</sub>O and Cu [6-8] are often added. These chemical promoters are thought to facilitate the reduction of the catalyst as well as the adsorption and dissociation of CO [9-17].

It is also well known that the intimate contacts between iron and chemical promoters result in an important influence on the catalyst activity and selectivity [8, 15, 18]. On an iron-based catalyst incorporated with SiO<sub>2</sub>, the existence of Fe-SiO<sub>2</sub> interaction has been extensively discussed in the literature [5, 19]. Nevertheless, little attention has been focused on the effect of SiO<sub>2</sub> on the interaction between iron and chemical promoters, especially for multi-component catalysts.

Also most of the studies reported have focused on the effect of SiO<sub>2</sub> as a structural promoter and not as a chemical promoter [23, 26]. The present study was undertaken to investigate the effect of SiO<sub>2</sub> content on the interaction of Fe/Cu and Fe/K<sub>2</sub>O, as well as FTS performances.

## 6.2 Experimental

All the catalysts employed in this Chapter were prepared using the precipitation method as explained in Chapter 3. Several characterisation techniques such as N<sub>2</sub> physisorption, H<sub>2</sub> TPR and “in situ” DRIFTS were employed to characterise the iron-promoters contacts and to illustrate the function of SiO<sub>2</sub> in the catalyst. The way in which the characterisation experiments were carried out is comprehensively discussed in Chapter 3. These results will be discussed first and will be followed by the results from the FTS reactor studies.

## 6.3 Results and discussion

### 6.3.1 Catalyst characterization

#### 6.3.1.1 N<sub>2</sub> physisorption

The textural properties of the catalysts were determined using N<sub>2</sub> physisorption as illustrated in Table 6.1. The effect of SiO<sub>2</sub> content on the interaction of Cu and K<sub>2</sub>O on Fe was studied. The weight loading of SiO<sub>2</sub> was varied from 1 wt. % to 10 wt. % and the amounts of Cu and K<sub>2</sub>O were kept constant (Table 6.1).

Table 6.1 The composition and textural properties of the catalysts

Catalyst (parts by weight)	Surface area (m <sup>2</sup> /g) <sup>a</sup>	Pore volume (cm <sup>3</sup> /g)
1SiO <sub>2</sub> /2K <sub>2</sub> O/5Cu/100Fe	65.2	0.14
3SiO <sub>2</sub> /2K <sub>2</sub> O/5Cu/100Fe	99.0	0.16
5SiO <sub>2</sub> /2K <sub>2</sub> O/5Cu/100Fe	130	0.17
10SiO <sub>2</sub> /2K <sub>2</sub> O/5Cu/100Fe	142	0.17

<sup>a</sup> Maximum error = ± 2 %

It is noticed that as the weight loading of SiO<sub>2</sub> is increased the total surface area of the catalyst increases. This is expected and is in agreement with work carried out by Hayakawa [20] and Hou et al. [24]. This explains the reason why SiO<sub>2</sub> is always incorporated into precipitated Fe-based FTS catalysts; the SiO<sub>2</sub> enhances the surface area of the active Fe crystallites. This surface area provided by SiO<sub>2</sub> also allows the Fe crystallites to be well dispersed and not to easily come together or sinter. Sintering produces larger Fe crystallites which are deemed less active for the FTS reaction and also lead to deactivation of the catalyst [21, 26].

### 6.3.1.2 H<sub>2</sub> TPR

The reduction behaviour of the Fe catalysts as determined using H<sub>2</sub>-TPR are shown in Fig 6.1. All Fe catalysts show two distinct peaks at 280-290 °C and 700-760 °C, which are assigned to the reduction of Fe<sub>2</sub>O<sub>3</sub> → Fe<sub>3</sub>O<sub>4</sub> and Fe<sub>3</sub>O<sub>4</sub> → Fe reactions respectively [22, 23].

Increasing the SiO<sub>2</sub> loading does not alter the reduction temperature of the first peak; in fact it is only when 10 wt. % SiO<sub>2</sub> loading is added that we see a temperature shift. Increasing SiO<sub>2</sub> loading increases the total surface area, leading to an improved dispersion of the Fe oxide crystallites.

However this has no effect on the reduction behaviour of the catalyst. The Fe<sub>3</sub>O<sub>4</sub> → Fe reduction step is represented by the second peak. This peak shifts from 760 °C when SiO<sub>2</sub> loading is 1 wt.% to 702 °C for 10 wt.% SiO<sub>2</sub> loading. Here the increased SiO<sub>2</sub> content, unexpectedly leads to an increase in reducibility.

Hou et al. [24] have found that increasing the SiO<sub>2</sub> content for a  $x\text{SiO}_2/4.2\text{K}/5\text{Cu}/100\text{Fe}$  catalyst ( $x = 15$  to  $40$ , catalyst composition based on parts by weight) facilitates the dispersion of Fe<sub>2</sub>O<sub>3</sub> and CuO and decreases the crystallite size of Fe<sub>2</sub>O<sub>3</sub>, leading to more Fe<sub>2</sub>O<sub>3</sub> being exposed to the surface of the catalyst. Other researchers have also published similar findings [25, 26].



It is also known that Cu improves the reduction of the iron oxide to metallic iron via a “spillover phenomenon” [17]. It may be that the dispersion of copper species caused by SiO<sub>2</sub> allows CuO to be easily reduced to metallic Cu allowing the crystallites formed to provide H<sub>2</sub> dissociation sites [13, 14, 16], which in turn lead to reactive hydrogen species that are able to reduce Fe oxides at lower temperatures [17].

It is also noticeable that as the SiO<sub>2</sub> loading is increased, the total area under the two peaks gets smaller. In fact the area under the two peaks represents the amount of H<sub>2</sub> being consumed during the reduction reaction. To quantitatively get a better sense of the amount of H<sub>2</sub> being consumed. The area of each peak was measured for each TPR profile. The area under peak 1 represents the Fe<sub>2</sub>O<sub>3</sub> → Fe<sub>3</sub>O<sub>4</sub> reduction step and the area under peak 2 illustrates the Fe<sub>3</sub>O<sub>4</sub> → Fe reduction step.

The results of these calculations are displayed in Table 6.2. It is noticed that as the SiO<sub>2</sub> loading is increased the area of peak 1 increases while the area of peak 2 decreases.

These results imply that SiO<sub>2</sub> favours the reduction of Fe<sub>2</sub>O<sub>3</sub> → Fe<sub>3</sub>O<sub>4</sub> but restrains the reduction of Fe<sub>3</sub>O<sub>4</sub> → Fe. The results may also mean that as the SiO<sub>2</sub> loading is increased it becomes extremely difficult to completely reduce the Fe<sub>2</sub>O<sub>3</sub> phase to the metallic Fe phase or the increment of SiO<sub>2</sub> loading results in the amount of available iron oxide for reduction to be decreased. It is to be noted that increasing the SiO<sub>2</sub> content may lead to increased Fe-SiO<sub>2</sub> interaction and this could have also played a role in restraining the Fe<sub>3</sub>O<sub>4</sub> → Fe reaction.

Overall the reduction of the Fe catalyst becomes difficult as shown by a decrease in the total area of peaks with increasing SiO<sub>2</sub> content. This would make sense and may mean that more of the SiO<sub>2</sub> is located at the surface masking some of the iron oxide species, making it difficult for reactive H<sub>2</sub> species to interact with them. Certainly XPS surface analysis experiments would be required to back this assertion.

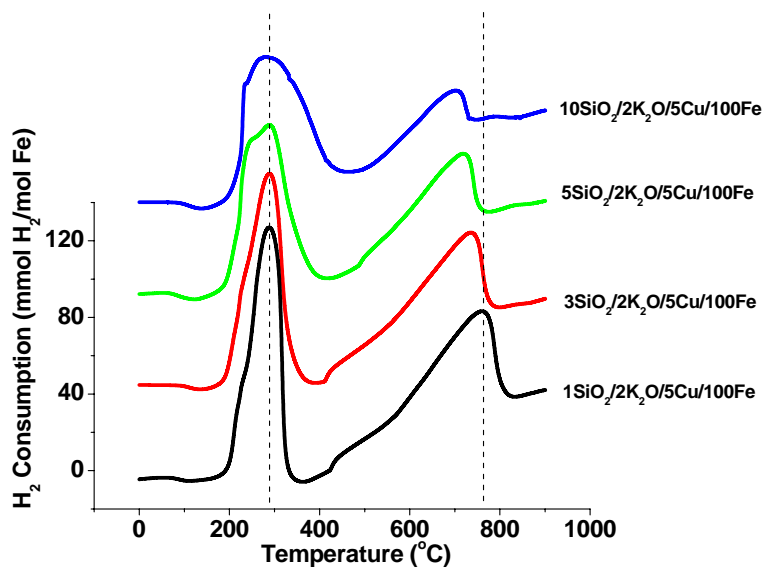


**Figure 6.1** H<sub>2</sub> TPR profiles for all catalysts

Table 6.2 Reduction temperatures for peak 1 and peak 2 as well as their areas

Catalyst composition	Reduction		Areas		
	Temperature [°C]		Peak 1	Peak 2	Total Area
	Peak 1	Peak 2			
1SiO <sub>2</sub> /5Cu/2K <sub>2</sub> O/100Fe	288	760	10300	8905	19205
3SiO <sub>2</sub> /5Cu/2K <sub>2</sub> O/100Fe	288	735	10967	8001	18968
5SiO <sub>2</sub> /5Cu/2K <sub>2</sub> O/100Fe	289	718	11211	7201	18412
10SiO <sub>2</sub> /5Cu/2K <sub>2</sub> O/100Fe	281	702	11271	6210	17481

Total area = Area of Peak 1 + Area of Peak 2

### 6.3.1.3 “In situ” CO adsorption using DRIFTS

CO adsorption measurements were carried out as outlined in Chapter 3. The results are illustrated in Figures 6.2 and 6.3. Fig 6.2 compares CO adsorption on all the catalysts studied. It is evident that two CO bands were identified for all the catalysts. These two bands (2014 and 2034  $\text{cm}^{-1}$ ) can be assigned to CO linearly bound to a Fe (0) species [27].

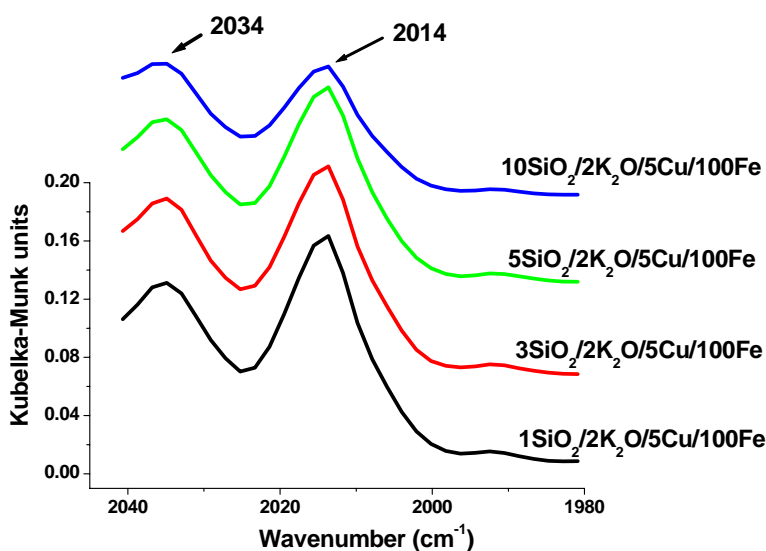


**Figure 6.2** CO adsorption on all the catalysts; Conditions: CO reduction for 1 hour (Flow rate = 12 ml/min, T = 350°C, P = 2 bar), CO adsorption for 30 min (CO Flow rate = 12 ml/min, T = 25°C, P = 2 bar)

This Fe<sup>0</sup> species may be Fe carbides or metallic Fe [30]. This is possible since Fe carbides can directly form from iron oxides or via the carburization of metallic iron [23].

The reason why it is difficult to differentiate between metallic Fe species and Fe carbide species is because the adsorption features of probe molecules on iron carbides are quite

similar to those on metallic iron particles. This is greatly supported by the adsorption features of CO on H<sub>2</sub> reduced iron samples performed in our lab (not reported herein). Also Bian et al [30] have shown that the adsorption of CO on the iron carbide phase produces adsorption bands with only a small shift in wavenumber from that on metallic iron.

So the CO species at 2014 and 2034 cm<sup>-1</sup> may represent the adsorption of CO on Fe-carbides. This has been reported before by Bian et al. [30]. Unfortunately bridged CO species could not be identified. They normally appear in the wavenumber region 1800 – 2000 cm<sup>-1</sup>) [28, 29].

The intensity of the peak at 2014 cm<sup>-1</sup> was compared for all the catalysts. This is illustrated in Fig 6.3. It was found that as the SiO<sub>2</sub> loading is increased above 3 wt. %, the intensity of this peak decreases. This means that increasing the SiO<sub>2</sub> loading above 3 wt. % results in the decrease of Fe<sup>0</sup> type species. Obviously this would mean a smaller number of Fe<sub>2</sub>O<sub>3</sub> crystallites were present at the surface, when they were exposed to CO reduction. This result ties in well with postulation made earlier on (for the H<sub>2</sub>-TPR results) that SiO<sub>2</sub> interacts with the iron oxide crystallites, leading to a decreased reduction of the iron oxide species.

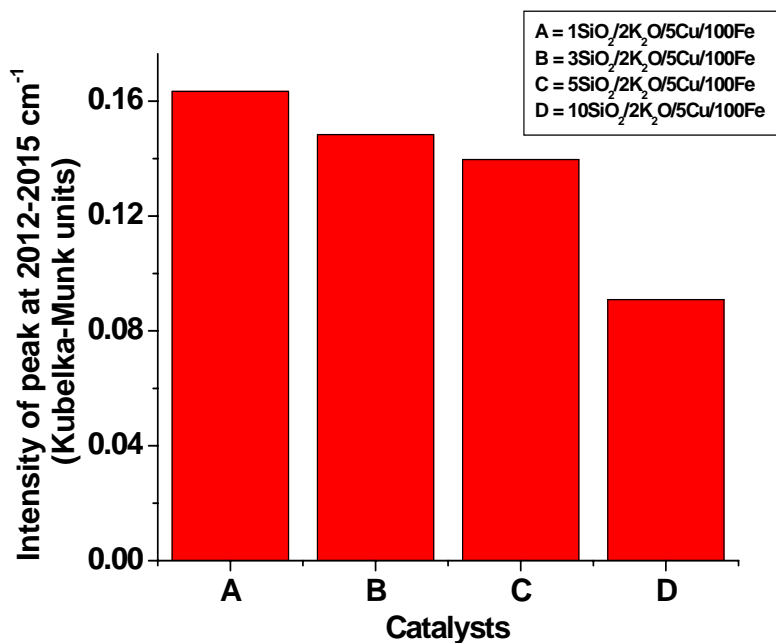


**Figure 6.3** Comparing the intensity of peak at 2014 cm<sup>-1</sup> for all the catalysts

It is also well known that K<sub>2</sub>O increases the extent of CO adsorption for iron based catalysts [13, 31] and this is due to Fe coming into contact with K<sub>2</sub>O [26]. A decrease in intensity of the peak at 2014 cm<sup>-1</sup> as the SiO<sub>2</sub> loading is increased, suggests that the incorporation of SiO<sub>2</sub> into the catalyst overwhelms the effect of the Fe/K<sub>2</sub>O contact. In summary – a clear relationship between SiO<sub>2</sub> and CO adsorption exists and that is, increasing the SiO<sub>2</sub> loading suppresses the adsorption of CO.

### 6.3.1.4 “In situ” FTS using DRIFTS

Fischer Tropsch synthesis reactions were also performed using the DRIFTS reactor. They were monitored in-situ. Only the wavenumber region 2800-3100  $\text{cm}^{-1}$  which showcases the production of C-H type species will be presented here. Hydrocarbons produced from the FTS reaction can be monitored using this part of the DRIFTS spectrum. The spectra for all catalysts after 5 hours of reaction are illustrated in Fig. 6.4.

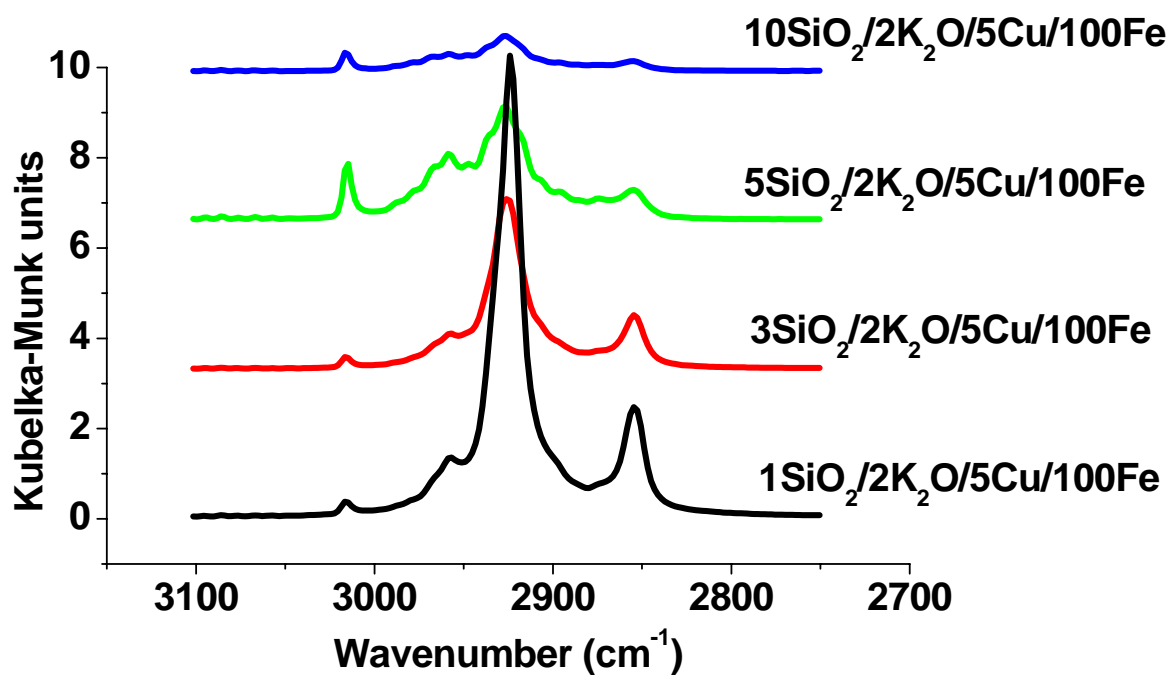


**Figure 6.4** DRIFTS spectra showcasing FTS reactions for all catalysts;

Conditions: Reduction for 1 hour ( $\text{H}_2/\text{CO} = 2/1$ , Flow rate = 12 ml/min,  $T = 350^\circ\text{C}$ ,  $P = 2$  bar), FTS reaction for 5 hours ( $\text{H}_2/\text{CO} = 2/1$ , Flow rate = 12 ml/min,  $T = 275^\circ\text{C}$ ,  $P = 10$  bar)

When the loading of SiO<sub>2</sub> is increased the intensities of C-H peaks are lowered. This invariably means that SiO<sub>2</sub> lowers the production of the C-H species. It also suggests that the Fe-SiO<sub>2</sub> interaction is more expected than Fe/Cu and Fe/K<sub>2</sub>O interactions. This postulation is further confirmed in Fig. 6.5 where spectra showcasing SiO<sub>2</sub> containing catalysts are compared to a catalyst only containing Cu and K<sub>2</sub>O. It is clear from Fig. 6.5 that SiO<sub>2</sub> does inhibit the Fe/Cu and Fe/K<sub>2</sub>O interactions. The intensity of the C-H species are drastically lowered immediately after the addition of 1 wt. % SiO<sub>2</sub> and becomes worse with higher loadings of SiO<sub>2</sub>.

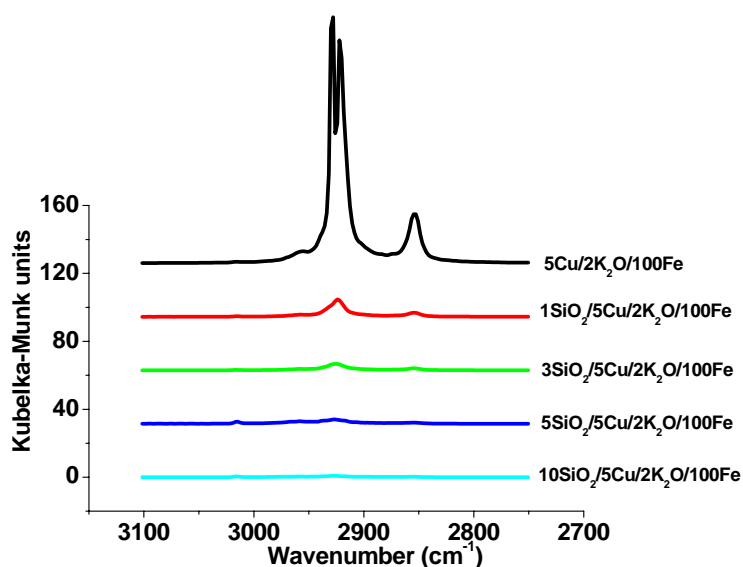
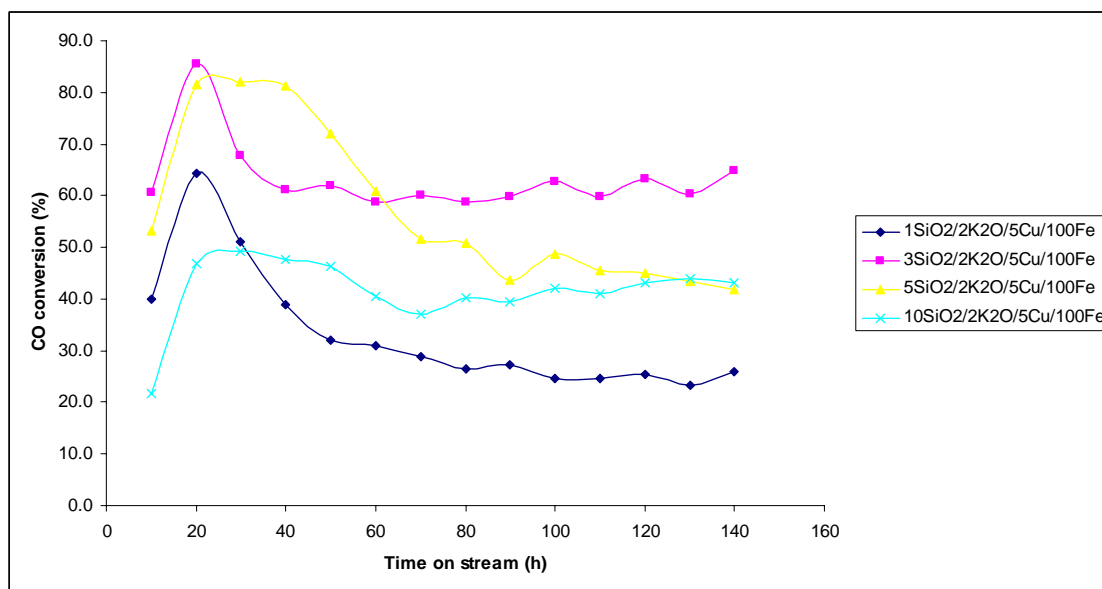


**Figure 6.5** DRIFTS spectra comparing FTS reactions for SiO<sub>2</sub> loaded catalysts to a non-loaded SiO<sub>2</sub> catalyst; Conditions: Reduction for 1 hour (H<sub>2</sub>/CO = 2/1, Flow rate = 12 ml/min, T = 350 °C, P = 2 bar), FTS reaction for 5 hours (H<sub>2</sub>/CO = 2/1, Flow rate = 12 ml/min, T = 275°C, P = 10 bar)



### 6.3.2 FTS reactor studies

The carbon monoxide (CO) and hydrogen (H<sub>2</sub>) conversions with time on stream for all catalysts are displayed in Fig. 6.6, Fig 6.8 and Table 6.2. It can be seen from Figure 6.6 and 6.8 that increasing the SiO<sub>2</sub> content has an effect on both CO and H<sub>2</sub> conversions. To get a sense of this effect, CO and H<sub>2</sub> conversion values at steady state conditions (constant CO and H<sub>2</sub> conversion) were plotted for all the catalysts. These plots are illustrated by Figures 6.7 and 6.9. Fig. 6.7 shows the CO conversion for all catalysts and it is noticeable that CO conversion goes through a maximum at 3 wt. % SiO<sub>2</sub> loading. The same trend is observed with the H<sub>2</sub> conversion plot (Fig 6.9). At a fixed set of process conditions, the CO conversion can be used as an indication of FTS activity [24]. So it is clear that 3 wt. % SiO<sub>2</sub> leads to the maximum activity when incorporated into an Fe-based catalyst. Even before steady state is reached the 3 wt. % SiO<sub>2</sub> loaded catalyst has the highest activity (Fig. 6.6).



Figures 6.6 The carbon monoxide conversion with time on stream for all catalysts

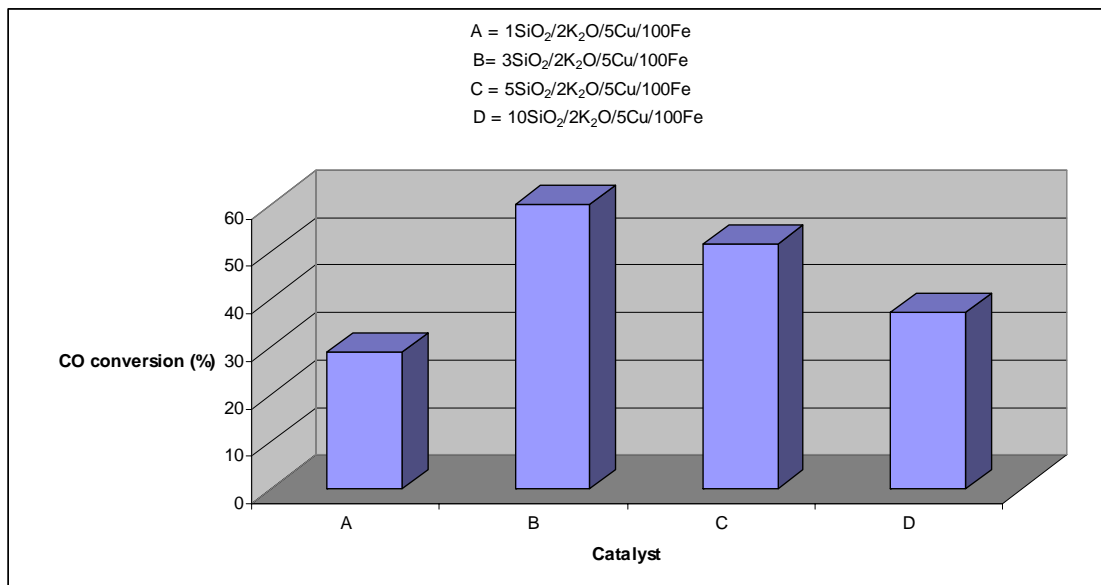
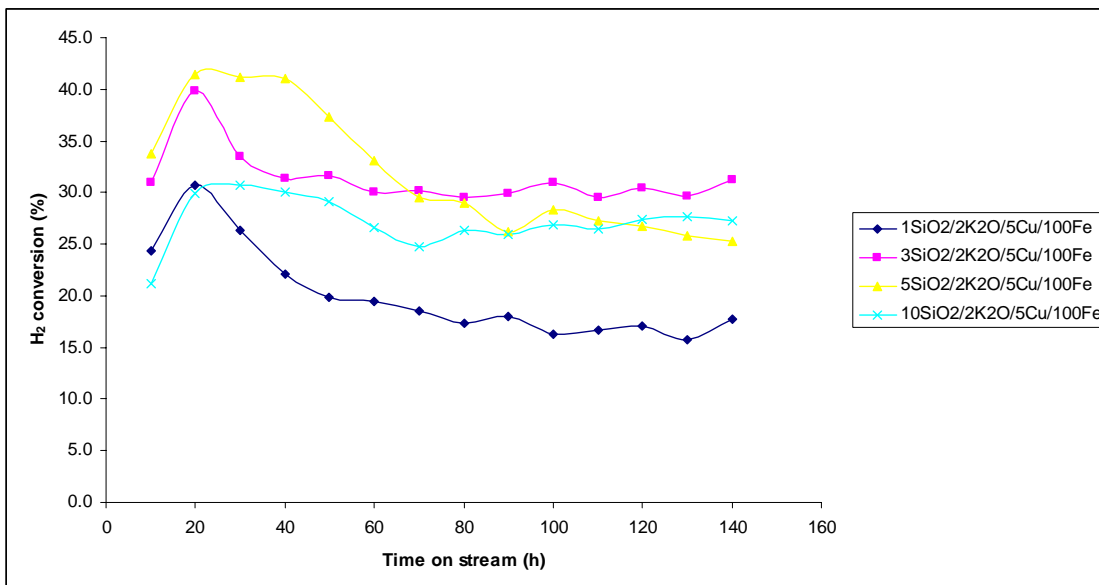


**Figure 6.7** Comparing CO conversion for all catalysts at steady state conditions

It is also interesting to note that the 3 wt. % SiO<sub>2</sub> loaded catalyst reaches stability fairly quickly and appears to be more stable on stream for a long time when compared to the other catalysts. Another interesting observation on the stability of all the catalysts is that the 3 wt. % and 5 wt. % SiO<sub>2</sub> loaded catalysts have similar maximum activities before reaching steady state. But the activity of 1 wt. % SiO<sub>2</sub> loaded catalysts continues to decrease with time on stream whereas the activity of the 10 wt. % SiO<sub>2</sub> remains stable and tends to increase with time on stream. This clearly illustrates that increasing the loading amount of SiO<sub>2</sub> improves the catalyst's stability.



Figures 6.8 The hydrogen conversion with time on stream for all catalysts

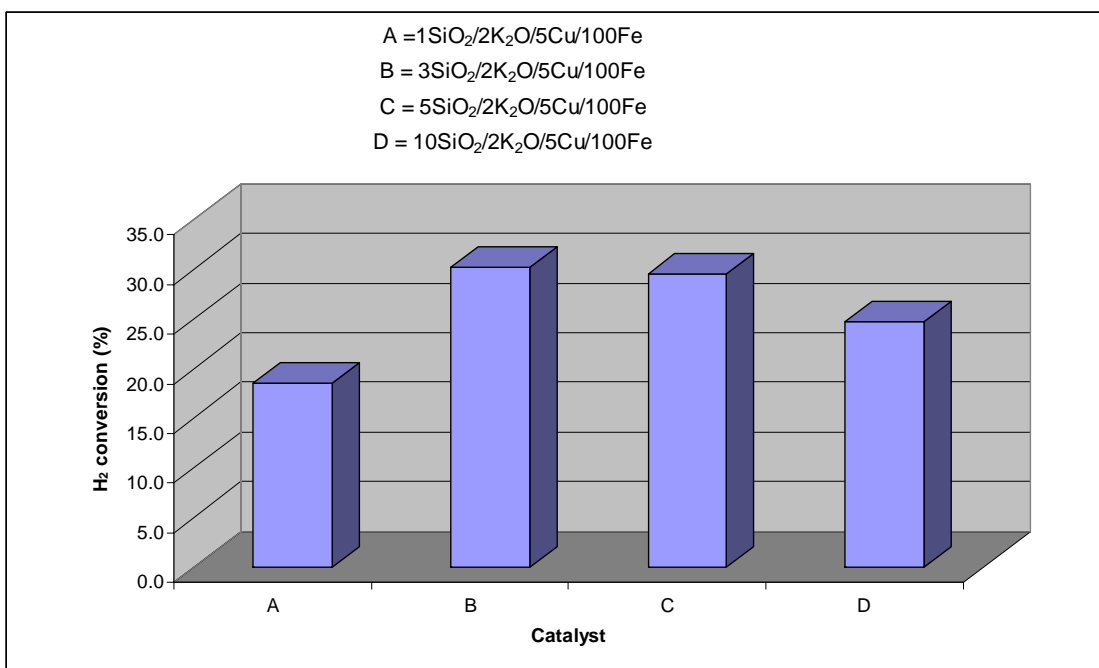


Figure 6.9 Comparing H<sub>2</sub> conversion for all catalysts at steady state conditions

Table 6.3 Reaction performances of all catalysts at steady state conditions

Catalyst <sup>a</sup>	1SiO <sub>2</sub> /100Fe	3SiO <sub>2</sub> /100Fe	5SiO <sub>2</sub> /100Fe	10SiO <sub>2</sub> /100Fe
<b>CO conversion (%)</b>	28.9	60.0	51.6	37.1
<b>H<sub>2</sub> conversion (%)</b>	18.5	30.2	29.5	24.8
<b>Rate CO (mol/s)</b>	-7.3 x 10 <sup>-7</sup>	-1.9 x 10 <sup>-6</sup>	-1.1 x 10 <sup>-6</sup>	-1.0 x 10 <sup>-6</sup>
<b>Rate CO<sub>2</sub> (WGS) (mol/s)</b>	1.95 x 10 <sup>-7</sup>	7.0 x 10 <sup>-7</sup>	3.34 x 10 <sup>-7</sup>	3.58 x 10 <sup>-7</sup>
<b>Rate FT</b>	5.39 x 10 <sup>-7</sup>	1.16 x 10 <sup>-6</sup>	7.95 x 10 <sup>-7</sup>	6.67 x 10 <sup>-7</sup>
<b>Activity (μmol/sec.gFe)</b>	7.34	18.6	11.3	10.2
<b>α</b>	0.69	0.64	0.68	0.61
<b>C<sub>2</sub> olefin %<sup>b</sup></b>	39.7	45.2	44.1	34.3
<b>Selectivity</b>				
<b>C<sub>1</sub></b>	19.3	19.8	20.4	23.3
<b>C<sub>2</sub>-C<sub>4</sub></b>	36.9	43.1	40.7	42.7
<b>C<sub>5</sub>-C<sub>11</sub></b>	38.2	31.2	33.4	28.0
<b>C<sub>12</sub><sup>+</sup></b>	4.40	4.56	4.46	4.49
<b>CO<sub>2</sub></b>	2.88	10.3	4.92	5.28

<sup>a</sup> All catalysts contained 2K<sub>2</sub>O and 5Cu

<sup>b</sup> C<sub>2</sub> = / (C<sub>2</sub> + C<sub>2</sub>=) [olefin to total C<sub>2</sub> hydrocarbon weight ratio]

Data consists of ± 5% experimental error

**Catalyst mass:** 0.1 g

**Reduction:** CO, flow rate = 12 ml/min, t = 20-24 h, T = 350 °C, P = 2 bar

**Reaction conditions:** H<sub>2</sub>/CO = 2, flow rate = 12 ml/min, t = 140 h, T = 275 °C, P = 10 bar

The effect of silica content on the product selectivity in the FTS reaction is shown in Table 6.3. It can be seen that SiO<sub>2</sub> loading greater than 1 wt. % increases selectivity to C<sub>2</sub>-C<sub>4</sub> hydrocarbons. It can also be noticed that the highest loading of SiO<sub>2</sub> (10 wt. %) gives the highest the methane selectivity and the lowest selectivity to C<sub>5</sub>-C<sub>11</sub> hydrocarbons and C<sub>2</sub> olefins. The  $\alpha$  value (0.61) for this catalyst is also the lowest. All of these results imply that chain growth is restrained whereas the hydrogenation reaction is enhanced. This could be attributed to SiO<sub>2</sub> retarding the Fe/K<sub>2</sub>O interaction, since potassium is known to promote the chain propagation reaction and olefin selectivity [8, 12, 25, 32, 37].

It has also been reported that potassium enhances the dissociative adsorption of CO and suppresses H<sub>2</sub> adsorption. Because it is an alkali promoter, it increases the basicity of the iron surface leading to increased CO adsorption [26, 33]. These chemical effects lead to the promotion of chain growth and olefin selectivity.

Previous reports have also suggested that K<sub>2</sub>O can interact with SiO<sub>2</sub> and this may lead to the promotional effect of potassium on FTS activity and selectivity to be decreased [8, 33, 34, 35, 36]. It is logical to think that a K<sub>2</sub>O-SiO<sub>2</sub> interaction could suppress the promotional effect of potassium since SiO<sub>2</sub> is acidic in nature [33]. This means that the interaction of SiO<sub>2</sub> with K<sub>2</sub>O could decrease the basicity of the iron surface, leading to the dissociative adsorption of CO to be suppressed, thereby retarding the chain growth reaction [20, 26]. This will result in a lower coverage of carbon species on the Fe surface whereas the H<sub>2</sub> present will enhance chain termination rates and the production of light paraffins due to olefins being hydrogenated [26].

CO adsorption results presented earlier demonstrated that as the SiO<sub>2</sub> content is increased the adsorption ability of the Fe surface is decreased. This may serve as evidence that as the K<sub>2</sub>O-SiO<sub>2</sub> interaction increases the Fe-K<sub>2</sub>O interaction diminishes.

#### **6.4 Conclusion**

The effect of SiO<sub>2</sub> content on an unpromoted precipitated iron-based catalyst was studied in the previous chapter. Interesting observations were noted and were all attributed to the presence of SiO<sub>2</sub>. In this chapter the effect of SiO<sub>2</sub> content on the promoted precipitated iron-based catalyst was studied. Incorporation of SiO<sub>2</sub> to the promoted precipitated iron-based catalyst was found to have a significant influence into the reduction and adsorption behaviours, as well as the catalytic activity of the catalyst. The changes in catalytic activity could primarily be attributed to the effects of SiO<sub>2</sub> on the Fe/Cu and Fe/K<sub>2</sub>O interactions, which led to different degrees of H<sub>2</sub> reduction and CO adsorption and further significantly affected the FTS performances of the catalyst.

SiO<sub>2</sub> stabilized the iron oxide crystallites by providing adequate surface area. This facilitated the high dispersion of Fe<sub>2</sub>O<sub>3</sub> and CuO and enhanced the contact between Fe<sub>2</sub>O<sub>3</sub> and CuO. The enhanced Fe/Cu contact promoted the reduction of Fe<sub>2</sub>O<sub>3</sub> to Fe<sub>3</sub>O<sub>4</sub>, whereas the transformation of Fe<sub>3</sub>O<sub>4</sub> to Fe was suppressed. Furthermore, due to the K<sub>2</sub>O-SiO<sub>2</sub> interaction, the catalyst loaded with 10 wt. % SiO<sub>2</sub> (highest SiO<sub>2</sub> loading) had a weak contact between Fe and K<sub>2</sub>O, which reduced the surface basicity of the catalyst and severely suppressed the CO adsorption.

In the FTS reaction, the FTS activity went through a maximum at 3 wt. % loading of SiO<sub>2</sub> and further increments of SiO<sub>2</sub> loading decreased the catalyst activity. The SiO<sub>2</sub> content also affected the hydrocarbon selectivity. At the highest SiO<sub>2</sub> loading, the product distribution shifted to light hydrocarbons and the C<sub>5</sub>-C<sub>11</sub> hydrocarbons and C<sub>2</sub> olefins selectivity were suppressed.

## References

- [1] M.A. Vannice, R.L. Garten, *J. Catal.* 66 (1980) 242
- [2] H.J. Jung, P.L. Walker, M.A. Vannice, *J. Catal.* 75 (1982) 416
- [3] H.N. Pham, A. Viergutz, R. Gormley, A.K. Datye, *Powder Technol.* 110 (2000) 196
- [4] R. Zhao, J.G. Goodwin, K. Jothimurugesan Jr., S.K. Gangwal, J.J. Spivey, *Ind. Eng. Chem. Res.* 40 (2001) 1065
- [5] C.H. Zhang, H.J. Wan, Y. Yang, H.W. Xiang, Y.W. Li, *Catal. Comm.* 7 (2006) 733
- [6] A.F.H. Wielers, A.J.H.M. Kock, C.E.A. Hop, J.W. Geus, A.M. van der Kraan, *J. Catal.* 117 (1989) 1
- [7] M.V. Cagnoli, S.G. Marchetti, N.G. Gallegos, M. Alvarez, R.C. Mercader, A.A. Yeramian, *J. Catal.* 123 (1990) 21
- [8] D.B. Bukur, X. Liang, D. Mukesh, W.H. Zimmerman, M.P. Rosynek, C. Li, *Ind. Eng. Chem. Res.* 29 (1990) 1588
- [9] M.E. Dry, G.J. Oosthuizen. *J. Catal.* 11 (1968) 18
- [10] M.E. Dry, T. Shingles, L. Boshoff, G.J. Oosthuizen. *J. Catal.* 15 (1969) 190
- [11] J. Benziger, R. Madix, *Surf. Sci.* 94 (1980) 119
- [12] D.B. Bukur, D.S. Mukesh, S.A. Patel, *Ind. Eng. Chem. Res.* 29 (1990) 194
- [13] R. J. O'Brein, L. Xu, R. L. Spicer, S. Bao, D. R. Milburn, B. H. Davis, *Catal. Today* 36 (1997) 325
- [14] S. Li, A. Li, S. Krishnamoorthy, E. Iglesia *Catal. Lett.* 77 (4) (2001) 197
- [15] Y. Jin, A.K. Datye, *J. Catal.* 196 (2000) 8
- [16] R.J. O'Brein, B.H. Davis, *Catal. Lett.* 94 (2004) 1
- [17] I.E. Wachs, D.J. Dwyer, E. Iglesia, *Appl. Catal.* 12 (1995) 35
- [18] Y. Yang, H.W. Xiang, Y.Y. Xu, L. Bai, Y.W. Li, *Appl. Catal. A: Gen.* 266 (2004) 181
- [19] W. Hou, B. Wu, X. An, T. Li, Z. Tao, H. Zheng, H. Xiang, Y. Li, *Catal. Lett.* 119 (2007) 353
- [20] H. Hayakawa, H. Tanaka, K. Fujimoto, *Appl. Catal. A: Gen.* 328 (2007) 117

- [21] B.H. Davis, E. Iglesia, *Technology Development for Iron and Cobalt Fischer-Tropsch Catalysis*, Final Report, Contract No. DE-FC26-98FT40308, University of Kentucky Research Foundation, Lexington, 2002
- [22] R. Brown, M.E. Cooper, D.A. Whan, *Appl. Catal.* 3 (1982) 177
- [23] D.B. Bukur, C. Sivaraj, *Appl. Catal. A Gen.* 231 (2002) 201
- [24] W. Hou, B. Wu, Y. Yang, Q. Hao, L. Tian, H. Xiang, Y. Li, *Fuel Process. Technol.* 89 (2008) 284
- [25] Y. Yang, H.W. Xiang, L. Tian, H. Wang, C.H. Zhang, Z.C. Tao, Y.Y. Xu, B. Zhong, Y.W. Li, *Appl. Catal. A: Gen.* 284 (2005) 105
- [26] H.J. Wan, B.S. Wu, Z.C. Tao, T.Z. Li, X. An, H.W. Xiang, Y.W. Li, *J. Mol. Catal. A: Chemical* 260 (2006) 255
- [27] A.F.H. Wielers, A.J.H.M. Kock, C.E.C.A. Hop, J.W. Geus, A.M. Van der Kraan, *J. Catal.* 117 (1989) 1
- [28] M.J. Heal, E.C. Leisegang, R. Torrington, *J. Catal.* 51 (1978) 314
- [29] G. Blyholder, L.D. Neff, *J. Phys. Chem.* 66 (1962) 1464
- [30] G. Bian, A. Oonuki, Y. Kobayashi, N. Koizumi, M. Yamada, *Appl. Catal. A: Gen.* 219 (2001) 13
- [31] D.G. Miller, M. Moskovits, *J. Phys. Chem.* 92 (1998) 6081
- [32] S. Mørup, H. Topsøe, *Appl. Phys.* 11 (1976) 63
- [33] G. Zhao, C. Zhang S. Qin, H. Xiang, Y. Li, *J. Mol. Catal. A: Chemical* 286 (2008) 137
- [34] M.E. Dry, *Catal. Today* 71 (2002) 227
- [35] M.E. Dry, in: J.R. Anderson, M. Boudart (Eds.), *Catalysis Science and Technology*, Vol. 1, Springer, New York, 1981, p. 160.
- [36] M.E. Dry, *Catal. Lett.* 7 (1990) 241
- [37] T.J. Donnelly, C.N. Satterfield, *Appl. Catal.* 52 (1989) 93



## Chapter 7

### Evaluating indium as a chemical promoter in Fe-based Fischer-Tropsch synthesis

#### **7.1 Introduction**

Although the impact of copper as a promoter on the activity of Fe-based catalysts has been extensively studied, amazingly, the effects of few other potential promoters have not been significantly investigated or compared directly to the effects caused by copper when carrying out a systematic study. In this study the impact of adding indium as a promoter (which is suspected to have similar chemical properties to copper) on the catalytic properties of precipitated bulk Fe-based catalysts was investigated using the same preparation method and reaction conditions.

Copper is normally added to Fe-based Fischer Tropsch catalysts as a chemical promoter. It is added to enhance hematite reducibility [1]. When copper oxide is reduced to metallic Cu, the crystallites formed provide H<sub>2</sub> dissociation sites [1-4], which in turn lead to reactive hydrogen species that are able to reduce Fe oxides at lower temperatures. This phenomenon is often referred to as H<sub>2</sub> spillover [5]. Increased loading of copper onto Fe FTS catalysts increases the FTS rate as well as the water gas shift (WGS) reaction [3]. Copper also has a positive effect on product selectivity over a wide range of conversions [2].

Work carried out by several researchers over the years has highlighted relationships that exist between various elements of the periodic table. A less known relationship is the “*Knight’s Move relationship*” [6]. It takes its name from the knight’s move in the game of chess, referring to a move of one step in any direction followed by two steps in a direction at right angles to the first movement (Fig. 7.1).

Cu	Zn	Ga				
Ag	Cd	In	Sn	Sb		
Au	Hg	Tl	Pb	Bi	Po	
				114		

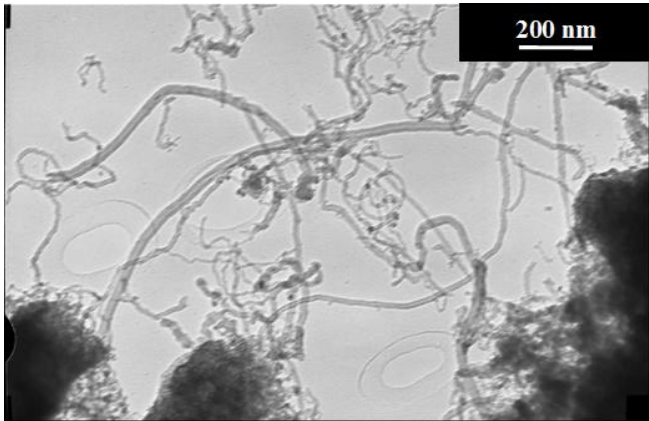
**Figure 7.1** Elements that show knight's move relationships (after E.R. Scerri [6])

Fig. 7.1 suggests that elements like Zn and Sn should show a “*Knight's Move relationship*” and have similar properties [7]. For example both are used for plating steel such as in the case of food cans [6]. Not only do layers of both metals successfully delay the onset of corrosion in the iron, but they are also non-poisonous.

With this in mind we decided to examine the use of indium as a catalyst promoter in the FTS reaction and compare the results with those of copper, since both copper and indium are in a position to each other to exhibit the “*Knight's Move relationship*”. Indeed not much work has been carried to evaluate indium's effects as a potential promoter and to the best of our knowledge no work has been published to compare the promotional effects of indium to copper for Fe-based FTS catalysts.

### 7.2 Motivation to compare indium to copper as a chemical promoter

Recent work in our laboratory to synthesise carbon nanotubes from acetylene, has shown that indium can exhibit similar chemical properties to copper [8]. Employing a  $\text{CaCO}_3$  supported Fe-Ni catalyst results in the synthesis of nanotubes as shown in Fig. 7.2.



**Figure 7.2** Carbon nanotubes synthesized using the Fe-Ni/ $\text{CaCO}_3$  catalyst

But adding copper to a  $\text{CaCO}_3$  supported Fe-Ni catalyst, results in the formation of tubes as well as *coils* (Fig. 7.3). To our amazement, the same effect was observed when indium was added to the Fe-Ni/ $\text{CaCO}_3$  (Fig. 7.4).

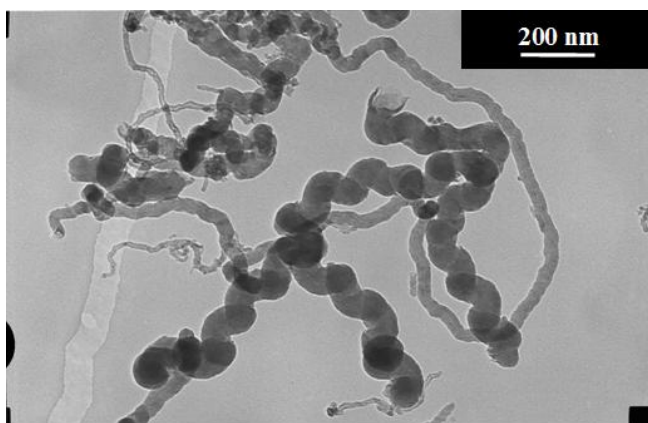


**Figure 7.3** Carbon nanotubes and coils synthesized using the Fe-Ni-Cu/ $\text{CaCO}_3$  catalyst

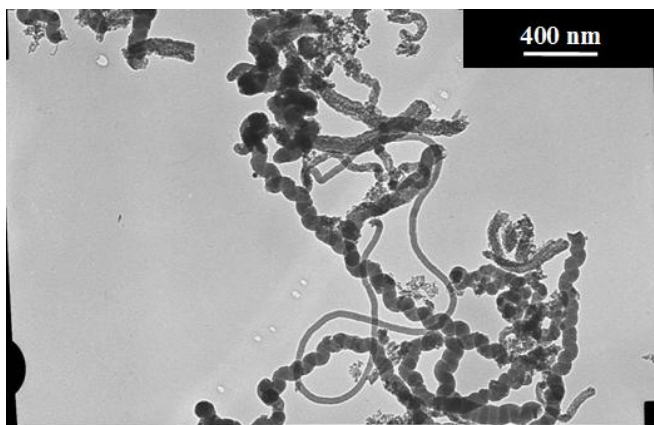


**Figure 7.4** Carbon nanotubes and coils synthesized using the Fe-Ni-In/CaCO<sub>3</sub> catalyst

Furthermore the ratio of the tubes to coils produced for the copper and indium promoted catalysts were found to be comparable (Fig. 7.5).

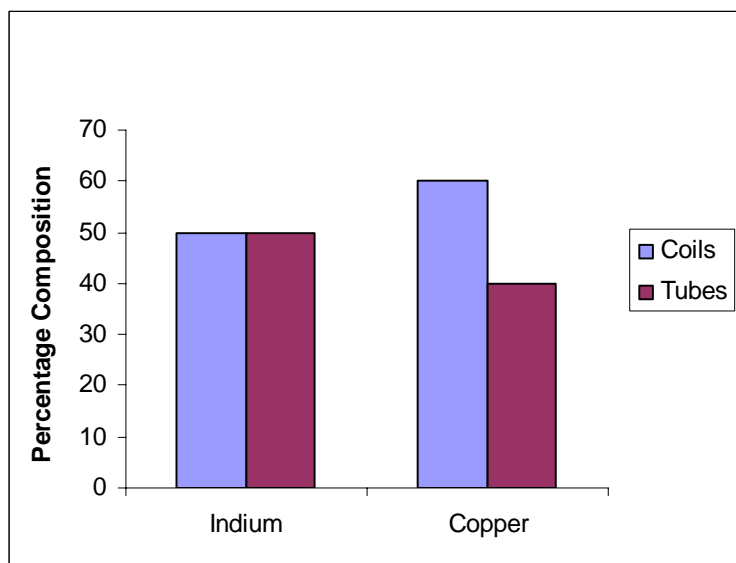


**Figure 7.5** Percentage composition of coils and tubes produced for the copper and indium promoted catalysts

Therefore with this possible link that exists between the chemical properties of copper and indium, we decided to carry out a study to compare the promotional properties of the two elements on the precipitated Fe-based FTS catalyst.

### **7.3 Experimental**

Five catalysts were prepared using the precipitation method as explained in Chapter 3. They include two copper-promoted catalysts and two indium promoted catalysts. The weight loading for the promoters was 1 and 3 wt. %. The fifth catalyst prepared was the unpromoted catalyst (100Fe) which was used as the benchmark catalyst. It is important to note that this catalyst is not the same as the one used in Chapters 5. The characterization results and a comparison of the properties of the catalysts are given below.

### **7.4 Results and discussion**

#### **7.4.1 N<sub>2</sub> physisorption results**

Table 7.1 The composition and textural properties of the catalysts

Catalyst composition <sup>a</sup> (parts by weight)	BET surface <sup>b</sup> area (m <sup>2</sup> /g)	Pore volume <sup>b</sup> (cm <sup>3</sup> /g)
100Fe	18.6	0.073
100Fe/1Cu	19.4	0.077
100Fe/3Cu	19.9	0.077
100Fe/1In	25.8	0.12
100Fe/3In	26.5	0.12

<sup>a</sup>Weight loadings verified using XRF, Maximum error =  $\pm 5\%$

<sup>b</sup>Maximum error =  $\pm 2\%$

Copper appears not to alter the surface area as well as the pore volume of Fe. Indium increases the surface area and pore volume of the Fe-based catalyst.

#### **7.4.2 Hydrogen Temperature Programmed Reduction (H<sub>2</sub> TPR)**

A comparison of TPR results for all catalysts is shown in Table 7.2 and Figures 7.6 and 7.7. All promoted catalysts were compared directly to the unpromoted Fe catalyst (Fe<sub>2</sub>O<sub>3</sub>). It is reasonable to assume that only the Fe<sub>2</sub>O<sub>3</sub> is detected after calcination based on the similar TPR profiles obtained for all the Fe catalysts prepared in this study. XRD work carried out (not reported herein) has also shown Fe<sub>2</sub>O<sub>3</sub> to be the predominant Fe phase after calcination.

All TPR profiles show 2 distinct reduction peaks. It has been suggested that the H<sub>2</sub> reduction of Fe<sub>2</sub>O<sub>3</sub> occurs via 2 main steps: Fe<sub>2</sub>O<sub>3</sub> → Fe<sub>3</sub>O<sub>4</sub> → Fe. These 2 elementary reactions have been assigned to the first and second peaks in the H<sub>2</sub> TPR profiles, respectively (Fig 7.6) [9-11].

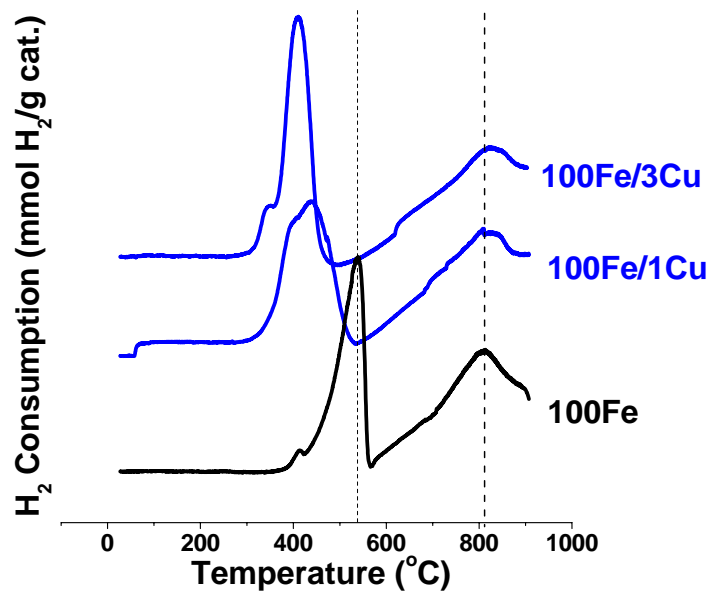


Figure 7.6 H<sub>2</sub> TPR profiles of Cu promoted catalysts

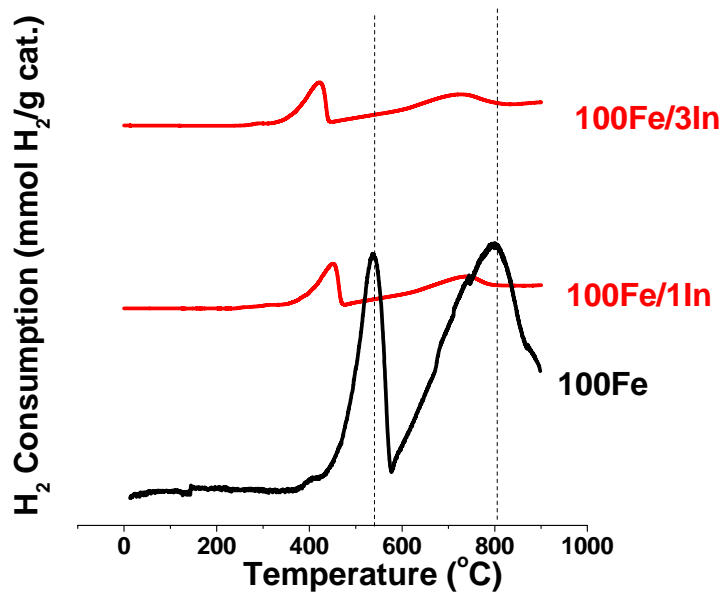


Figure 7.7 H<sub>2</sub> TPR profiles of indium promoted catalysts

It is noticeable that copper lowers the reduction peaks of iron oxide to metallic iron. This same effect has been observed by other authors [4, 12, 13]. A similar effect is noticed with the indium promoted catalysts. But a striking effect with these results is that, the H<sub>2</sub> reduction peaks of the indium promoted catalysts are smaller than those of the copper promoted catalysts. To get a sense of the size of the peaks, we calculated the moles of H<sub>2</sub> consumed by the catalysts. Thereafter, the Fe reducibility was calculated in the same way as reported in literature [15].

Table 7.2 Comparing the reducibility of Fe-based catalysts using H<sub>2</sub> TPR

Catalyst	H <sub>2</sub> TPR		
	Peak temperature (°C)	H <sub>2</sub> Consumption (mmol/molFe)	Fe reducibility (%)
100Fe	536	72	15
100Fe/1Cu	436	217	46
100Fe/3Cu	411	189	38
100Fe/1In	451	9.8	2
100Fe/3In	422	9.8	2

From Table 7.2, it is evident that the percentage amount of iron reduced in the indium promoted catalysts is relatively low compared to the copper promoted catalysts. This quantifies the small size of the reduction peaks and suggests that indium decreases the %Fe reducibility.

#### 7.4.3 X-Ray diffraction (XRD)

The XRD technique was employed to determine the crystallite size of Fe<sub>2</sub>O<sub>3</sub>. The objective was to see how both copper and indium affect the crystallite size of iron oxide. Table 7.3 depicts the crystallite size determined using Rietvelt refinement (as explained in Chapter 3).



Table 7.3 Fe<sub>2</sub>O<sub>3</sub> crystallite size determined using Rietveld refinement

Catalyst	Crystallite size (nm)
100Fe	32.8
100Fe/1Cu	43.6
100Fe/3Cu	48.6
100Fe/1In	41.6
100Fe/3In	40.9

The addition of copper and indium increases the crystallite size of Fe<sub>2</sub>O<sub>3</sub>. An explanation for this effect could be that during the preparation of the catalysts, the introduction of promoters (precursors) modifies the precipitation behaviour of ions in the solution. This leads to the net repulsive effect of the Fe<sup>3+</sup> ions to be neutralized, hence making the Fe<sup>3+</sup> particles to come together. This is the same analogy that can be used to explain the destabilization of colloidal systems [14].

#### 7.4.4 CO adsorption measurements using DRIFTS

A study of adsorbed CO provides information about the extent of, and number of types of adsorbed CO on the Fe. It can also act as a probe molecule with which to study the metal on which it is adsorbed. Carbon monoxide is an ideal probe molecule for the characterisation of Fischer-Tropsch catalysts using DRIFTS. The CO is able to accept electron density from metal surface sites, resulting in formation of metal–carbonyl complexes that can readily be monitored by the CO stretching frequency.

The complexes are characterized by IR absorption bands at 2100–1800 cm<sup>-1</sup>. The shift from the vibrational energy of gas-phase CO (2143 cm<sup>-1</sup>) can be explained in terms of simple molecular orbital (MO) theory. The 5σ orbital of the CO molecule forms a σ bond with an empty orbital on the metal, and for electron-rich surfaces, back-donation from the metal *d*-orbitals into the antibonding π\*-orbitals of the CO molecule occurs, weakening the C≡O bond. The result is a red shift of the CO stretching frequency (compared with

“free” CO gas) and the appearance of bands caused by CO linearly and bridged bonded to the metal surface. The precise position of these bands can provide valuable information about the electron density of the metal sites [16-18].

When CO adsorption was performed on the unpromoted iron catalyst (100Fe), two peaks were obtained at 2033 and 2013  $\text{cm}^{-1}$ , showcasing CO linearly adsorbed on  $\text{Fe}^0$  (Fig. 7.8). This is consistent with work carried out by other researchers [19-21].

These peaks decreased in intensity during thermal desorption until they were completely desorbed at 300°C (Fig. 7.9). The introduction of Cu to Fe produced a red shift of the peak at 2013  $\text{cm}^{-1}$  to *ca.* 2011  $\text{cm}^{-1}$  (Fig. 7.8) highlighting the increased backdonation ability of the *d*-orbitals of Fe. These results are in agreement with the  $\text{H}_2$  TPR results for the Cu promoted catalysts. No other peaks were observed, although it is possible that some were hidden by the gaseous CO peaks (2173 and 2115  $\text{cm}^{-1}$ ), since a pressure of 2 bar CO was employed in the experiments.

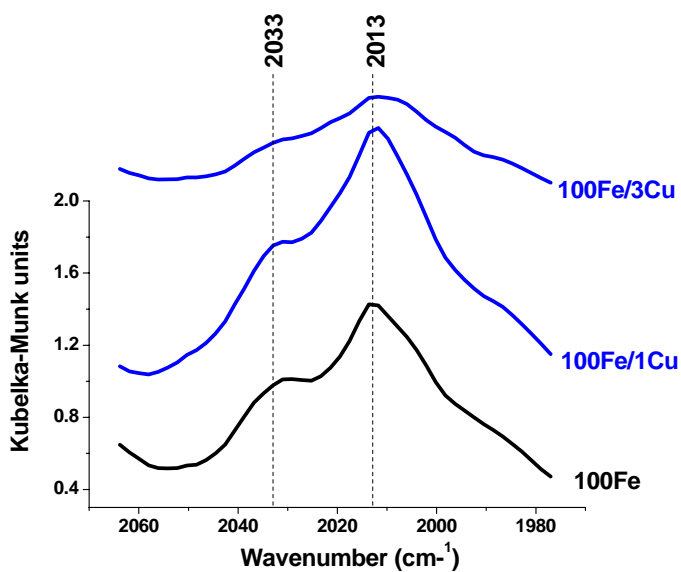


**Figure 7.8** Comparison of CO adsorption on the unpromoted iron catalyst and copper promoted iron catalysts; Conditions: CO reduction for 1 hour (Flow rate = 12 ml/min, T = 350°C, P = 2 bar), CO adsorption for 30 min (CO Flow rate = 12 ml/min, T = 25°C, P = 2 bar)

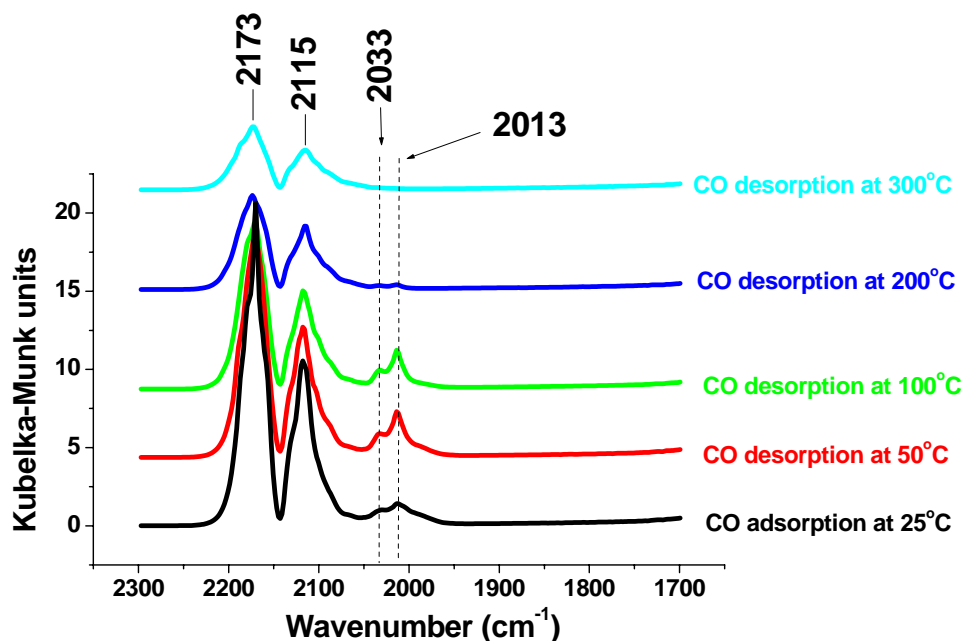


**Figure 7.9** Thermal desorption of CO on the unpromoted iron catalyst

Fig. 7.10 shows the adsorption of CO on indium promoted Fe catalysts. It is evident that the intensity of species at 2033 and 2013  $\text{cm}^{-1}$  has decreased with indium addition to Fe. A comparison of the intensities of these peaks for copper promoted and indium promoted catalysts is shown in Figures 7.11 and 7.12. This is to give a sense of CO adsorption ability of these catalysts. It is clear from both figures that the intensity of the adsorbed CO bands of the Cu promoted catalysts is at least seven times more than the intensity of the indium promoted catalysts.

It is also noticed that the 2013  $\text{cm}^{-1}$  peak intensity of the 3Cu case is lower than that of the 1 Cu case. This could be due to the copper particles covering some Fe active sites available for CO adsorption as a result of the higher loading of Cu. We do acknowledge

that at this point this is a mere speculation and confirmatory evidence in a form of XPS data would be required to back this assertion

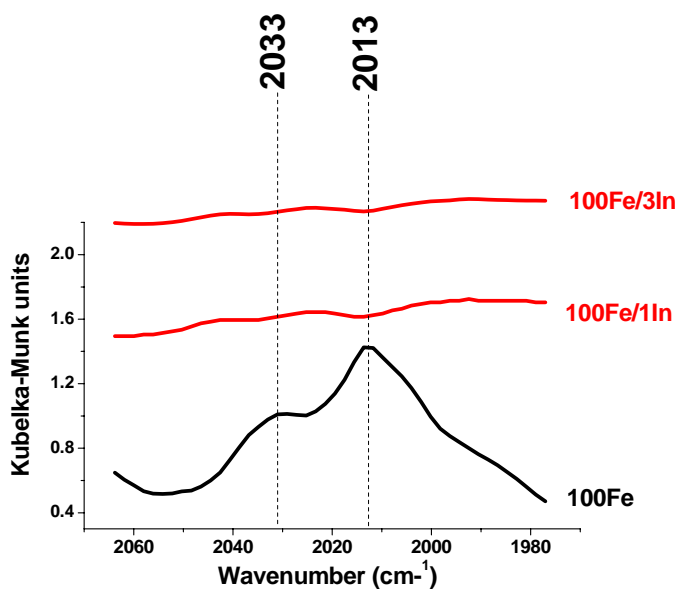


Figure 7.10 CO adsorption on the indium promoted iron catalysts

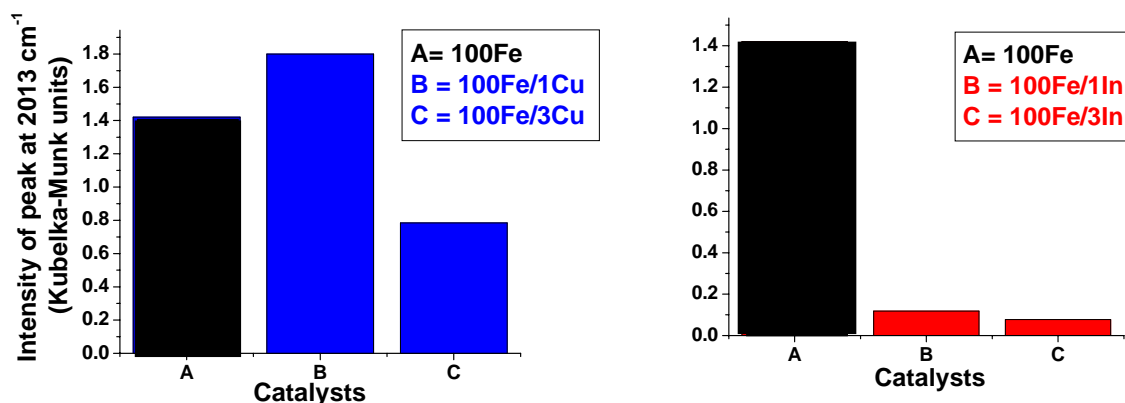
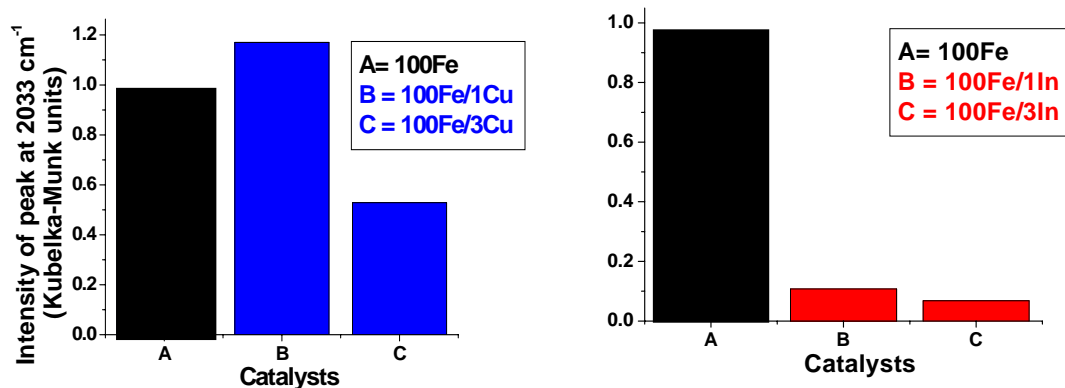
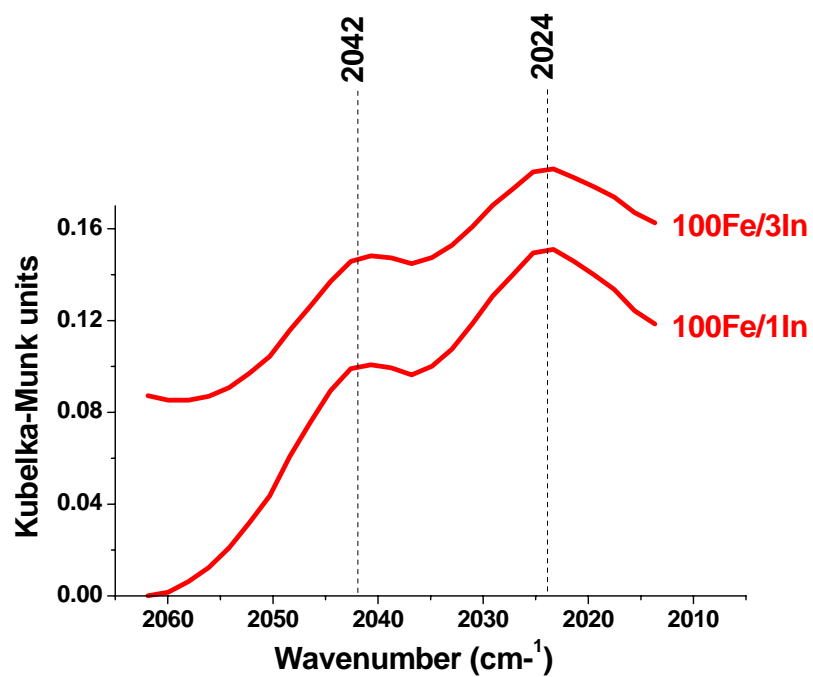


Figure 7.11 Intensity of peak at 2013 cm<sup>-1</sup> for CO adsorption on the copper promoted and the indium promoted iron catalysts



**Figure 7.12** Intensity of peak at 2033 cm<sup>-1</sup> for CO adsorption on the copper promoted iron catalysts and the indium promoted iron catalysts

It is also noted that the CO adsorption spectra of the indium promoted catalysts reveal CO adsorption peaks at 2024 and 2042 cm<sup>-1</sup> (Fig. 7.13). This might indicate the presence of a different type of iron species or simply a blue shift of the 2013 and 2033 cm<sup>-1</sup> peaks. If the emergence of these peaks is more likely as a result of the blue shift of the 2013 and 2033 cm<sup>-1</sup> peaks, then this might suggest that indium inhibits the backdonation ability of iron. This suggesting that indium acts as a poorer promoter for the Fe-based FTS catalyst. It therefore appears that indium lowers the CO adsorption ability of the Fe catalyst.



**Figure 7.13** CO adsorption on the indium promoted iron catalysts showing the adsorbed CO species at 2024 and 2042 cm<sup>-1</sup>

#### 7.4.5 In situ FTS performances using DRIFTS

After performing the FTS reaction for the copper and indium promoted catalysts for 5 hours, spectra were recorded. These are shown in Fig 7.14 and Fig 7.15. All the spectra are compared to that of the spectrum showing FTS reaction performed over the unpromoted Fe catalyst.

The peak at  $3016\text{ cm}^{-1}$  is associated with gaseous methane ( $\text{CH}_4$ ), whereas peaks at  $2957\text{ cm}^{-1}$  and  $2929\text{ cm}^{-1}$  represent the asymmetric CH stretching vibration of the methyl species ( $-\text{CH}_3$ ) and the asymmetric CH stretching of methylene species ( $-\text{CH}_2-$ ) respectively. The peak at  $2878\text{ cm}^{-1}$  is assigned to a symmetric CH stretching vibration of the methyl species ( $-\text{CH}_3$ ) and the one at  $2854\text{ cm}^{-1}$  is assigned to the symmetric CH stretching vibration of the methylene species ( $-\text{CH}_2-$ ) [19, 29].



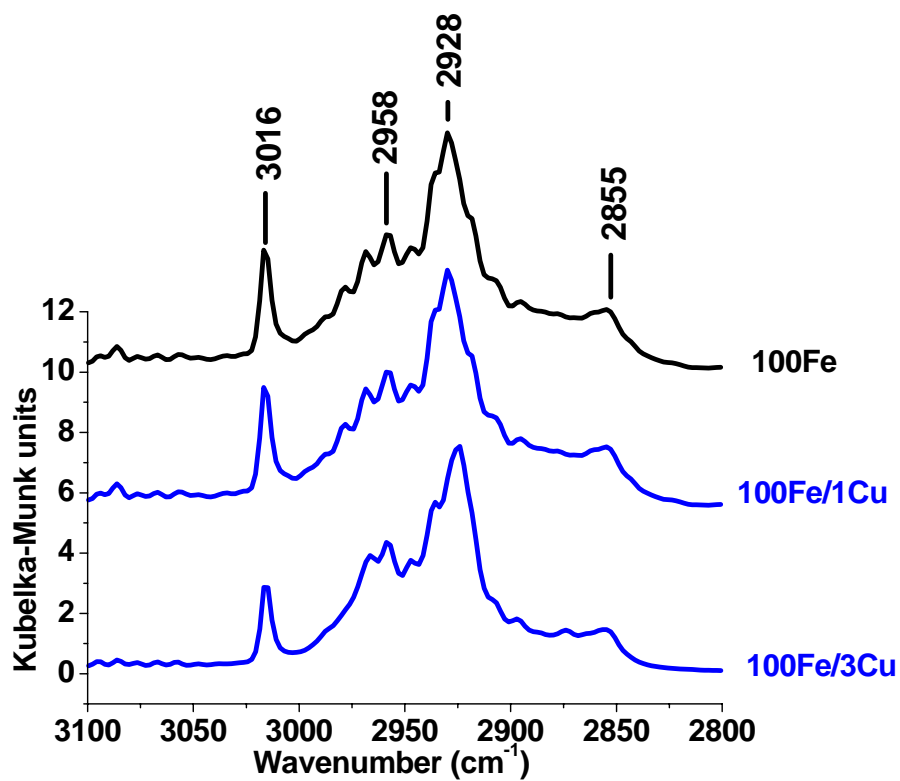


**Figure 7.14** Comparison of the FTS reaction over the unpromoted iron catalyst (100Fe) and the copper promoted catalysts; P = 10 bar, T = 275 °C, H<sub>2</sub>/CO = 2, H<sub>2</sub>/CO flow rate = 12 ml/min, Time = 5 h)

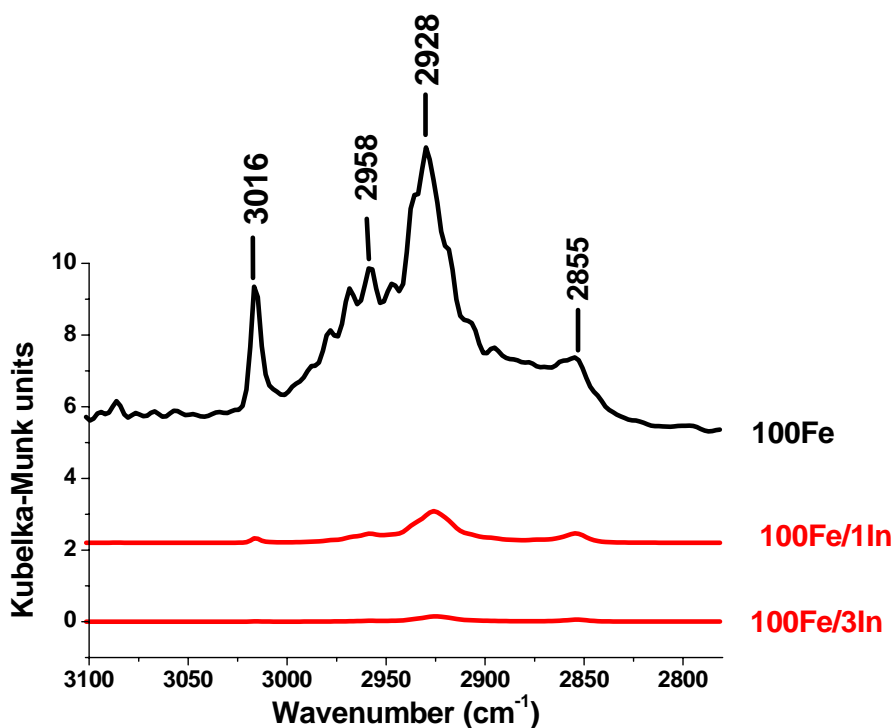


**Figure 7.15** Comparison of the FTS reaction over unpromoted iron catalyst (100Fe) and indium promoted catalysts; P = 10 bar, T = 275 °C, H<sub>2</sub>/CO = 2, H<sub>2</sub>/CO flow rate = 12 ml/min, Time = 5 h)

It is evident that the addition of indium to the Fe catalyst lowers the intensity of the C-H peaks obtained after 5 hours of reaction whereas copper has a negligible effect on the intensity of the C-H peaks. This tells us that the addition of indium to the Fe catalyst hampers its activity. From this observation it appears that indium has a deleterious effect on the activity of the Fe catalyst.

To estimate the average carbon chain length of the hydrocarbon molecules produced after 5 hours of reaction, the ratio of CH<sub>2</sub>/CH<sub>3</sub> species was calculated using the following formula:

$$\frac{\text{Area}(-\text{CH}_2 - \text{species})}{\varepsilon_1} / \frac{\text{Area}(-\text{CH}_3 - \text{species})}{\varepsilon_2}$$

where

- 1) Area of -CH<sub>2</sub>- species is the area of the peak at 2925-2930 cm<sup>-1</sup> representing the asymmetric stretch of CH<sub>2</sub> species
- 2) Area of -CH<sub>3</sub> species is the area of the peak at 2955-2960 cm<sup>-1</sup> representing the asymmetric stretch of CH<sub>3</sub> species
- 3) ε<sub>1</sub> is the molar extinction coefficient of the CH<sub>2</sub> species (75 mole<sup>-1</sup>.l.cm<sup>-1</sup>) [22]
- 4) ε<sub>2</sub> is the molar extinction coefficient of the CH<sub>3</sub> species (70 mole<sup>-1</sup>.l.cm<sup>-1</sup>) [22]

The calculated ratios are given in Table 7.4. It is evident that both indium and copper lead to an increase in the average chain length of the hydrocarbons. This suggests that both copper and indium can induce similar effects properties to the Fe FTS catalyst.

Table 7.4 Calculated ratios of CH<sub>2</sub>/CH<sub>3</sub> bands for all catalysts

Catalyst	Ratio of CH <sub>2</sub> /CH <sub>3</sub>
100Fe	1
100Fe/1Cu	7
100Fe/3Cu	7
100Fe/1In	4
100Fe/3In	5

From the results presented above it is clear that indium has similar properties to copper but it is a poorer promoter than copper. In fact indium lowers the activity of the precipitated Fe-based FTS catalyst. It is thought that indium poisons the active sites of the catalyst by interacting with them. Our postulation is that during calcination,  $\text{In}(\text{NO}_3)_3$  (which was used as the indium precursor) is transformed to  $\text{In}_2\text{O}_3$  and during pretreatment (before reaction)  $\text{In}_2\text{O}_3$  is reduced to indium metal which has a low melting point (157 °C) [23] causing it melt during the FTS reaction and this resulted in some of the active sites to be covered by this melted indium rendering them inactive.

## 7.5 Conclusion

The ability of indium to act as a chemical promoter for the Fe-based FTS catalyst was evaluated. Its effect on Fe was evaluated and compared to that of copper. This was to evaluate if both indium and copper possessed similar promotional abilities for the Fe-based FTS catalyst. N<sub>2</sub> physisorption, temperature programmed reduction (TPR), X-ray diffraction (XRD) and diffuse reflectance infrared fourier transform spectroscopy (DRIFTS) were employed to characterize the catalysts. “*In situ*” Fischer Tropsch synthesis (FTS) reactions were also performed in the DRIFTS reactor. It was found via TPR studies that indium exhibited similar chemical properties to that of copper. Results obtained from XRD and N<sub>2</sub> physisorption showed indium promoted catalysts give comparable results to those of copper promoted catalysts. It therefore appears that indium does exhibit similar chemical properties to copper.

However indium decreased the reducibility and CO adsorption ability of the Fe catalyst. Indium also lowered the FTS activity of the Fe-based catalyst. It is thus concluded that indium is a poorer promoter for the iron-based FTS catalyst and acts as a poison for this catalyst.

## References

- [1] S. Li, A. Li, S. Krishnamoorthy, E. Iglesia, *Catal. Lett.* 77 (2001) 197
- [2] R. J. O'Brein, L. Xu, R. L. Spicer, S. Bao, D. R. Milburn, B. H. Davis, *Catal. Today* 36 (1997) 325
- [3] R.J. O'Brein, B.H. Davis, *Catal. Lett.* 94 (2004) 1
- [4] Y. Jin, A.K. Datye, *J. Catal.* 196 (2000) 8
- [5] I.E. Wachs, D.J. Dwyer, E. Iglesia, *Appl. Catal.* 12 (1995) 35
- [6] E.R. Scerri, *The Periodic Table, Its Story and Its Significance*, Oxford University Press, New York, 2007
- [7] M. Laing, The Knight's Move in the Periodic Table, *Education in Chemistry*, 36 (1999) 160
- [8] A. Shaikjee, N.J. Coville, *in preparation*.
- [9] D.B. Bukur, C. Sivaraj, *Appl. Catal. A: Gen.* 231 (2002) 201
- [10] K. Jothimurugesan, J.G. Goodwin, Jr., S.K. Gangwal, J.J. Spivey, *Catal. Today* 58 (2000) 335
- [11] I.S.C Hughes, J.O.H. Newman, G.C. Bond, *Appl. Catal.* 30 (1987) 303
- [12] R. J. O'Brien, L. Xu, R. L. Spicer, S. Bao, D. R. Milburn, B. H. Davis, *Catal. Today* 36 (1997) 325
- [13] U. Lindner, H. Papp, *Appl. Surf. Sci.* 32 (1988) 75
- [14] N. Lohitharn, J. G. Goodwin, Jr., E. Lotero, *J. Catal.* 255 (2007) 104
- [15] <http://en.wikipedia.org/wiki/Colloid>
- [16] F. Morales, E. de Smit, F. M.F. de Groot, T. Visser, B. M. Weckhuysen *J. Catal.* 246 (2007) 91
- [17] J. Ryczkowski, *Catal. Today* 68 (2001) 263
- [18] G. Blyholder, L.D. Neff, *J. Phys. Chem.* 66 (1962) 1464
- [19] G. Bian, A. Oonuki, Y. Kobayashi, N. Koizumi, M. Yamada, *Appl. Catal. A: Gen.* 219 (2001) 13
- [20] E. Boellaard, A.M. van der Kraan, J.W. Geus, *Appl. Catal. A: Gen.* 147 (1996) 207
- [21] E. Guglielminotti, F. Boccuzzi, F. Pinna, G. Strukul, *J. Catal.* 167 (1997) 153

[22] K. Nakanishi, *Infrared Absorption spectroscopy – PRACTICAL -*, Nankodo Company Limited, Japan, 1964

[23] <http://www.chemicalelements.com/elements/cu.html> (01 February 2009)

## Chapter 8

### Chemical promotion of a multi-promoted Fe-based Fischer-Tropsch synthesis catalyst by indium

#### ***8.1 Introduction***

In Chapter 7 it was reported that indium does exhibit some chemical properties similar to those of copper. It was decided to employ indium as a promoter and evaluate its effect on a multi-promoted precipitated iron catalyst. It was also noticed that at loadings of > 1 wt. % indium had a deleterious effect on the chemical properties of the precipitated iron catalyst. This prompted us to evaluate wt. % loadings of less than 1 wt. % for this study. The aim of this study was thus to evaluate the effect of low loadings of indium on a multi-promoted precipitated iron catalyst.

#### ***8.2 Experimental***

The catalysts were prepared in the same manner as those reported in Chapter 6 and the detailed experimental procedure is discussed in Chapter 3. The three catalysts prepared contained indium, potassium, silica and iron and their compositions are shown in Table 8.1. All these catalysts were characterized using N<sub>2</sub> physisorption, TPR and DRIFTS. Their FTS performances were also evaluated.



### 8.3 Results and discussion

#### 8.3.1 N<sub>2</sub> physisorption measurements

The BET surface area measurements are given in Table 8.1. It is seen that upon addition of indium on the promoted precipitated iron based FTS catalyst, both the surface area and pore volume are decreased. The decrease in surface area could be due to indium filling the pores of the SiO<sub>2</sub>.

Table 8.1 The composition and N<sub>2</sub> physisorption results of the catalysts

Catalyst composition (parts by weight)	BET Surface area <sup>a</sup> (m <sup>2</sup> /g)	Pore volume (cm <sup>3</sup> /g)
2K <sub>2</sub> O/5SiO <sub>2</sub> /100Fe	87.3	0.15
0.01In/2K <sub>2</sub> O/5SiO <sub>2</sub> /100Fe	78.7	0.14
0.1In/2K <sub>2</sub> O/5SiO <sub>2</sub> /100Fe	64.3	0.14

<sup>a</sup>Maximum error = ± 2%

SiO<sub>2</sub> is known to provide a high surface area [1, 2]. Thus as more promoters are added to the catalyst, the high surface area of SiO<sub>2</sub> diminishes.

### 8.3.2 Temperature programmed reduction (TPR)

#### 8.3.2.1 H<sub>2</sub> TPR

H<sub>2</sub> TPR measurements were also performed on the catalysts. The results for all the catalysts studied are shown in Fig. 8.1 and Table 8.2. In all the TPR profiles there are two peaks and these two peaks illustrate the transformation of Fe<sub>2</sub>O<sub>3</sub> to Fe via a two step process [3-6]. The first peak represents the transformation of Fe<sub>2</sub>O<sub>3</sub> → Fe<sub>3</sub>O<sub>4</sub> and the second one shows the transformation of Fe<sub>3</sub>O<sub>4</sub> → Fe. It is noticed that the addition of indium shifts the two reduction peaks to *higher* temperatures. This means that indium suppresses the reduction of Fe<sub>2</sub>O<sub>3</sub>.

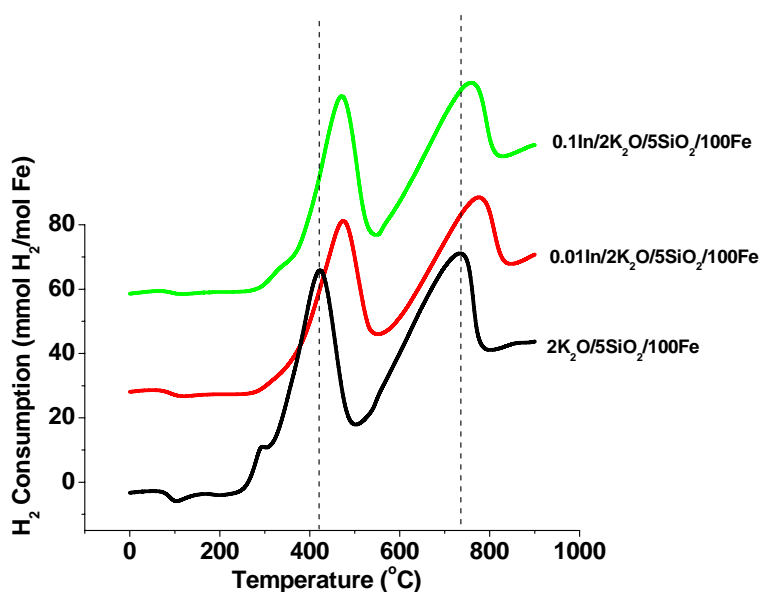


**Figure 8.1** H<sub>2</sub> TPR profiles for all the catalysts

Table 8.2 shows that the first peak is shifted from 422 °C to 473 °C and the second peak from 733 °C to *ca.* 768-772 °C. This change occurs for both the indium loaded catalysts. It is interesting to note that this trend occurs even if the loading amount of indium is increased tenfold (0.01 – 0.1 wt. %). This signifies that the suppression ability of indium is complete after addition of very small amounts of indium.

Table 8.2 H<sub>2</sub> Reduction temperatures for all the catalysts in Figure 8.1

Catalyst composition	Reduction Temperature [°C]	
	Peak 1	Peak 2
2K <sub>2</sub> O/ 5SiO <sub>2</sub> /100Fe	422	733
0.01In/2K <sub>2</sub> O/ 5SiO <sub>2</sub> /100Fe	473	772
0.1In/2K <sub>2</sub> O/ 5SiO <sub>2</sub> /100Fe	473	768

### 8.3.2.2 CO TPR

CO TPR measurements were also performed on the catalysts and the results are given in Fig. 8.2 and Table 8.3. All the profiles show four peaks. The first peak is in the temperature range 120 – 150 °C and may be the reduction of easily reducible iron-oxide crystallites. Luo et al. [7] have shown that Fe<sub>2</sub>O<sub>3</sub> occurs via a two step process as given by Eqs. 8.1 and 8.2.

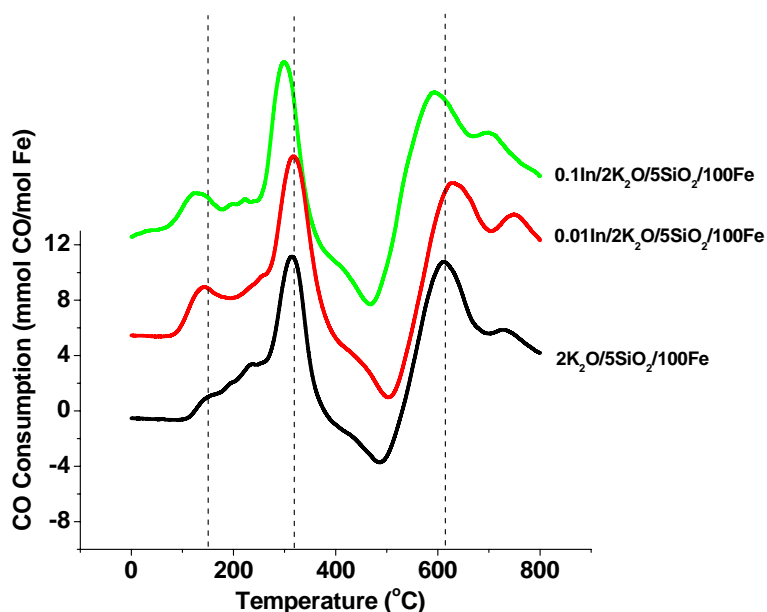
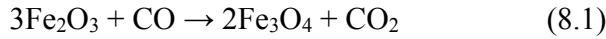


Figure 8.2 CO TPR profiles for all the catalysts



The second peak located in the 290 – 315 °C range is ascribed to the reduction of Fe<sub>2</sub>O<sub>3</sub> to Fe<sub>3</sub>O<sub>4</sub> as illustrated by Eq. 8.1. It is noticeable that this peak is unaffected by the addition of a small amount of indium. However, when the indium loading is increased to 0.1 wt. % the peak is shifted to 296 °C. This indicates that indium promotes the reduction of Fe<sub>2</sub>O<sub>3</sub> to Fe<sub>3</sub>O<sub>4</sub> and Fe<sub>2</sub>O<sub>3</sub> is more easily reduced using CO than using H<sub>2</sub>.

Table 8.3 CO reduction temperatures for all the catalysts in Figure 8.2

Catalyst composition	Reduction Temperature [°C]			
	Peak 1	Peak 2	Peak 3	Peak 4
2K <sub>2</sub> O/5SiO <sub>2</sub> /100Fe	146	315	622	736
0.01In/2K <sub>2</sub> O/5SiO <sub>2</sub> /100Fe	138	314	626	739
0.1In/2K <sub>2</sub> O/5SiO <sub>2</sub> /100Fe	127	296	593	699

The third peak in the temperature range 590 – 630 °C corresponds to the carburization of iron oxides as illustrated by Eq. 8.2, and the fourth peak corresponds to the carburization of the difficult to reduce iron oxide species. These difficult to reduce iron oxide species could be present as a result of the Fe-SiO<sub>2</sub> interaction, which many researchers have widely reported [8-11]. Nonetheless, the addition of indium (especially 0.1 wt. %) has a marked effect on the carburization peaks. Both the carburization peaks are shifted to lower temperatures. This suggests that indium promotes the carburization of the iron oxide phase. It is known that K<sub>2</sub>O promotes the dissociative adsorption of CO [12-14] and in doing this it promotes the carburization of the iron oxide phase. This could mean that indium plays a role in enhancing the carburization ability of K<sub>2</sub>O and of also enhancing the Fe-K<sub>2</sub>O contact.

### 8.3.3 DRIFTS

#### 8.3.3.1 “In situ” CO adsorption measurements

The CO adsorption results are shown in Figures 8.3 and 8.4. CO adsorption peaks at 2014 and 2034  $\text{cm}^{-1}$  were obtained and these bands represent the adsorption of CO on  $\text{Fe}^0$  species [15]. The intensity of the 2014  $\text{cm}^{-1}$  band gives a qualitative measure of the adsorption of CO and this is used to compare the CO adsorption for all the catalysts. This is illustrated in Fig. 8.4.

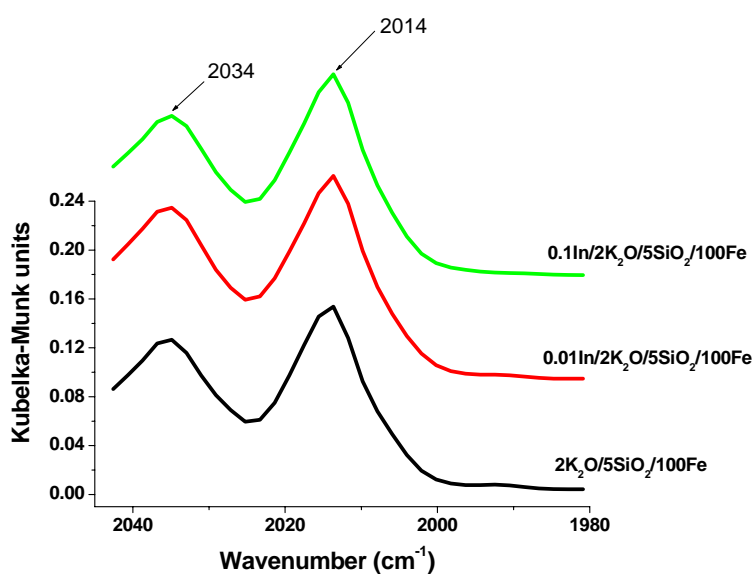


**Figure 8.3** CO adsorption on all the catalysts; Conditions: CO reduction for 1 hour (Flow rate = 12 ml/min, T = 350°C, P = 2 bar, CO adsorption for 30 min (CO Flow rate = 12 ml/min, T = 25°C, P = 2 Bar)

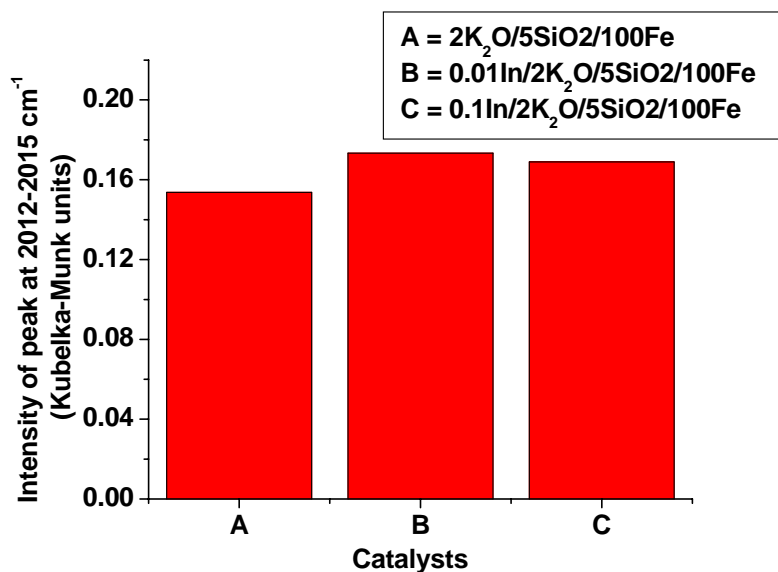


**Figure 8.4** Comparison of the intensities of 2014 cm<sup>-1</sup> peak

The 2014 cm<sup>-1</sup> peak intensity is slightly increased when indium is added to the catalyst. This implies that CO adsorption is slightly enhanced when indium is added. It may be that indium improves carburization as shown by the CO TPR results and it also enhances the Fe-K<sub>2</sub>O contact for the adsorption of CO. This would mean that K<sub>2</sub>O improves the ability of Fe to adsorb CO. It is widely accepted that K<sub>2</sub>O promotes the CO adsorption ability of Fe [14, 16].

### 8.3.3.2 “In situ” FTS

The IR spectra showing the production of C-H peaks after 5 hours of FTS reaction performed in a DRIFTS reactor for all the catalysts are shown in Fig. 8.5. It appears as if indium has no marked effect on the production of C-H peaks as illustrated in Fig. 8.5.

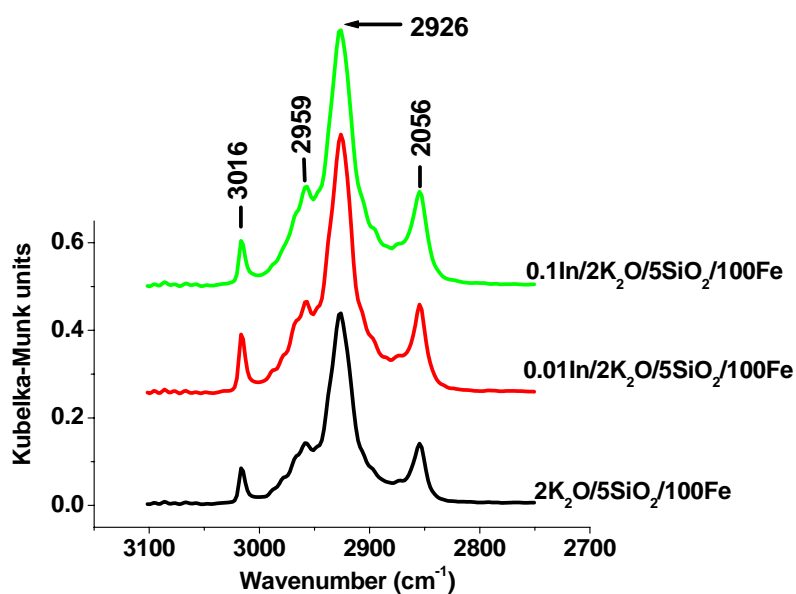


**Figure 8.5** DRIFTS spectra for the FTS reaction of all catalysts

Reaction conditions:  $H_2/CO = 2/1$ , Flow rate = 12 ml/min,  $T = 275^\circ C$ ,  $P = 10$  bar,  $t = 5$  h

### 8.3.4 FTS performances

#### 8.3.4.1 Catalyst activity and stability

The conversions of carbon monoxide and hydrogen over the catalysts with time on stream are shown in Fig. 8.6, Fig. 8.7 and Table 8.4. It is noticeable that the addition of indium to the catalyst has a marked effect on both the CO and  $H_2$  conversions. In fact changing the loading of indium also has an effect on both the CO and  $H_2$  conversions.

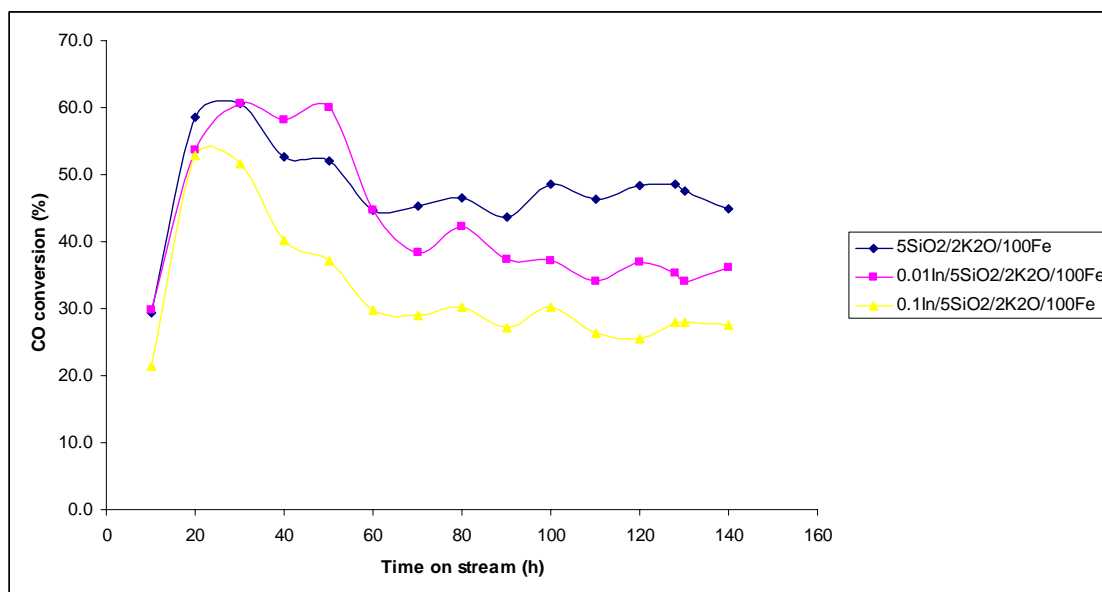


**Figure 8.6** CO conversion with time on stream



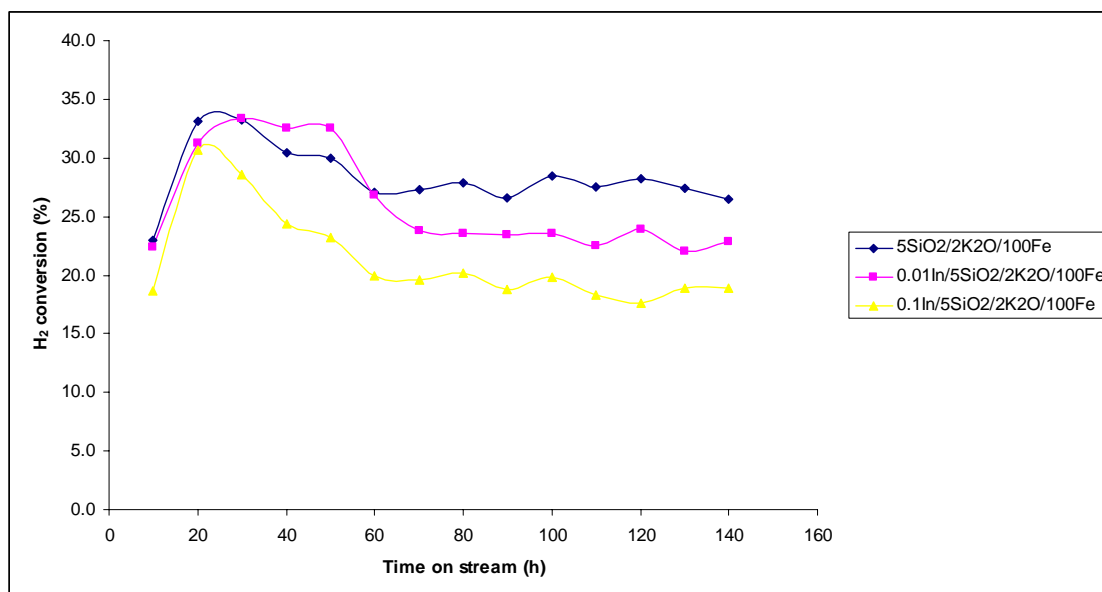


**Figure 8.7** H<sub>2</sub> conversion with time on stream

Figures 8.8 and 8.9 respectively show a comparison of CO and H<sub>2</sub> conversion at steady state conditions for all catalysts. It is noticeable that the addition of indium lowers the activity of the catalyst, since both the CO and H<sub>2</sub> conversions are decreased. The calculated activity (Table 8.4) confirms this point. The activity decreases from 14.5 to 10.8  $\mu\text{mol}/\text{sec.gFe}$ . The activity is further decreased when the loading amount of indium is increased from 0.01 wt. % to 0.1 wt. % (i.e. from 10.8 to 7.0  $\mu\text{mol}/\text{sec.gFe}$ ). It is also noticeable from Table 8.4 that the rate of CO conversion is lowered from  $-1.1 \times 10^{-6}$  mol/s to  $-7.0 \times 10^{-7}$  mol/s as the indium content is increased to 0.1 wt. %.

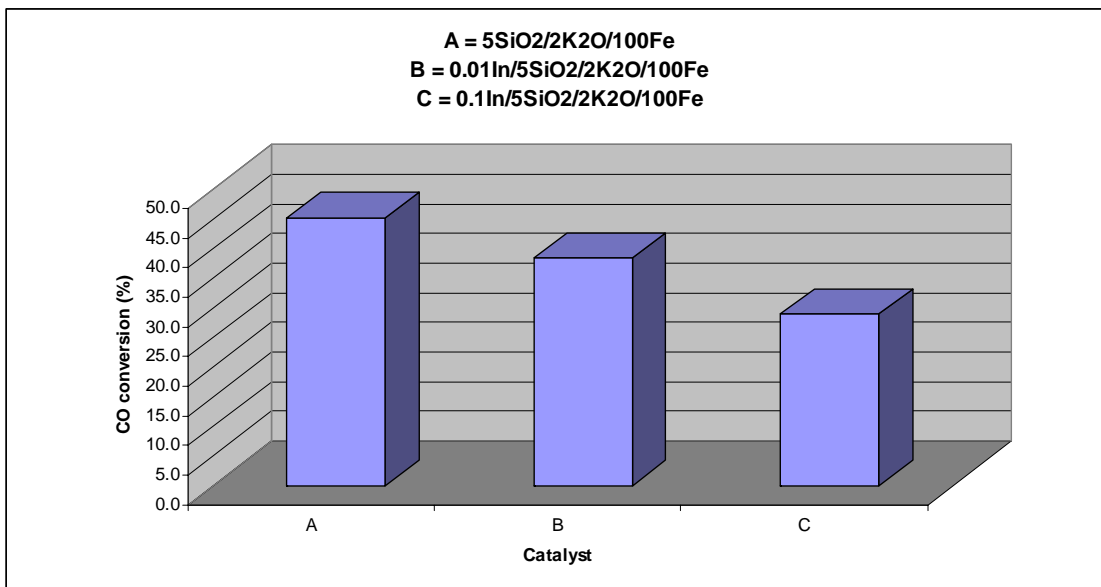


**Figure 8.8** Comparison of the CO conversion for all catalysts at steady state

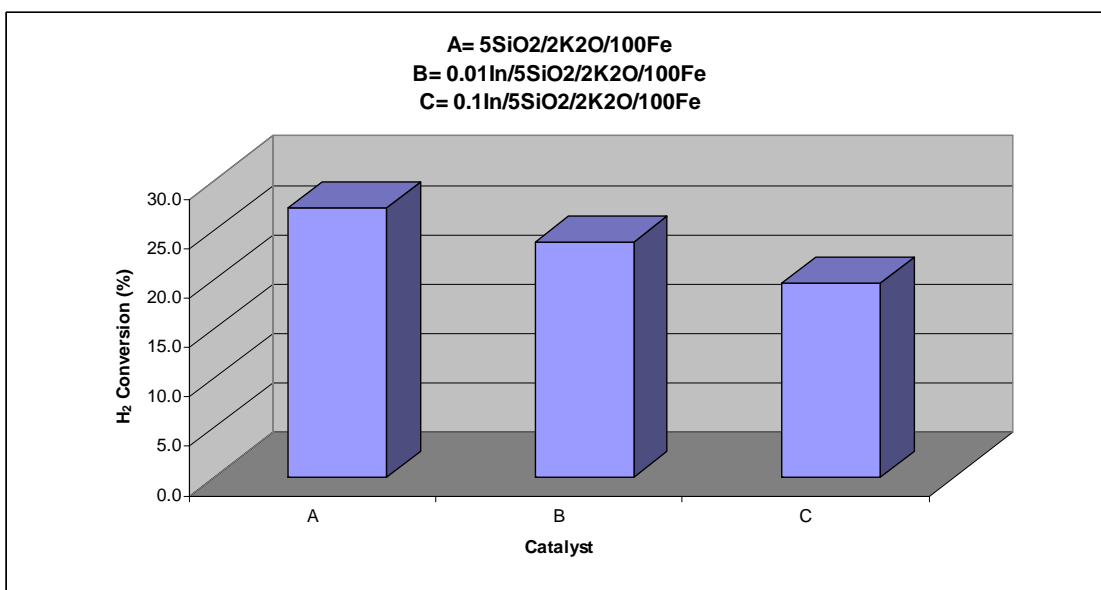


**Figure 8.9** Comparison of the H<sub>2</sub> conversion for all catalysts at steady state conditions

The decrease in activity could be attributed to a decrease in surface area as confirmed by the N<sub>2</sub> physisorption results. It may also be that a suppression of the reduction properties of the catalyst (H<sub>2</sub> TPR results) is responsible for a decrease in the catalyst's activity. It is noted that the catalyst was activated in CO for the FTS runs. CO TPR results suggest that indium improves the reduction/carburization of the iron oxide phase. It thus appears as if a decrease in surface area of the catalyst is a logical explanation for the decrease in activity.

It is also noticed that after 70 hours of reaction the activity of the indium promoted catalysts continued to decline indicating that they had not reached stability.

Table 8.4 FTS reaction performances for all the catalysts

Catalyst	5SiO <sub>2</sub> /2K <sub>2</sub> O/100Fe	0.01In/5SiO <sub>2</sub> /2K <sub>2</sub> O/100Fe	0.1In/5SiO <sub>2</sub> /2K <sub>2</sub> O/100Fe
<b>CO conversion (%)</b>	49.9	38.4	26.3
<b>H<sub>2</sub> conversion (%)</b>	28.5	23.8	18.0
<b>Rate CO (mol/s)</b>	-1.4 x 10 <sup>-6</sup>	-1.1 x 10 <sup>-6</sup>	-7.0 x 10 <sup>-7</sup>
<b>Rate CO<sub>2</sub> (mol/s)</b>	4.67 x 10 <sup>-7</sup>	2.98 x 10 <sup>-7</sup>	1.80 x 10 <sup>-7</sup>
<b>Rate FT (mol/s)</b>	9.79 x 10 <sup>-7</sup>	7.76 x 10 <sup>-7</sup>	5.22 x 10 <sup>-7</sup>
<b>Activity (μmol/sec.gFe)</b>	14.5	10.8	7.0
<b>α</b>	0.48	0.60	0.62
<b>C<sub>2</sub> olefin %<sup>a</sup></b>	44.0	40.7	36.8
<b>Selectivity</b>			
<b>C<sub>1</sub></b>	19.8	18.4	20.4
<b>C<sub>2</sub>-C<sub>4</sub></b>	39.8	34.9	34.6
<b>C<sub>5</sub>-C<sub>11</sub></b>	25.1	30.5	27.7
<b>C<sub>12</sub><sup>+</sup></b>	10.2	11.7	11.9
<b>CO<sub>2</sub></b>	6.89	4.40	2.66

Data has ± 5% experimental error

<sup>a</sup> C<sub>2</sub> = / (C<sub>2</sub> + C<sub>2</sub>=) [olefin to total C<sub>2</sub> hydrocarbon weight ratio]

**Catalyst mass:** 0.1 g, **Reduction:** CO, flow rate = 12 ml/min, t = 20-24 h, T = 350 °C, P = 2 bar,

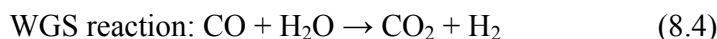
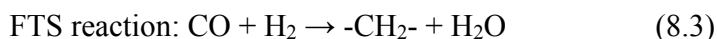
**Reaction conditions:** H<sub>2</sub>/CO = 2, flow rate = 12 ml/min, t = 140 h, T = 275 °C, P = 10 bar

### 8.3.4.2 Product selectivity

The selectivity to FTS products produced is illustrated in Table 8.4. The introduction of indium lowers the selectivity to low weight hydrocarbons ( $C_2$ - $C_4$  and  $C_2$  olefins), whereas the selectivity to heavy weight hydrocarbons ( $C_5$ - $C_{11}$  and  $C_{12+}$ ) is increased. This trend stays the same even when the loading of indium is increased. It may be that the addition of indium enhances the Fe- $K_2O$  contact leading to  $K_2O$  promotion to be boosted.

$K_2O$  promotion leads to enhanced CO adsorption and this in turn increases the concentration of C atoms on the Fe surface, which promotes the chain growth reaction over chain termination reactions [16]. CO adsorption results presented earlier did show a slight increase in CO adsorption when indium was added, so this assertion could be true.

Indium addition also lowers  $CO_2$  selectivity.  $CO_2$  production may be a qualitative way of evaluating a catalyst's effect on the Water Gas Shift reaction (WGS) (Eq. 8.4). It is also important to note that  $CO_2$  can be produced by the Boudouard reaction (Eq. 8.5).



Assuming that most of the  $CO_2$  produced is from the WGS reaction. This then suggests that adding indium to the catalyst decreases the WGS activity. This could be true since the rate of the WGS reaction is mainly controlled by the amount of  $H_2O$  available. This  $H_2O$  is produced as a byproduct of the FTS reaction (Eq. 8.3). It is seen from Table 8.4 that the FTS rate is decreased when indium is added and when its loading amount is increased. This would invariably slow down the production rate of  $H_2O$  and this would in turn decrease the formation rate of  $CO_2$ . It is noticeable from Table 8.4 that the rate of  $CO_2$  formation is also lowered from  $4.67 \times 10^{-7}$  to  $2.98 \times 10^{-7}$  mol/s when indium is added. Increasing the loading amount of indium still results in a decrease as well. The

rate of the FTS reaction is also decreased further with an increment in the loading amount of indium.

It is suggested that indium acts more as a 'poison' than a promoter for the FTS reaction. As it was suggested in Chapter 7, it may be possible that during calcination and reduction indium moves to the surface of the catalyst to cover some of the active sites of the catalyst.

During calcination  $\text{In}(\text{NO}_3)_3$  is transformed into  $\text{In}_2\text{O}_3$  (indium oxide) and this  $\text{In}_2\text{O}_3$  is transformed into In (indium) metal during reduction. Since indium has a very low melting point ( $157^\circ\text{C}$ ) [17], it melts during the FTS reaction and covers some of the active sites of the Fe-based FTS catalyst. To verify this postulate an  $\text{H}_2$  TPR experiment of indium oxide was carried out (Fig. 8.10).  $\text{In}_2\text{O}_3$  was reduced to metallic indium at ca.  $250\text{-}350^\circ\text{C}$  and this temperature range is well within the temperature conditions employed for the FTS reaction. The broad peak stretching from  $440\text{-}950^\circ\text{C}$  is ascribed to the volatilization of indium.

The broadness of this peak may suggest that as In volatilizes, it is picked up by the TCD detector and since a TCD detector was used which monitors the change in conductivity of the effluent gas stream. It may be that as a component of In was volatilizing, a change in conductivity of the effluent stream occurred and the detector picked it up, consequently resulting in a broad peak on our TPR profile.

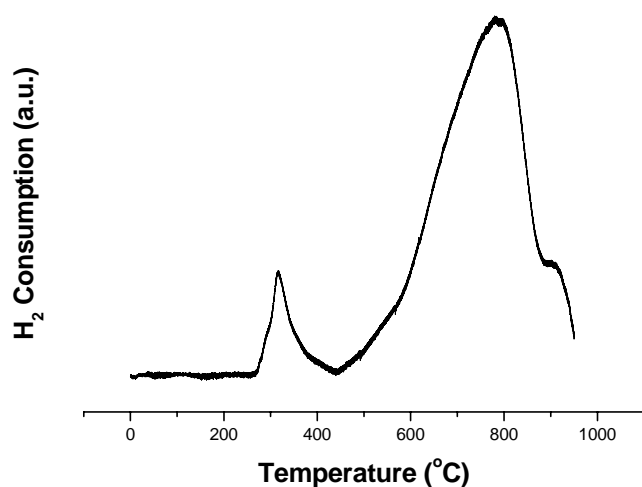


**Figure 8.10** H<sub>2</sub> TPR profile of In<sub>2</sub>O<sub>3</sub>

#### **8.4 Conclusion**

The effect of adding indium to a multi-promoted Fe-based FTS catalyst was investigated. The addition of indium suppressed the reduction properties of the catalyst when H<sub>2</sub> was employed as a reductant. When CO was employed as a reductant, the reduction/carburization properties were improved. This improved the CO adsorption ability of Fe and resulted in a selectivity shift to heavy weight hydrocarbons during the FTS reaction, whereas low weight hydrocarbons were suppressed. Adding indium to the promoted catalyst also lowered the catalyst surface area which resulted in a decrease to the FTS activity.

## References

- [1] M.E. Dry, in *Applied Industrial Catalysis*, B.E. Leach (Ed.) 2, Academic Press, New York, 1983
- [2] V.U.S. Rao, G.J. Stiegel, G.J. Cinquegrane, R.D. Strvastava, *Fuel Proc. Tech.* 30 (1992) 83
- [3] H. Lin, Y. Chen and C. Li, *Thermochimica Acta* 400 (2003) 61-67
- [4] D. B. Bukur, K. Okabe, M. P. Rosynek, C. P. Li, D. J. Wang, K. R. P. M. Rao G. P. Huffman, *J. Catal.* 155 (1995) 353
- [5] Y. Jin, A. K. Datye, *J. Catal.* 196 (2000) 8
- [6] R. Brown, M.E. Cooper, D.A. Whan, *Appl. Catal.* 3 (1982) 177
- [7] M. Luo, R. J. O'Brien, S. Bao, B. H. Davis, *Appl. Catal. A: Gen.* 239 (2003) 111
- [8] C.H. Zhang, H.J. Wan, Y. Yang, H.W. Xiang, Y.W. Li, *Catal. Comm.* 7 (2006) 733
- [9] H. Dlamini, T. Motjope, G. Joorst, G.T. Stege, M. Mdleleni, *Catal. Lett.* 78 (2002) 201
- [10] P.K. Basu, S.B. Basu, S.K. Mitra, S.S. Dasandhi, S.S. Bhattacharjee, P. Samuel, *Stud. Surf. Sci. Catal.* 113 (1998)
- [11] J.J. Jothimurugesan, S.K. Spiey, S.K. Gangwal, J.G. Goodwin, *Stud. Surf. Sci. Catal.* 119 (1998) 215
- [12] R. J. O'Brein, L. Xu, R. L. Spicer, S. Bao, D. R. Milburn, B. H. Davis, *Catal. Today* 36 (1997) 325
- [13] D.G. Miller, M. Moskovits, *J. Phys. Chem.* 92 (1998) 6081
- [14] G. Zhao, C. Zhang S. Qin, H. Xiang, Y. Li, *J. Mol. Catal. A: Chemical* 286 (2008) 137
- [15] G. Bian, A. Oonuki, Y. Kobayashi, N. Koizumi, M. Yamada, *Appl. Catal. A: Gen.* 219 (2001) 13
- [16] H.J. Wan, B.S. Wu, Z.C. Tao, T.Z. Li, X. An, H.W. Xiang, Y.W. Li, *J. Mol. Catal. A: Chemical* 260 (2006) 255
- [17] <http://www.chemicalelements.com/elements/cu.html> (01 February 2009)



## Chapter 9

### *General conclusions*

This study describes the effects that copper, potassium, silica and indium have on a precipitated Fe-based Fischer Tropsch synthesis catalyst.

Chapters 1-3 were introductory chapters contained background material relevant to the thesis. Chapter 4 described studies in which the optimum weight loadings of Cu and K<sub>2</sub>O were investigated. For both the promoters a weight % loading range of 1-5 wt. % was studied. It was established that the 5 wt. % loading was the optimal weight loading for the copper promoter since it gave optimal reduction properties as well as the CO adsorption properties of the Fe catalyst. For the K<sub>2</sub>O promoter it was concluded that 2 wt. % K<sub>2</sub>O loading was also optimal for the Fe-based catalyst. At this loading the reduction properties and the CO adsorption properties of the Fe-based catalyst were optimal. These weight loadings were then employed to prepare catalysts containing Cu and K<sub>2</sub>O.

The effect that silica content had on the Fe-based catalyst was presented in Chapter 5. It was found that increasing the SiO<sub>2</sub> content increased the surface area of the catalyst which improved the dispersion of the iron oxide crystallites, resulting in a decrease in the average size of the iron oxide crystallites. But a decrease in the average size of the iron oxide crystallites strengthened the Fe-SiO<sub>2</sub> interaction. An XPS surface analysis of the catalysts confirmed that as the SiO<sub>2</sub> loading was increased, more of the SiO<sub>2</sub> stayed on the surface allowing the Fe-SiO<sub>2</sub> interaction to be enhanced. This resulted in the reduction and carburization ability of the catalyst being suppressed. This affected the FTS performance of the catalyst and lowered its activity.

In Chapter 6 the effect of silica content on the Fe-based Fischer Tropsch synthesis catalyst that was promoted with potassium and copper was presented. The conclusions reached from this study were that silica stabilized the iron oxide crystallites by providing adequate surface area. This facilitated the high dispersion of Fe<sub>2</sub>O<sub>3</sub> and CuO and

enhanced the contact between  $\text{Fe}_2\text{O}_3$  and  $\text{CuO}$ . The enhanced Fe/Cu contact promoted the reduction of  $\text{Fe}_2\text{O}_3$  to  $\text{Fe}_3\text{O}_4$ , whereas the transformation of  $\text{Fe}_3\text{O}_4$  to Fe was suppressed. Furthermore, due to the  $\text{K}_2\text{O}$ - $\text{SiO}_2$  interaction, the catalyst loaded with the highest  $\text{SiO}_2$  loading had a weak contact between Fe and  $\text{K}_2\text{O}$ , which reduced the surface basicity of the catalyst and severely suppressed the CO adsorption.

In the FTS reaction, the FTS activity went through a maximum at 3 wt. % loading of  $\text{SiO}_2$  and further addition of  $\text{SiO}_2$  decreased the catalyst activity. The  $\text{SiO}_2$  content also affected the hydrocarbon selectivity. At the highest  $\text{SiO}_2$  loading, the product distribution shifted to light hydrocarbons and the  $\text{C}_5$ - $\text{C}_{11}$  hydrocarbons and  $\text{C}_2$  olefins selectivity were suppressed.

In Chapter 7 the effect of indium on the Fe-based Fischer Tropsch catalyst was evaluated and the results obtained were compared to those of the effects caused by copper on the Fe-based Fischer Tropsch synthesis catalyst. It was found that indium exhibited similar promotional properties to copper. However indium decreased the reducibility and CO adsorption ability of the Fe catalyst. It also lowered the FTS activity of the Fe-based catalyst. It was thus concluded that indium was a poorer promoter for the iron-based FTS catalyst and acted as a poison for this catalyst.

Finally in Chapter 8 the effect of indium on an Fe-based Fischer Tropsch synthesis catalyst promoted with potassium and silica was investigated. It was determined that indium suppressed the reduction properties of the catalyst when  $\text{H}_2$  was employed as a reductant, whereas when CO was employed as a reductant, the reduction/carburization properties were improved. This improved the CO adsorption ability of Fe and resulted in a selectivity shift to heavy weight hydrocarbons during the FTS reaction whilst low weight hydrocarbons were suppressed. Adding indium to the promoted catalyst also lowered the catalyst surface area which resulted in a decrease to the FTS activity.